Saniye Aylin Ceylan

A Master's Thesis

AGU 2023

INFLUENCE OF 3D BIOPRINTING PARAMETERS ON PRINTABILITY AND MECHANICAL BEHAVIOR OF THE PCL SCAFFOLDS

A THESIS
SUBMITTED TO THE DEPARTMENT OF BIOENGINEERING
AND THE GRADUATE SCHOOL OF ENGINEERING AND SCIENCE
OF ABDULLAH GUL UNIVERSITY
IN PARTIAL FULFILLMENT OF THE REQUIREMENTS
FOR THE DEGREE OF
MASTER OF SCIENCE

By
Saniye Aylin Ceylan
June 2023

INFLUENCE OF 3D BIOPRINTING PARAMETERS ON PRINTABILITY AND MECHANICAL BEHAVIOR OF THE PCL SCAFFOLDS

A THESIS

SUBMITTED TO THE DEPARTMENT OF BIOENGINEERING

AND THE GRADUATE SCHOOL OF ENGINEERING AND SCIENCE OF ABDULLAH GUL UNIVERSITY

IN PARTIAL FULFILLMENT OF THE REQUIREMENTS

FOR THE DEGREE OF

MASTER OF SCIENCE

By

Saniye Aylin Ceylan

June 2023

SCIENTIFIC ETHICS COMPLIANCE

I as a result of this declare that all information in this document has been obtained in accordance with academic rules and ethical conduct. I also declare that, as required by these rules and conduct, I have fully cited and referenced all materials and results that are not original to this work.

Name-Surname: Saniye Aylin Ceylan

Signature :

REGULATORY COMPLIANCE

M.Sc. thesis titled INFLUENCE OF 3D BIOPRINTING PARAMETERS ON PRINTABILITY AND MECHANICAL BEHAVIOR OF THE PCL SCAFFOLD has been prepared in accordance with the Thesis Writing Guidelines of the Abdullah Gül University, Graduate School of Engineering & Science.

Prepared By	Advisor
Saniye Aylin CEYLAN	Assoc. Prof. İsmail Alper İŞOĞLU

Head of the Bioengineering Program

Asst. Prof. Altan ERCAN

ACCEPTANCE AND APPROVAL

M.Sc. thesis titled INFLUENCE OF 3D BIOPRINTING PARAMETERS ON PRINTABILITY AND MECHANICAL BEHAVIOR OF THE PCL SCAFFOLDS and prepared by Saniye Aylin Ceylan has been accepted by the jury in the Bioengineering Graduate Program at Abdullah Gül University, Graduate School of Engineering & Science.

05/06 / 2023

(Thesis Defense Exam Date)

JURY:

Advisor : Assoc. Prof. İsmail Alper İŞOĞLU

Member: Assoc. Prof. Murat TOPUZOĞULLARI

Member: Assoc. Prof. Burak BAL

APPROVAL:

The acceptance of this M.Sc. thesis has been approved by the decision of the Abdullah Gül University, Graduate School of Engineering & Science, Executive Board dated ….. /….. / …….. and numbered ……..…… .

…….. /…….. / ……..

(Date)

Graduate School Dean

Prof. Dr. İrfan Alan

ABSTRACT

INFLUENCE OF 3D BIOPRINTING PARAMETERS ON PRINTABILITY AND MECHANICAL BEHAVIOR OF THE PCL SCAFFOLD

Saniye Aylin CEYLAN

MSc. in Bioengineering

Advisor: Assoc. Prof. İsmail Alper İŞOĞLU

June 2023

Polycaprolactone (PCL) is a synthetic polymer that exhibits desirable properties such as biodegradability, tolerable mechanical properties, and biocompatibility for a diverse range of tissue engineering applications. In this study, we analyzed the effects of polymer concentration (10%, 25%, 50% and 75% w/v), solvent effect (dichloromethane, chloroform and acetic acid), and device parameters (pressure, speed, nozzle-surface distance, nozzle gauge, infill density) on printed scaffolds fabricated through 3D Bioprinting. Scanning electron microscopy (SEM) and optical microscopy were used to assess printability, and uniaxial tensile testing was performed to evaluate mechanical behavior. The aim of this study was to investigate the effects of different printing speeds (5 mm/s, 10 mm/s, and 15 mm/s) on the mechanical properties of PCL_DCM and PCL_CF scaffolds. The scaffolds printed at the lowest speed exhibited the highest ultimate tensile strength (UTS) values. Scaffolds printed at 5 mm/s with the highest printing pressure (480 kPa) demonstrated a remarkably high Young's modulus of 39.69 MPa and a UTS value of 6.4 for PCL_DCM, as well as Young's modulus of 26.80 MPa and a UTS value of 6.3 MPa for PCL_CF. Additionally, we investigated the influence of polymer concentrations (50% and 75%) and infill densities (50%, 70%, and 90%). The results showed that increasing the infill density and using a lower concentration (50%) led to improvements in Young's modulus and UTS values for both PCL_DCM and PCL_CF scaffolds. These results highlight the importance of carefully controlling printing parameters to optimize the mechanical properties of the printed scaffolds.

Keywords: 3D Bioprinting, extrusion-based 3D Bioprinting, polycaprolactone (PCL), mechanical analysis.

ÖZET

3D BİYOBASKI PARAMETRELERİNİN PCL İSKELESİNİN BASILABİLİRLİĞİ VE MEKANİK DAVRANIŞI ÜZERİNDEKİ ETKİSİ

Saniye Aylin CEYLAN

Biyomühendislik Anabilim Dalı Yüksek Lisans

Tez Yöneticisi: Doç. Dr. İsmail Alper İŞOĞLU

Haziran-2023

Polikaprolakton (PCL), çeşitli doku mühendisliği uygulamaları için uygun özelliklere sahip, biyolojik olarak parçalanabilen sentetik bir polimerdir. Çalışmada polimer konsantrasyonu (%10, %25, %50 ve %75 w/v), çözücü etkisi (diklorometan, kloroform ve asetik asit) ve cihaz parametrelerinin (basınç, hız, nozul-yüzey mesafesi, nozul,dolgu yoğunluğu) etkisi basılabilirlik için tarama elektronu (SEM) ve optik mikroskopi ve mekanik davranış için tek eksenli çekme testi kullanılarak analiz edildi. Farklı baskı hızlarının (5, 10 ve 15 mm/sn) PCL_DCM ve PCL_CF yapı iskelelerinin mekanik özellikleri üzerindeki etkilerini araştırması amaçlamıştır. En düşük hızdaki iskeleleri, en yüksek nihai gerilme mukavemeti (UTS) değerlerini sergiledi. En yüksek baskı basıncıyla (480 kPa), 5 mm/s'de yazdırılan yapı iskeleleri PCL_DCM için 39,69 MPa'lık oldukça yüksek bir Young modülü ve 6,4'lük bir UTS değeri ve 26,80 MPa'lık bir Young modülü ve 6,3 MPa'lık bir UTS değeri gösterdi. Polimer konsantrasyonlarının (%50 ve %75) ve dolgu yoğunluklarının (%50, %70 ve %90) etkisini araştırmıştır. Dolgu yoğunluğunu artırmanın ve daha düşük konsantrasyonun (%50) hem PCL_DCM hem de PCL_CF yapı iskeleleri için Young modülü ve UTS değerlerinde iyileşmelere yol açtığını gösterdi. Bulgular, iskelelerin mekanik özelliklerini optimize etmek için baskı parametrelerini dikkatli bir şekilde kontrol etmenin önemini vurgulamaktadır.

Anahtar kelimeler: 3B Biyoyazıcı, Püskürtmeli 3B Biyoyazıcı, polikaprolakton (PCL), mekanik analiz

Acknowledgements

I would like to thank you my supervısor Assoc. Prof. İsmail Alper İŞOĞLU, for his support, extremely patience, guidance during my thesis study. Besides, I am grateful to Assoc. Prof. Burak Bal for valuable support and guidace my research work. I am deeply thankful to Prof. Dr. Sevil Dinçer İŞOĞLU for her guidance and contributions. Furthermore, I would like to express my special thank you to Nazende Nur Bayram and Ferdi Caner Bayram for supporting and helping during the experimental parts of my thesis study. Besides, I am extremely grateful to my laboratory mates Seray Zora Tarhan and Enes Hamdi Demirci for their motivation. Also, I would like to thank deeply my close friends Selma Abay, Ümmügülsüm Yıldız, Melek Ersoy and all friends for their endless support and motivation. Finally, I would like to thank my family for believing in me throughout my education.

TABLE OF CONTENTS

LIST OF FIGURES

LIST OF TABLES

LIST OF ABBREVIATIONS

ECM	Extracellular Matrix
3DP	Three-Dimensional Printing
RP	Rapid Prototyping
FDM	Fused Deposition Modeling
SLA	Stereolithography Apparatus
SLS	Selective Laser Sintering
CT	Computed Tomography
MRI	Magnetic Resonance Imaging
CAD	Computer-Aided Design
SCPL	Solvent Casting/Particle Leaching
TIPS	Thermally-Induced Phase Separation
FDM	Fused Deposition Modeling
SLS	Selective Laser Sintering
EBB	Extrusion-Based Bioprinting
PLLA	Poly-L-Lactic Acid
PGA	Polyglycolic Acid
PEG	Polyethylene Glycol
PLGA	Poly-Dl-Lactic-Co-Glycolic Acid
PCL	Polycaprolactone
UTS	Ultimate Tensile Strength
SEM	Scanning Electron Microscopy
DCM	Dichloromethane
CF	Chloroform
AA	Acedic Acid
FTIR	Fourier Transform Infrared Spectroscopy

To My Family

Chapter 1

Introduction

1.1 Tissue Engineering

Tissue engineering is an interdisciplinary field that uses combination of cells, engineering, materials methods, and appropriate biochemical and physicochemical factors to repair, maintain, and heal different tissues [1]. In order to repair the damaged tissues, some specific artificial materials have been produced and implanted in the body or on the surface of the body so that the cells can grow and regain their functionality. These structures act as natural extracellular matrix (ECM) and create a three-dimensional (3D) structure for cells [2]. The ECM provides structural support and a physical environment for cell growth, proliferation, and activation of intracellular signaling pathways, as shown in Figure 1.1. In addition, the ECM provides information about the structure of the tissue. ECM defines hardness and elastic properties. For example, while bone tissue has high strength, its elastic properties are weak; on the other hand, tendon tissues are very resistant to stretching thanks to type 1 collagen bundles and have high elastic properties [3-4]. Collagen and elastin fibers are responsible for the elastic behavior of the tissue. At the same time, since it supports intercellular signaling pathways, regeneration and migration of cells will be limited in case of tissue loss for any reason. For this reason, tissue engineering produces structures called scaffolds that mimic the ECM for cells, which are suitable for attachment [3-5-6].

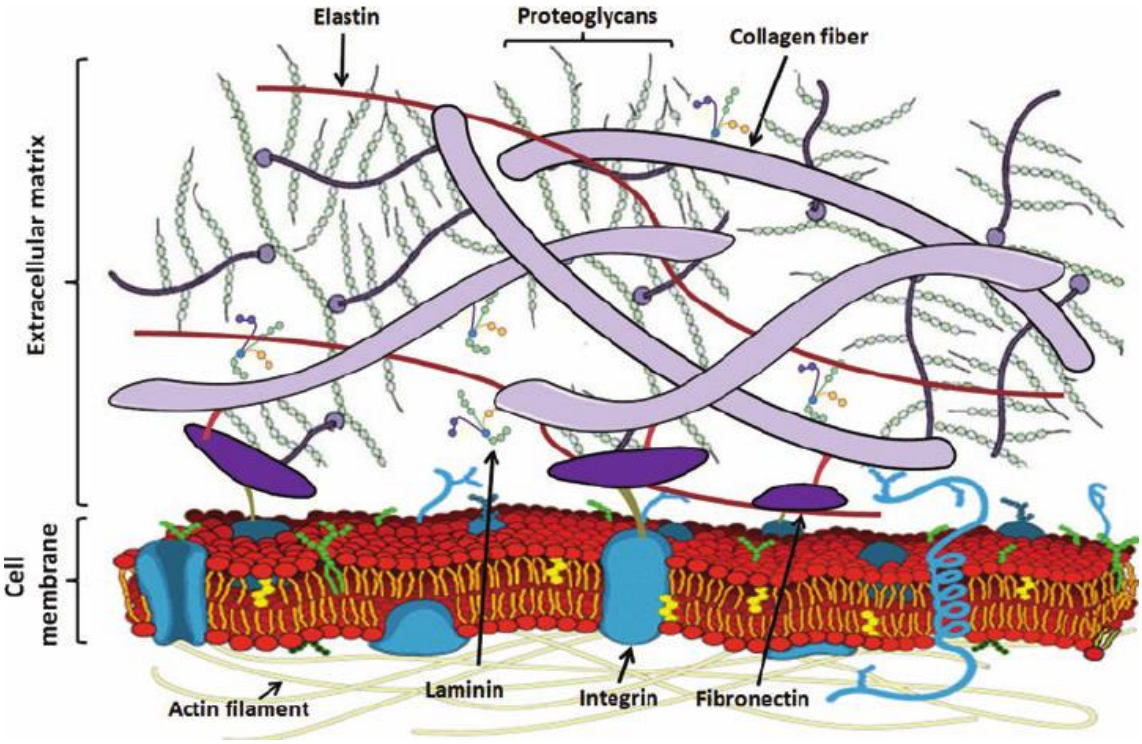

Figure 1.1 Components of Extracellular matrix (ECM) [7].

Tissue engineering is based on the interaction between cells, signals (growth factors, small molecules, etc.), and biomaterials. As of the 1990s, the use of scaffolds which provide cell attachments and cellular signaling pathways, has increased significantly developing in the field of tissue engineering. Scaffolds are three-dimensional structures that ensure mechanical and biological supports [8]. Scaffolds should be biocompatible and biodegradable, have mechanical properties suitable for tissues, and show porosity appropriate for attachment, proliferation, and migration of cells [9-10-11]. Scaffolds with these features accelerate healing by creating an appropriate host response for tissue healing [11]. The materials used in the production of scaffolds can be categorized as natural and synthetic biomaterials . Scaffolds made of biomaterials are produced using different production techniques [9].

1.2. Fabrication Techniques of the Scaffolds for the Tissue Engineering Applications

The primary classification for fabrication technique can be divided into two groups conventional techniques and rapid prototyping as depicted in Figure 1.2. Conventional fabrication techniques, also known as traditional manufacturing methods, constitute a wide range of fields in scaffolding production. The production techniques demonstrated in Figure 1.3 have been frequently preferred due to their many advantages such as fabrication possibilities with varying pore sizes, high interconnectivity. In spite of their advantages, there are critical drawbacks such as inadequate mechanical integrity, small pore size and, small-scale production [12]. But, in recent years new methods have also been developed due to the need for these requests, such as the production of rapid and higher precision, large-scale production, sufficient mechanical properties, and patient-specific manufacturing [13-14].

Additive manufacturing technologies, known as rapid prototyping (RP) have gained increasing interest in tissue engineering as they offer the ability to create 3D structures through repetitive deposition and processing of material layer by layer. Rapid prototyping techniques include three-dimensional printing (3DP), fused deposition modeling (FDM), stereolithography apparatus (SLA), and selective laser sintering (SLS) as described in Figure 1.4. RP has been primarily used for product designs and quick and easy prototyping in manufacturing industries. Recently, researchers have also used it for producing patient-specific implants such as artificial limbs, prosthetic implants. To create patient-specific models are formed a model using MRI (Magnetic resonance imaging), CT (computed tomography) scans of patients or computer-aided design (CAD) of an object directly with special software [15].

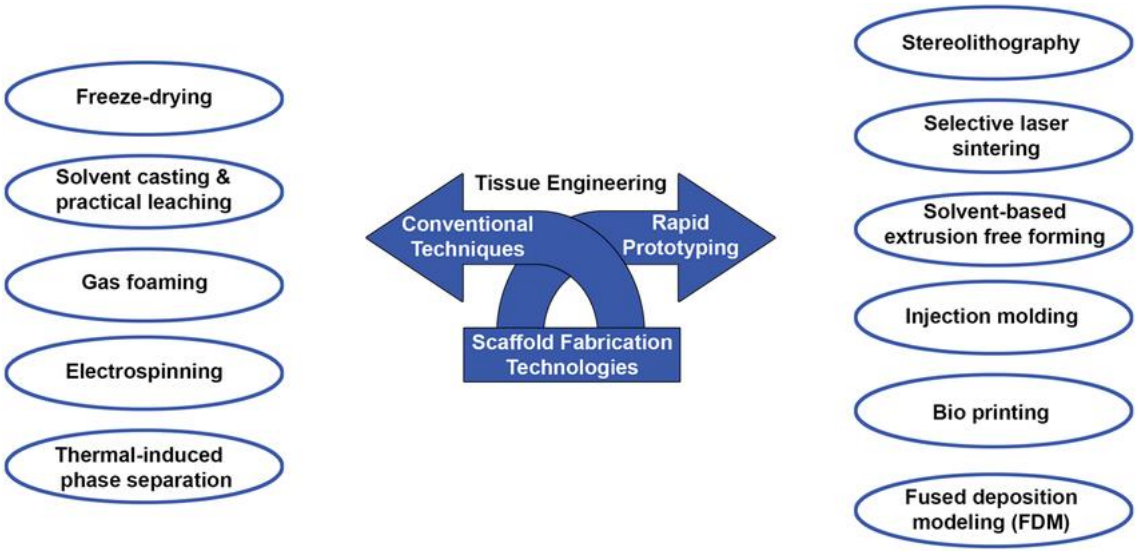

Figure 1.2 Classification of fabrication technique in tissue engineering [7].

1.2.1 Solvent Casting and Particle Leaching

Solvent casting/particle leaching is a commonly used technique for preparing porous scaffolds with controlled pore size and porosity. This method involves dissolving particles of different sizes and numbers in a solvent to create a mixture that is then cast into a mold. After the solvent is evaporated, the particles are leached out, leaving behind a porous structure. Various materials can be used as pore-forming agents in this technique, such as sodium chloride particles, sugar particles, ice particles, and paraffin microspheres. The pore size and porosity of the scaffold can be precisely controlled by adjusting the size and number of the particles, as well as the freezing temperature [16]. One of the significant challenges faced in this technique is the poor mechanical properties of high-porosity materials. To address this, researchers have studied different solvent systems and additives to improve the quality of the resulting scaffold. For example, the addition of plasticizers like glycerin, polyethylene glycol, and sorbitol can enhance the tensile strength and flexibility of the scaffold. Thus, reinforced tensile strength and improved flexibility make the scaffolds more suitable for tissue engineering applications.

Another limitation is that SCPL can not form homogenous distribution within the scaffold even it provides high porosity changing between 50% and 95% within the scaffold [18]. However, this technique is a relatively low-cost and straightforward method for producing porous polymer scaffolds, and it can be optimized to meet specific tissue engineering requirements.

1.2.2 Electrospinning

Electrospining is a versitale technology that produces micro and nanoscale fibers with a wide range of potential applications, including tissue engineering, medical, wound dresing, and drug delivery. The components of electrospinning consist fundamentally of three parts: a power supply, metallic needle, and collector. Taylor cone plays a crucial role in the electrospinning technique. Basically, a liquid polymer solution is electrically charged and afterward ejected from a syringe tip to form a nanofibrous scaffold. The Taylor cone is formed when the electric force at the polymer solution's surface overcomes the liquid's surface tension. This part result in a cone-shaped droplet produced from the syringe tip. As the electric field increases, the droplet elongates and eventually forms a jet that is deposited on a collector to form a nanofibrous scaffold [18-19]. By controlling various factors, such as polymer solution and environmental conditions, nanofibers can be designed with specific properties such as high porosity, roughness, and tunable mechanical properties [19-20]. Therefore, it is essential to optimize these variables to produce electrospun nanofibers with ideal properties for specific applications such as wound dressing and drug delivery [21].

Recent studies have shown that increasing the specific surface area and decreasing the fiber diameter of electrospun nanofibers can enhance scaffold performance to support the growth of cells and tissues due to high interconnected porosity [22]. Additionally, electrospun nanofibers allow cell attachment, proliferation, and differentiation to specific tissue types [23]. Despite its many advantages, electrospinning still has some limitations due to the use of solvents. Solvents are highly toxic and depend on a high environmental impact. Therefore, the use of large volumes of solvents in electrospinning is time-consuming and expensive as well as toxic effects [24].

1.2.3 Thermally-Induced Phase Separation

Thermally-induced phase separation (TIPS) is a widely used method for fabricating microporous membranes, which finds numerous applications in various fields such as tissue engineering and biomedical devices [25]. The TIPS process can be adapted to different polymers, solvents, and non-solvents to obtain membranes with specific properties such as pore size, morphology, mechanical strength, and chemical resistance [26]. The TIPS process involves several steps including polymer solution preparation,

film casting, quenching, and solvent extraction. The first step is to dissolve the polymer in a suitable diluent at an elevated temperature to obtain a homogeneous solution. The polymer concentration and the temperature are critical parameters that affect the polymer solubility and the phase separation behavior [27]. A higher polymer concentration or a lower temperature can promote phase separation and lead to smaller pore sizes. The next step is to cast the polymer solution into a film using a suitable method such as spin-coating, dip-coating, or extrusion TIPS provides the ability to prepare membranes from a variety of polymers and high interconnectivity of scaffolds. Even though its advantages, TIPS also has some drawbacks and challenges that must be considered. One of the significant limitations is controlling the morphology and pore size distribution of the membrane, which can be affected by factors such as the composition of the polymer solution and the extraction conditions. Another challenge is that the TIPS process is the control of membrane thickness. Controlling the membrane thickness is crucial since it can significantly affect the properties of the membrane such as its permeability, selectivity, and mechanical strength. For instance, the increased thickness of the membrane is to provide a favorable environment with a larger surface area for the attachment and proliferation of cells [28]. Furthermore, the TIPS process is sensitive to variations in processing conditions and requires careful optimization to achieve consistent and reproducible membrane properties. However, it can be carefully considered and optimized to achieve the desired membrane properties and performance to overcome these limitations [26-29].

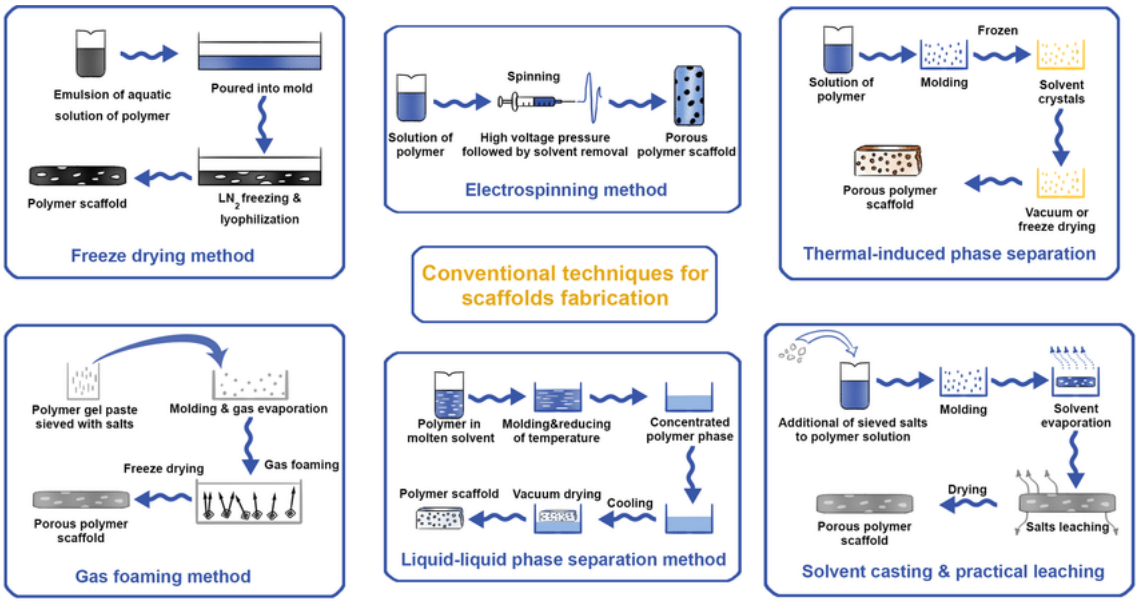

Figure 1.3 Demonstration of conventional prototyping techniques in scaffold fabrication [7].

1.2.4 Gas Foaming

Gas foaming is a promising fabrication technique in tissue engineering that allows the creation of porous structures. The technique involves introducing inert gases such as carbon dioxide or nitrogen into a modeled polymer sample and creating bubbles using a chemical blowing agent [30]. When the sample is brought to atmospheric pressure, CO_2 expands to create pores within the polymer. This technique can produce scaffolds with pore sizes ranging from 30-700 μm and porosity rates of up to 85% [31]. However, controlling pore size and interconnectivity remains a challenge, and inhomogeneous deposition can lead to reproducibility problems. This can limit the ability of gas foaming to create scaffolds with precisely controlled pore sizes and interconnectivity. Researchers continue to explore ways to improve the technique's reproducibility and control over pore size and interconnectivity to overcome these limitations and create more effective scaffolds for tissue engineering. Notwithstanding these limitations during fabricating scaffold, it has a significant advantage compared to most fabrication techniques such as electrospinning, TIPS using solvents. Gas foaming eliminates the risk of cytotoxicity associated with solvents and porogens, which can be harmful to cells [32].

1.2.5 Freeze Drying

Freeze drying, also known as lyophilization or cryodesiccation, is a dehydration technique used in various fields such as biomedicine, tissue engineering, and food preservation. The process involves freezing the sample and then reducing the pressure to allow the frozen water to sublimate directly from a solid to a gas without going through a liquid phase [33-34]. This process results in a dry and porous product that maintains its original shape. Freeze drying is a particularly preferable technique in tissue engineering, where it can be used to produce scaffolds with high porosity and controlled pore sizes. The porosity and pore size can be controlled by adjusting the freezing rate, polymer concentration, and temperature. However, one of the significant disadvantages of this technique is that the scaffolds have insufficient mechanical structure and cannot be used in load-bearing tissue engineering applications such as bone tissue [35]. One of the benefits of freeze drying is that it can dry samples at low temperatures, which prevents

product deterioration caused by heat. Additionally, the humidity of the final product can be controlled, and the product's structure can be preserved during the process [36].

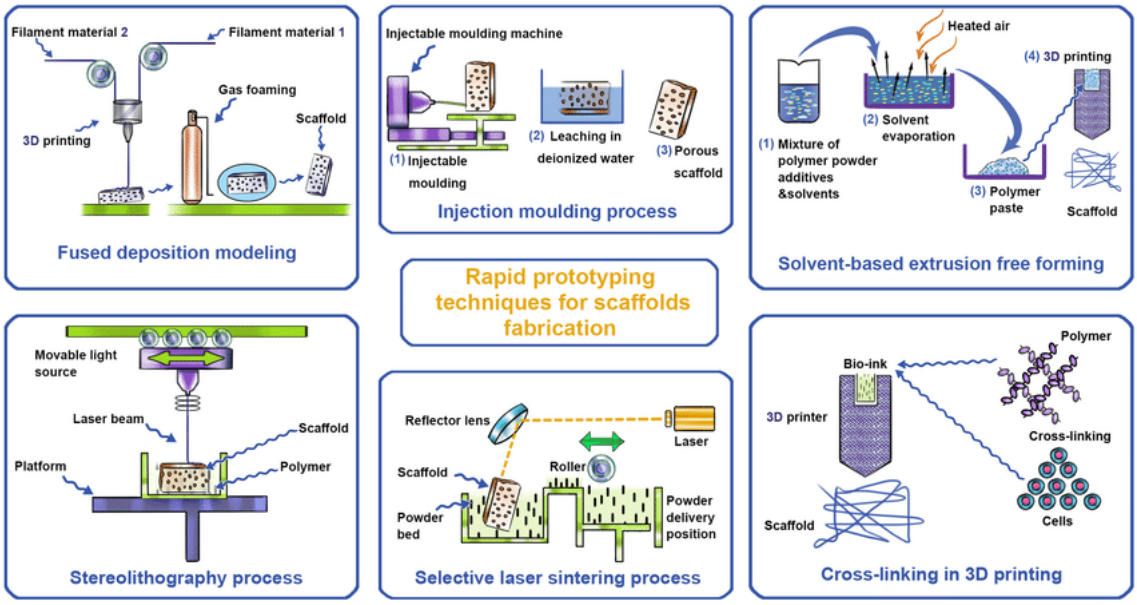

Figure 1.4 Demonstration of rapid prototyping techniques in scaffold fabrication [23].

1.2.6 Fused Deposition Modeling

Fused Deposition Modeling (FDM) is known for its ease of use and versatility, as it can produce complex geometries and functional parts with a variety of materials [37]. In recent years, FDM has been widely used in a range of industries, from aerospace and automotive to medical and dental. Its applications include prototyping, tooling, and even end-use parts. FDM has proven particularly useful in biomaterial research for fabricating scaffolds and implants with tailored mechanicalstructures and properties. In this process, the filament (usually made of thermoplastic material) is fed through a heated nozzle. Melting materials extrude onto a build platform layer by layer, following the path defined by the g-code instructions. Some of the critical advantages of FDM include its relatively low cost and high accuracy, as well as the ability to produce parts with a range of mechanical properties (e.g., flexibility, strength, and durability). Additionally, FDM does not require any post-processing steps and is generally faster than other 3D printing methods. But, the limited number of polymers to be used in this technique and the inability to work with different material combinations are the most limiting aspects of the system [37].

1.2.7 Stereolithography

Stereolithography (SLA) is an additive manufacturing process that uses an ultraviolet laser beam to cure a liquid photopolymer layer by layer. The system consists of four essential components: (i) a UV laser source, (ii) a photosensitive liquid resin tank, (iii) mirrors, (iv) and a movable platform. During the build process, the process involves a platform that sits in a vat of liquid epoxy resin or an acrylate resin. The platform is incrementally lowered after each layer of the photo-sensitive polymer has been exposed to the laser beam. In the SLA process, the laser scans the predefined area according to the slice information and cures the resin in a defined penetration depth. After each layer is cured, the platform is lowered, and new resin is applied to the surface of the previous layer. The next layer is then generated and bonded to the previous layer, and this process is repeated until the 3D object is complete. SLA offers several advantages, including the ability to produce 3D objects with relatively accurate geometries, create complex geometries, and produce smooth surfaces suitable for post-processing like coating and plating. Otherside, SLA requires support structures to be built to support overhanging features during the build, need thermal post-curing, and more post-processing time [38]. Additionally, SLA needs several post-processing parts such as removing support structures, cleaning, and extra curing in UV oven. Therefore this process can be challenging to predict and control because of these limitations.

1.2.8 Selective Laser Sintering

SLS is a method that enables the 3D structure to be obtained by compressing (sintering) the powder particles with the help of the laser energy of the powder sample [39]. Polymer, metal, or ceramics can be used in this method, and possible to work with composite materials [40-41]. It is beneficial for creating parts with intricate geometries, such as porous scaffolds for tissue engineering. The technique produces structures with excellent mechanical properties. As the sintered particles are tightly fused to each other, a dense and strong structure is obtained. The microstructures of the produced scaffold can be controlled by adjusting the percentage ratios of the mixture consisting of different materials. This process needs additional processes, such as bringing it from high temperature to room conditions after the sintering process [42].

1.3 3D Bioprinting

3D Bioprinting, also known as additive manufacturing, has started to attract more attention in recent years. 3D bioprinting has paved the way for developments in tissue engineering in recent years by producing layer-by-layer structures quickly and effectively with a bottom-up approach [43]. Additionally, it enables scalable and complex geometries with the help of three-dimensional(3D) computer tools [44-45]. It is possible to create different geometries in CAD / CAM programs, as can be obtained from images such as MRI and tomography from the patient [46]. The 3D bioprinter enables the utilization of various substances such as polymers, cells, bioactive particles, medications, and growth factors. Thanks to 3D Bioprinting, it becomes possible to generate heterocellular microenvironments, which have facilitated numerous types of research compared to conventional manufacturing methods. [47]. The structures that can imitate the natural cellular structure enable the tissues to capture their natural structure and functionality again. Moreover, these structures provide the appropriate 3D support structure for cells to adhesion, proliferation, and migration and accelerate the healing process of damaged tissues. As the 3D printer offers micropores, it supports gas and nutrient exchange between layers and provides appropriate porosity for intracellular and intercellular communication [48]. In this way, 3D Bioprinters are an excellent option for designing suitable conditions for obtaining physiological outputs before in vivo experiments.

Figure 1.5 illustrates using inks as biomaterials and bioink in 3D bioprinting. 3D bioprinters utilize bioinks containing living cells or biomaterial inks to produce 3D-printed tissues [49]. Biomaterial inks, unlike bioinks, do not have cells due to the limitations in the printing process, which may damage cells using organic solvents. Therefore, cell cultivation is carried out on the printed structure in cell culture [50]. The printing procedure starts with the preparation of the ink and the creation of the model to be printed. The desired structure is then obtained by the material deposition method, followed by necessary characterizations of the printed structure. With the help of bioprinting, a variety of research can be conducted in tissue engineering, pave the way for innovative solutions for organ loss, which is a major concern [51].

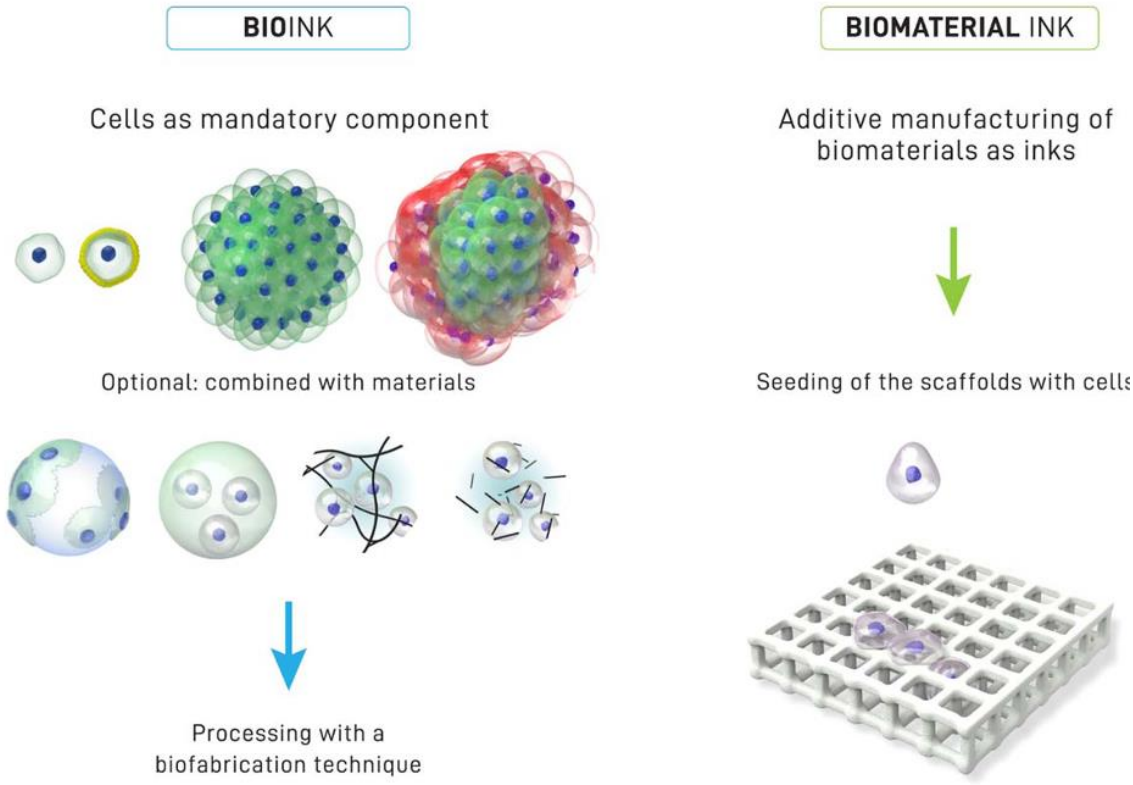

Figure 1.5 Inks using 3D Bioprinting [52].

3D Bioprinters can be classified into three main categories: inkjet-based, laser-assisted, and extrusion-based bioprinting shown in Figure 1.6. Different 3D bioprinters use different mechanisms for layer-by-layer deposition of materials to create 3D structures . The chose of a 3D bioprinter depends on the specific requirements of the intended application, including the viscosity of the ink, the presence of cells, the targeted resolution, accuracy, or shape of the geometry [53].

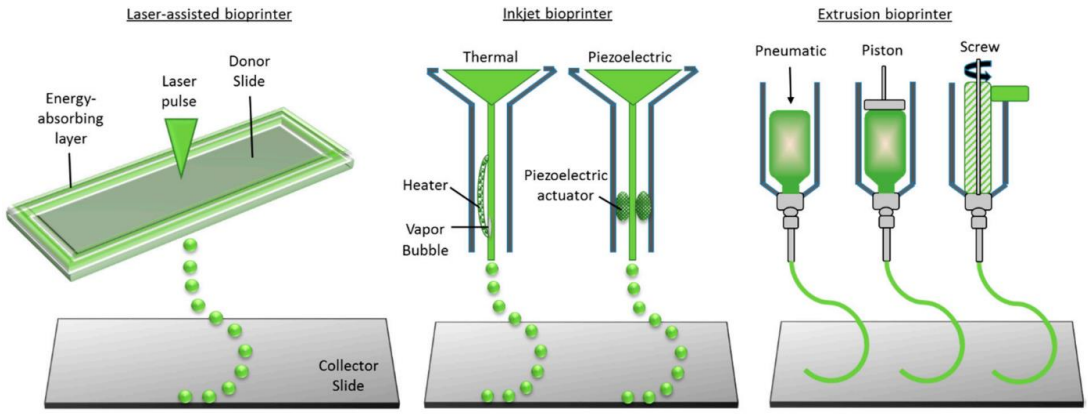

Figure 1.6 Types of 3D Bioprinting: (a) laser-assisted bioprinting; (b) inkjet bioprinting; (c) extrusion based bioprinting [54].

1.3.1 Inkjet Based 3D Bioprinting

Inkjet bioprinters have the ability to print complex tissue structures with high resolution and accuracy, making them ideal for a wide range of applications in tissue engineering and regenerative medicine. This technologhy allows for precise control over the size and shape of the droplets that are deposited onto the substrate. Ink-printed bioprinters are often preferred due to their easy accessibility, high printing control, and low cost [55]. Basically, inkjet bioprinters use thermal or acoustic energy to print of materials. Bioprinters with thermal ink rise up to high temperatures (200-300 °C) and allow the bioink to come out in the form of bubbles. However, prolonged exposure to high temperatures or repeated thermal cycles can lead to damage and death of the cells. Acoustic inkjet bioprinters are a promising technology for the field of bioprinting, with the potential to create complex and functional tissues and organs. Ongoing research accerates necessary to expand the range of materials that can be used, improve printing resolution and accuracy, and optimize the cross-linking process to achieve optimal outcomes. Acoustic inkjet bioprinters use piezoelectric crystals for printing and bioink pulses at the printhead to form droplets on the surface. Acoustic inkjet bioprinters use piezoelectric crystals to create pulses that generate the droplets of bioink. When a voltage is applied to the piezoelectric crystals, they vibrate at a high frequency generating pressure waves. These pressure waves create droplets that are ejected from the printhead and deposited onto the printing surface. Acoustic inkjet bioprinters allow for high-throughput printing, precise control over droplet size and placement, and the ability to print onto irregular and non-flat surfaces. Additionally, because the printing process is non-contact, there is minimal damage to the printed cells or tissues in contrast to thermal inkjet bioprinters. However, the range of materials that can be used with acoustic inkjet bioprinters is limited, since the bioink must have suitable viscosity to be sprayed from the nozzle. In addition, extra supporting elements may be required to maintain the structural integrity of the printed structure. As a solution to these limitations, cross-linking techniques can be used to transform the bioink into a more solid form, which can improve mechanical stability and strength [56].

1.3.2 Laser Assisted 3D Bioprinting or Laser Induced Forward Transfer

Laser-assisted 3D bioprinting is indeed a promising bioprinting technique that has the potential to produce high-resolution 3D structures for tissue engineering and regenerative medicine applications. Laser assisted 3D Bioprinting allows a cell-containing ink surface to be deposited on the surface using a pulsed laser light source [57]. The non-contact nature of the technique allows for precise control over the deposition of the bioink, which can result in more accurate and reproducible structures. They consist of three essential parts; a pulsed laser source,bioink and laser pulse. The laser sourse is placed on a strip and at the bottom a surface where the ink is deposited after the laser pulse. The bioink is coated on a plate that allows the laser to be transmitted. The laser pulse pushes the heat-sensitive ink "from the plate" to the surface (Figure 1.6) [58]. The transfer of cells and other biological materials from the bioink to the surface depends on various factors, including the properties of the bioink, the characteristics of the laser, and the properties of the surface [59]. A sacrificial layer can be used to improve the optical properties of the bioink and facilitate its transfer to the surface.In spite of their advantages, one of the main challenges of laser-assisted 3D bioprinting is the cost and complexity of the equipment. The pulsed laser source and associated optics required for this technique can be expensive, which limits its accessibility to many researchers and labs. Additionally, the process can be more difficult to control than other 3D bioprinting techniques, which can result in lower printing efficiency and higher failure rates.Moreover , the use of sacrificial layers and coatings may introduce additional steps and materials that can complicate the printing process.

1.3.3 Extrusion Based 3D Bioprinting

Extrusion-based bioprinting (EBB) is a widely used 3D bioprinting technique in tissue engineering applications due to its versatility and accessibility. One of the advantages of EBB is its ability to work with a wide range of viscosities, making it suitable for printing a variety of materials such as polymers, bioactive particles, and cells [60]. Additionally, EBB allows for the creation of desired strut diameters and pore structures by using different nozzle and needle types, making it highly customizable. Its commercial availability has made it even more important and preferred over other 3D bioprinting techniques [61].

The biomaterials used in bioink should have adequate fluidity, compressibility, suitable mechanical properties, and biocompatibility to ensure the success of the bioprinting process. The printability of the bioink refers to its ability to produce accurate and high-quality structures through bioprinting strategies [62]. The choice of biomaterials and their properties can greatly impact the printability and functionality of the final 3D-printed structures.

There are three types of EBB: pneumatic, piston, and screw bioprinting as shown in Figure 1.7. In pneumatic systems, air pressure is used to push the solution through the nozzle/needle, and the structures are quickly created in the desired geometries with movements on the x-y-z-axis [51-63]**.** Pneumatic systems are commonly used in tissue engineering applications because of their high printing speed and their accuracy.

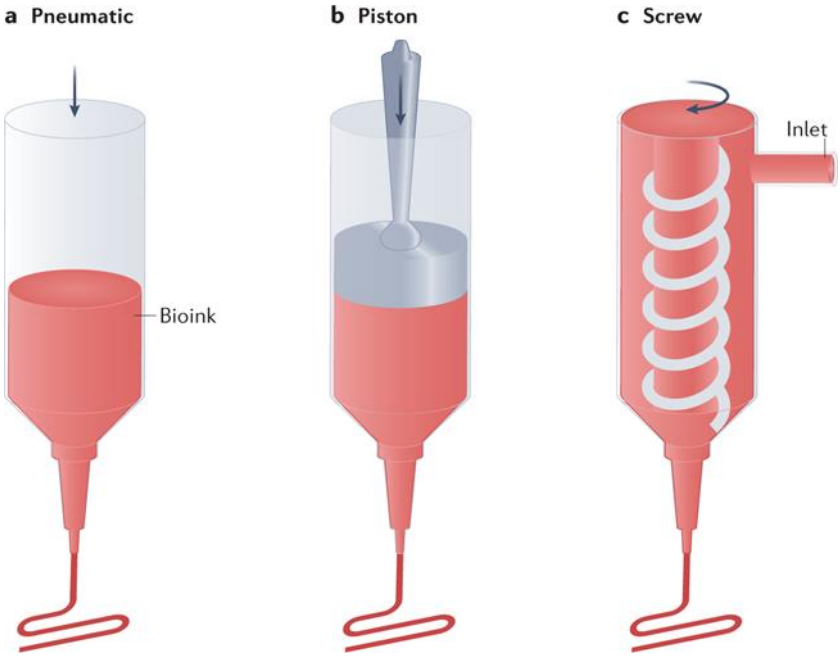

Figure 1.7 Types of extrusion-based bioprinting [64].

1.3.3.1 Printing Parameters in 3D Extrusion Printing

For tissue engineering and biomedical applications, it is essential to determine the appropriate parameter combinations that allow various types of bioprinting applications. 3D bioprinting encompasses a wide array of adjustable device parameters, as represented in Figure 1.8 (a), offering it a dynamic process with numerous variables that can be

controlled to achieve desired outcomes in terms of mechanical and biological. These parameters affect their structural integrity, the surface's smoothness, and strut and pore dimensions (Figure 1.8 (b)) of the produced scaffolds.

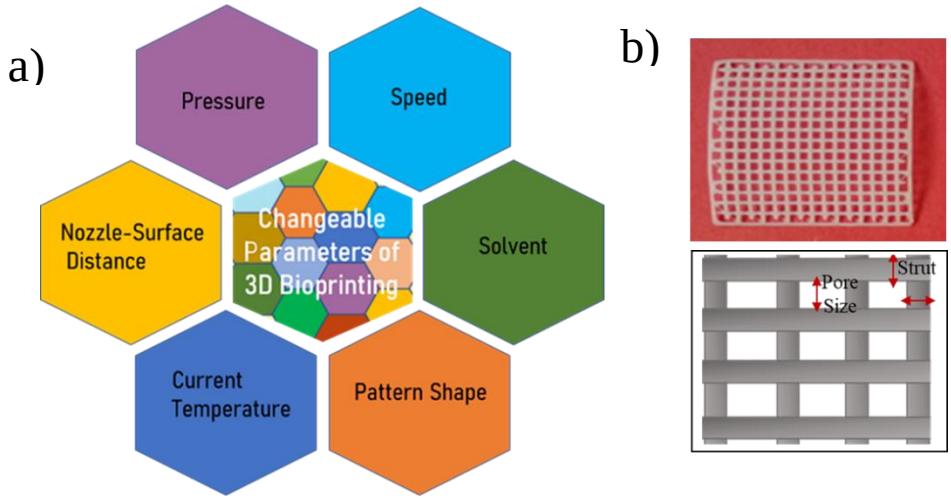

Figure 1.8 Changeable parameters on 3D Bioprinting during the printing process (a), representetive strut and pore size (b).

One of the most critical parameter affecting surface roughness is z-offset value. Z-offset value is the parameter that has a crucial impact on print quality in 3D printers and 3D bioprinters. This value represents the distance between the nozzle tip and the surface to be printed. As can be seen in Figure 1.9, the structure to be produced is directly affected by the increase or decrease in the z-offset value. As the distance decreases, it crushes the strut surface, or on the other hand, increasing distance causes deposits at the nozzle tip and nonhomogeneous struts [65-66].

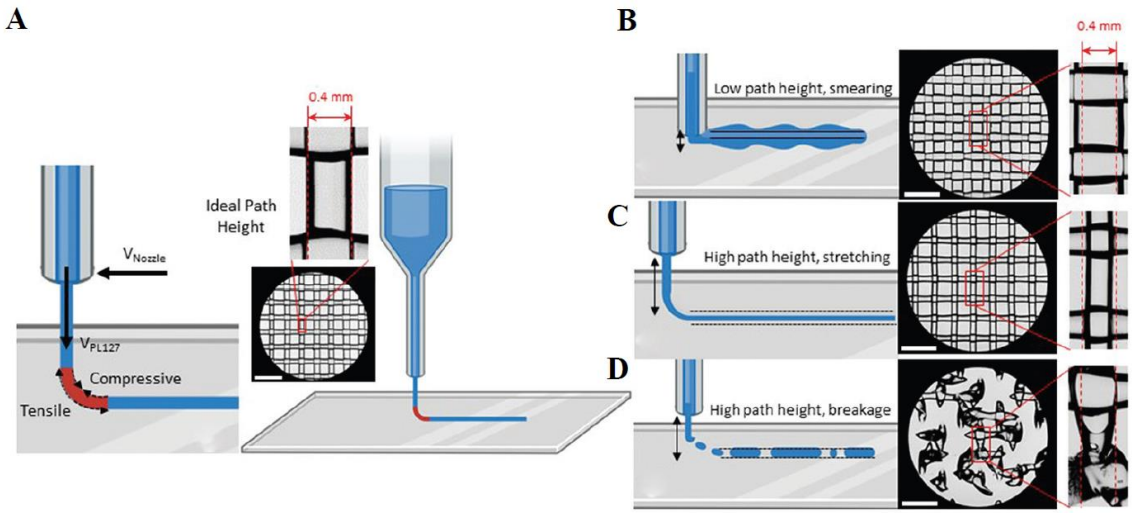

Figure 1.9 Representation of nozzle-to-surface height. (A) optimum height (B) height less than optimum (C) height leading to thinning lines (D) height resulting in breakage. The correct line width represented by your dashed line solid line width [67].

Strut size determine used nozzles and needles which can have different diameters with a variety of types (Figure 1.10). Choosing the appropriate nozzle or needle for applications is very important for printing process. Their geometry and the print length affect the shear stress. Especially in experiments with cells, the needle structure directly affects cell viability which can vary between 40% and 90%. The viability of the cells will decrease as the needle diameter decreases because higher pressures are required for decreasing needle diameter. In addition, narrow-diameter nozzle or needle in printing processes take longer than large-diameter nozzle or needle tips. Nozzles have larger diameters than needles. With this feature, they need a faster flow rate than needles. In addition, cells are more damaged with this feature. For this reason, the nozzle is more preferable in high-viscosity studies. Their diameters affect the diameter of the struts formed ; that is, they determine the pore size and porosity, which is key factor for tissue engineering applications[68-69]. Additionaly, Ozbolat defined that the nozzle diameter should be equal to the distance between the surface and the nozzle(z-offset value).

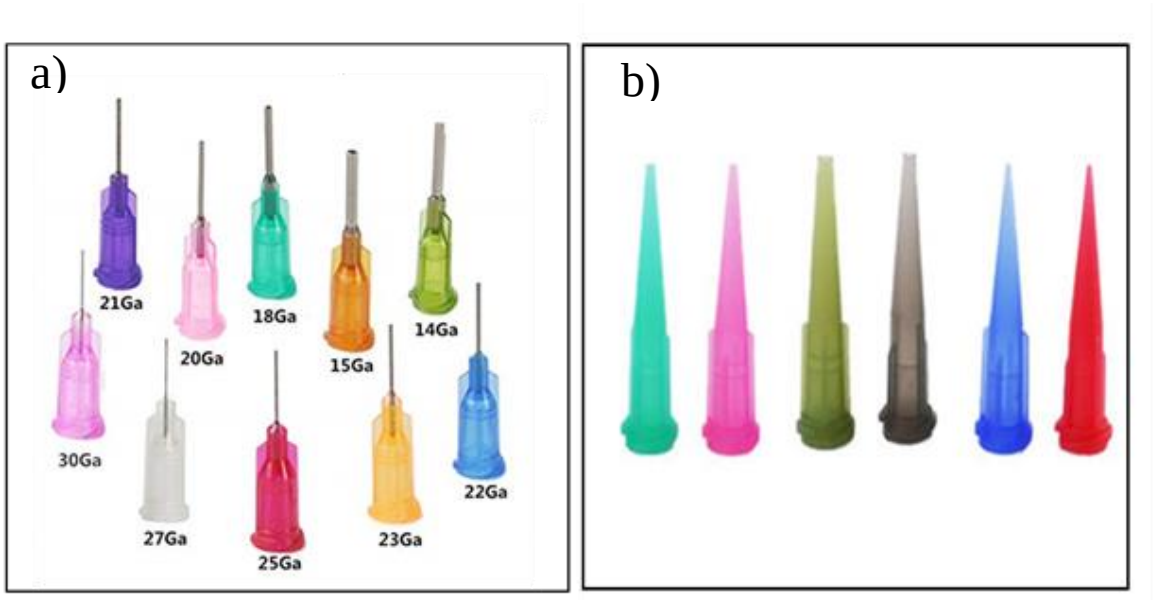

Figure 1.10 Needle and nozzle types used in EBB. (a) the types of needles, (b) dispensing nozzle.

Another significant parameters is infill density which determines the fill rate of the interior of the geometry to be printed. In the slicer programme (Repetitier Host), the geometry is defined with a infill rate between 0 and 100. The pore diameter, number of struts and weight of the part change with the infill ratio. As the infill density increases, the duration of the print increases. Increasing infill density affects the mechanical properties of the material sush as flexibility and stiffness. One of the remarkably advantages of 3D Bioprinting is the achievement of homogeneous and arrangeable pore structures. The infill density is a parameter used to adjust the desired pore diameters. As representative in Figure 1.11, as the infill density rate increases, the number of struts in the scaffold increases and pore size decreases[70-71].

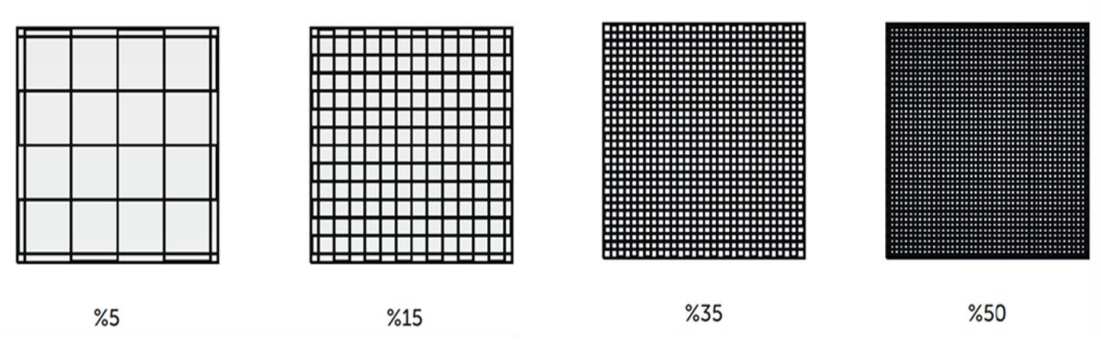

Figure 1.11 Representative images of different infill density rates.

1.4 Natural Polymers and Synthetic Polymers

Biomaterials are the main requirement for fabricating scaffolds in tissue engineering. Natural polymers have significant advantages compared to synthetic polymers for tissue engineering due to their similarity with ECM, biodegradation, and high biocompatibility. Natural polymers commonly studied for tissue engineering include proteins such as gelatin, collagens, and silk fibroin and polysaccharides like chitosan, alginate, and hyaluronic acid as shown in Figure 1.12 [72]. Since natural polymers are a part of the biological structure, they provide suitable conditions for cells.

Collagen is the most abundant protein in the human body and there are over 29 types of collagen, with type I being the most prevalent in bone tissue and type II in cartilage. Marine-derived collagen has also received attention as a cheaper alternative to mammalian collagen, which is easily extractable from marine waste residues [73]. Gelatin is a soluble protein derived from animal collagen through enzyme proccessing. Gelatin has elastic properties, lower antigenicity, excellent cell adhesion and accessible functional

parts for chemical modification [74]. It can effectively blend with natural and sythetic polymers to enchance bio-affinity and mechanical properties. Nanofibrous scaffolds made of gelatin are primarly used in large bone defect repair [75]. However, they have poor mechanical properties and a high degradation time for that need some modifications to eliminate these problem. Crosslinking and chemical modifications are often used to control the stiffness and structure of the scaffolds. Additionally, natural polymers are origin from natural sources, they are more difficult to produce easily and serially, unlike synthetic polymers. On the other hand, the mechanical properties, molecular weights, and physical forms of synthetic polymers can be easily manipulated. Synthetic polymers have the high strength and stiffness needed for tissue engineering due to their abbility to self-reinforce. However, most synthetic materials are poor in terms of cell adhesion. In order to reduce this effect, synthetic polymers are combined with bioceramics and natural polymers as opposed to their individual use to show a reduced inflammatory resonse [76].

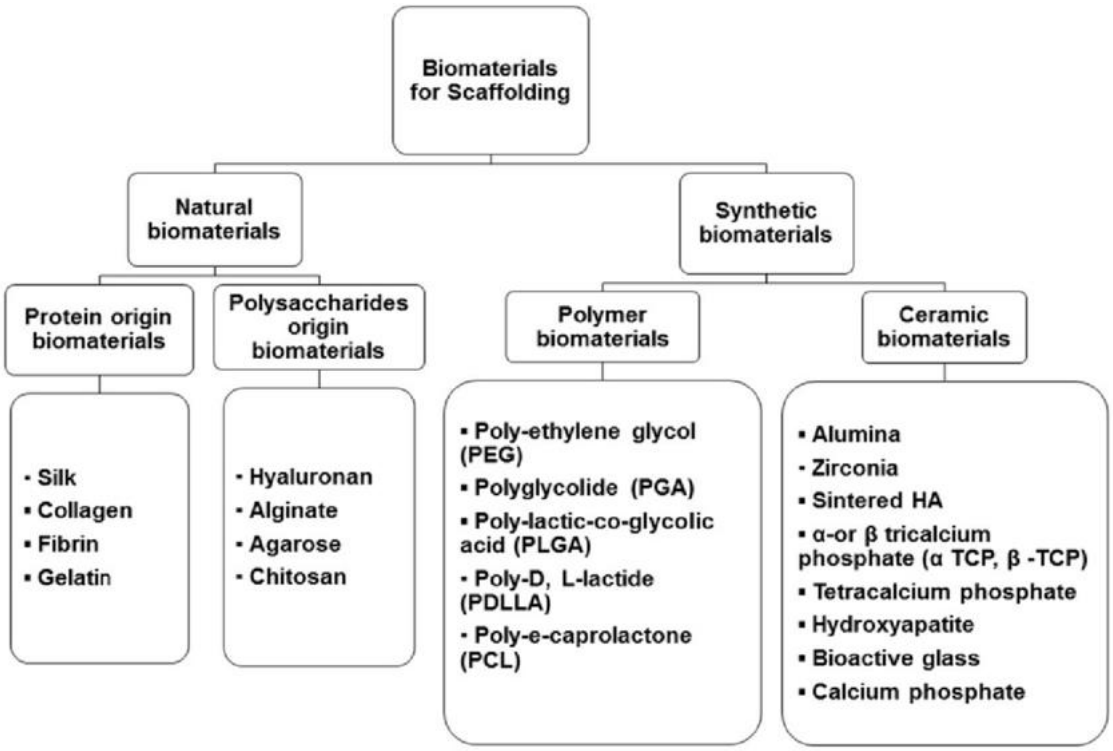

Figure 1.12 Biomaterials for scaffolding fabrications in tissue engineering [72].

Many of the synthetic polymers, including poly-l-lactic acid (PLLA), PCL, polyglycolic acid (PGA), polyethylene glycol (PEG), and poly-dl-lactic-co-glycolic acid (PLGA), are used due to their strong mechanical properties, controllable degradation

time, biocompatibility to support or repair damaged or diseased tissues. They show better mechanical properties than natural polymers. In addition, the mechanical properties of the polymer vary according to the molecular weight, their chain sequence and structure, degree of polymerization, and the proportions of the crystalline and amorphous regions [77]. Compared to natural polymers, they have more important advantages than ease of synthesis and use. However, cell adhesion rates are very low compared to natural polymers. For this reason, cell affinity is generally improved by mixing with natural polymers or by chemical modifications.

1.4.1 Polycaprolactone

Polycaprolactone (PCL) is a biocompatible, bioabsorbable, and non-toxic synthetic polymer approved by the U.S. Food and Drug Administration (FDA). It has been frequently preferred in tissue engineering and biomedical fields. PCL is biodegradable polyester belonging to the member of aliphatic polyester. It is an aliphatic semi-crystalline polymer with a glass transition temperature of -60°C and a melting temperature of 60°C. Its melting point provides easy-to-handle manufacturing, so it is used frequently with 3D printers [78]. Degradation occurs by hydrolysis of the aliphatic ester bond under physiological conditions, as explained in Figure 1.13. Degradation time is longer than other polyesters because it has repetitive –CH2 groups. It has been preferred in drug releases and implant applications due to its long biodegradation period (2-3 years). Scaffolds produced with PCL are resistant to erosion. Also, PCL can be easily blended with many polymers and bioactive particles. When used with a natural polymer, biodegradation times vary between 2-4 months.

Thanks to its viscoelastic properties, it is easy to use with many tissue production techniques, and thus nano and micro-scale structures are produced. PCL is frequently preferred in a variety of medical application areas, including medical implants, polymeric membranes for tissue engineering applications such as skin tissue cartilage tissue, and cardiovascular tissue engineering, has a high effect on bone regeneration and neural generation, wound dressing, and surgical sutures [79-80]. In addition, it can be widely used in studies in which prolonging release is needed due to its high control, encouraging encapsulation, and high bioavailability. PCL, which has good mechanical properties, has been used in several tissue engineering applications or in a variety of studies blending with other polymers and bioactive particles [81]. Merceron et al. used a multi-head system

on a 3D printer to create supporting structures for cells using PCL and PU polymers. Cell viability and elasticity were examined by filling the bioink consisting of hyaluronic acid, gelatin, and fibrinogen into the created frame and it was stated that the results were in accordance with the natural muscle-tendon structures [82].

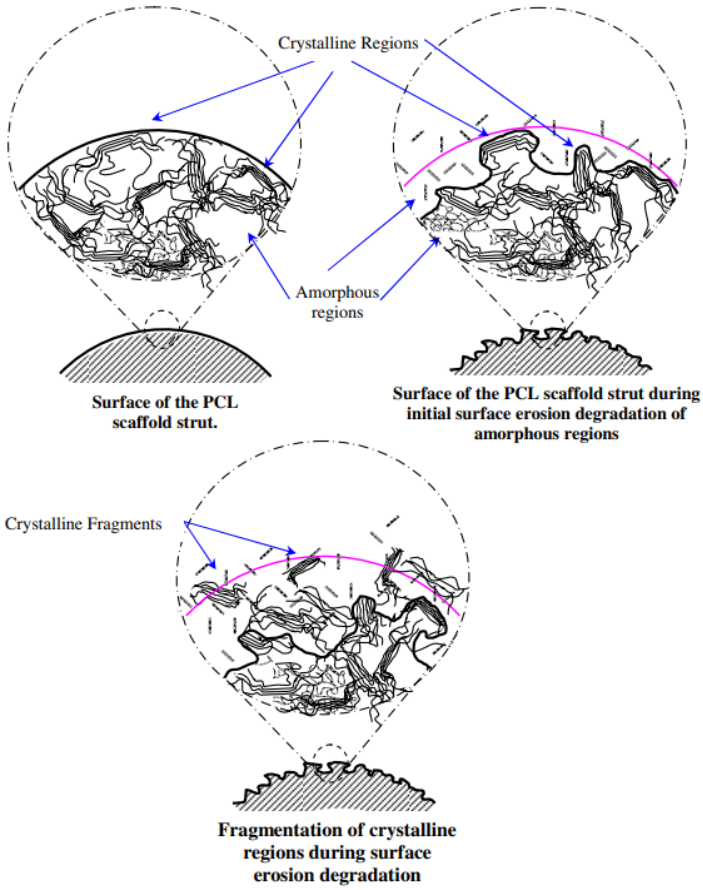

Figure 1.13 Visual diagram of degradation of PCL by organisms or under physiological conditions [83].

Recently developed EBB has been used with PCL to fabricate scaffolds for many tissues engineering fields. Dalya et al. created a structure consisting of PCL and bioink using a 3D bioprinter to increase endochondral bone formation, and therefore scaffold's stiffness was significantly increased with respect to without PCL [84]. Pati et al. synthesized PCL-PEG-PCL triple-block polymer to make a suitable hydrogel for bioprinting [85]. PCL was used to increase the crystallinity of the hydrogel as PEG showed poor mechanical properties. Shim et al. fabricated a construct for osteochondral tissue with alginate hydrogel and PCL, which was used as a framework to enhance mechanical behavior and increase strength [86]. Lee et al. printed hybrid scaffolds

consisting of cells (MC3T3-E1) for tissue regeneration. In their study, they used alginate for encapsulation of the cells and PCL to improve the elastic modulus of the structure [87]. Cantu et al. fabricated using GelMA and PCL to create scaffolds for nasal reconstructive surgeries. PCL formed a framework for chondrocyte-loaded GelMA hydrogel to provide better printing accuracy and provide structural support for the final structure. In addition, their study revealed that the Young's Modulus of the GelMA/PCL scaffold improved up to 37 times over GelMA [88], [89]. In another study, Koziol et al. used various polymers and bioactive particles for their layers to form osteochondral tissue with a heterogeneous multi-layered structure composed of both articular cartilage and subchondral bone. Previous studies generated PCL construct because it has osteogenic potential and load-bearing capabilities for subchondral bone [89]. Yu et al. developed a scaffold bipartite scaffold with PCL/Alginate for repairing osteochondral defects [90]. Park et al. formed artificial trachea with printed alginate hydrogels and PCL to generate elasticity and strength matchable native trachea. PCL was used to create an appropriate mechanical response during breathing to overcome variable pressure [10-91].

1.5 Mechanical Properties of Tissues

In tissue engineering, the mechanical properties of scaffolds play a crucial role in determining the success of tissue reconstruction. Different tissues in the human body have varying mechanical properties, such as stiffness, elasticity, and strength, which need to be considered when designing scaffolds. Stiffness is one of the most important properties of a material and is defined as the ratio of the applied load to the deformation that occurs in the material. The deformation rate that occurs when a structure is subjected to a load provides information about the rigidity of the structure.To fabricate scaffolds for tissue engineering applications, it is essential to have a complete understanding of the mechanical properties of living tissues. These properties can vary significantly among different tissue types, such as hard and soft tissues. Soft tissues, such as skin and cartilage, have lower stiffness and tensile strength than hard tissues like bone. Therefore, the load ratios to which soft and hard tissues are exposed differ significantly from each other [68].

To evaluate the mechanical properties of scaffolds, tensile and compression tests are commonly performed. The outputs obtained from these tests can help define the mechanical properties required for tissue reconstruction, such as the tensile strength,

Young's modulus, and elongation at break values. These values can vary depending on the specific application area, and the scaffold's design should be made accordingly to match the elastic properties and strength of the tissue and ensure successful tissue interaction. For example, the tensile strength of the skin is in the range of 5.0-30.0 MPa, the Young's Modulus in the range of 4.6-20.0 MPa, and the elongation at break values approximately between 35.0-115.0% [10-92]. Understanding the mechanical properties of living tissues is essential for designing scaffolds for tissue engineering applications. By considering factors such as stiffness, elasticity, and strength, scaffolds can be fabricated to match the specific mechanical properties of the target tissue and ensure successful tissue reconstruction. Guimaraes et al. identified detailed result of tissue stiffness of various tissue types as shown in Figure 1.14 Elastic modulus of tissues and Table 1.1

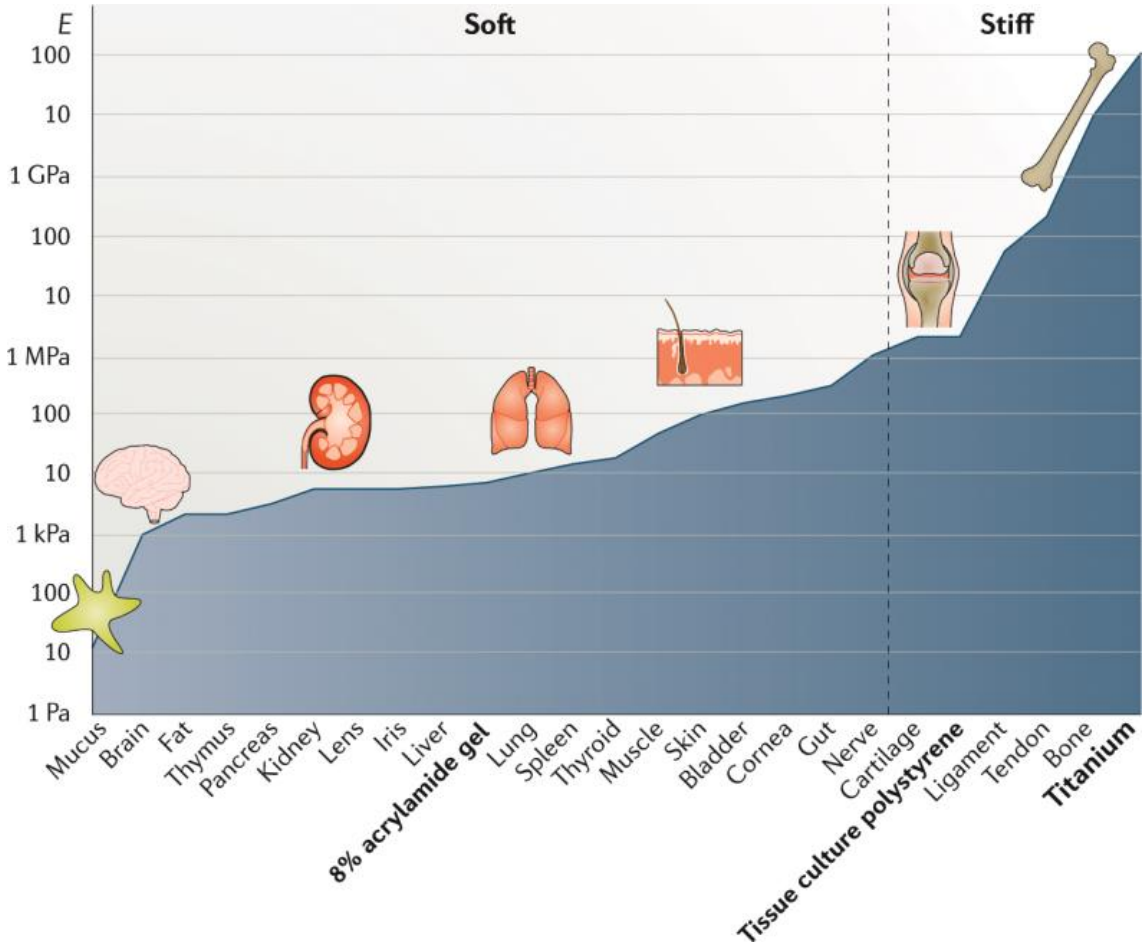

Figure 1.14 Elastic modulus of tissues [93].

To improve mechanical properties, several approaches can be used. One approach is to crosslink natural polymers, which involves chemically bonding the polymer chains

to increase their strength and stability. Another approach is to add bioactive particles, such as ceramics or metallic nanoparticles, which can improve the mechanical properties of the scaffold and enhance its biological functionality. Additionally, synthetic polymers can be used to form scaffolds that have specific mechanical properties and can be tailored to meet the needs of different tissues [94]. From another aspect, the mechanical properties of scaffolds can be affected by various factors during the fabrication process, such as the type and concentration of the biomaterials used, the porosity and pore size of the scaffold, and the fabrication technique employed. For instance, achieving homogeneity in porosity is crucial for obtaining consistent mechanical properties and optimal tissue regeneration.

Table 1.1 The elastic modulus of living tissues [93].

Tissue	**Elastic Modulus**
Nervous Tissue	
Brain (pig)	3.1 kPa (up to 6.5 kPa)
Spinal cord (human)	1.23 MPa
Sciatic nerve (mouse)	7 MPa
Sciatic nerve (rat)	0.5–4.0 MPa
Sciatic nerve (rabbit)	2 MPa[a]
Ulnar nerve (human)	5 MPa[a]
Connective Tissue	
Tibial trabecular bone (human)	10.4 Gpa
Tibial cortical bone (human)	18.6 Gpa
Articular cartilage (cow)	1.06 MPa
Articular cartilage (sheep)	5.0–12.9 MPa
Adipose tissue (human)	1.6–2.9 kPa
Plantaris tendon (mouse)	100–200 MPa
Ligaments (human)	25–93 MPa
Muscle	
Smooth muscle — blood vessels (human)	30–100 kPa
Smooth muscle — aortic rings (rat)	10–23 kPa
Cardiac muscle (rat, cow)	30–145 kPa
Cardiac muscle (human)	5–50 kPa
Cardiac muscle (pig)	110 kPa
Skeletal muscle (rat)	20 kPa single fibres; 200 kPa bundles
Skeletal muscle (mouse)	15–150 kPa
Skeletal muscle (pig)	Up to 800 kPa
Endothelial and epithelial tissues	
Skin (bat wing)	131 kPa

Skin dermis (pig)	50–150 kPa
Intestine (rat)	350 kPa
Small intestine (guinea pig)	430–441 kPa
Intestine (pig)	300–700 kPa
Viscera	
Bladder (pig)	200–320 kPa
Eye	
Cornea (pig)	0.23–2.89 MPa
Lens capsule (human)	2.3–3.3 MPa
Iris dilator (cow)	27 kPa
Iris (pig)	4–6 kPa

[a]Derived from the curves (that is, values were not directly reported by the authors).

1.5.1 Mechanical Properties Definition

Tensile testing is a destructive sample testing technique that gives information about the tensile strength, yield strength, and ductility of materials against a force. It gives information about the force required for the materials to break or fail and the change in the material structure while applying this force. Also, the tensile test gives information about the elongation of the material under force. Therefore, the tensile test is one of the most basic tests to characterize the behavior of materials. While performing the tensile test, the sample is fixed from two ends to the area called "grips" on the device. In a uniaxial tensile test, the specimen is fixed at one end, and force is applied at the other end. The amount of force versus elongation is obtained as a graph. The length and cross-sectional area of the placed sample are known, and other critical mechanical properties are calculated from the obtained data from the device [95]. Stress is defined as the force per unit area of the material required for elastic and permanent deformation of the externally applied force on the material.

Stress is given by the following formula in equation 1.1:

$$\sigma = FA \ (N/m^2) \qquad (1.1)$$

where σ is the stress applied, F is the force applied, and A is the area of the force application.

Two different stresses can be applied to the material: tensile stress and compressive stress. The tensile stress gives the force per unit of the material when the material is

exposed to an external force in a specific direction. Compressive stress is the force that causes material deformation by compressing the material and reducing its volume.

Strain gives information about the change in the dimensions of the material depending on the deformation in the direction of the applied force. It is also expressed as the initial length ratio of the change in length, as expressed in the equation 1.2 and 1.3.

$$\varepsilon = \Delta L / L_0 \quad (1.2)$$

$$\Delta L = L - L_0 \quad (1.3)$$

ε is the strain due to the applied stress, ΔL is the difference value between the final length and the initial length which presented as L0. Strain is a unitless value.

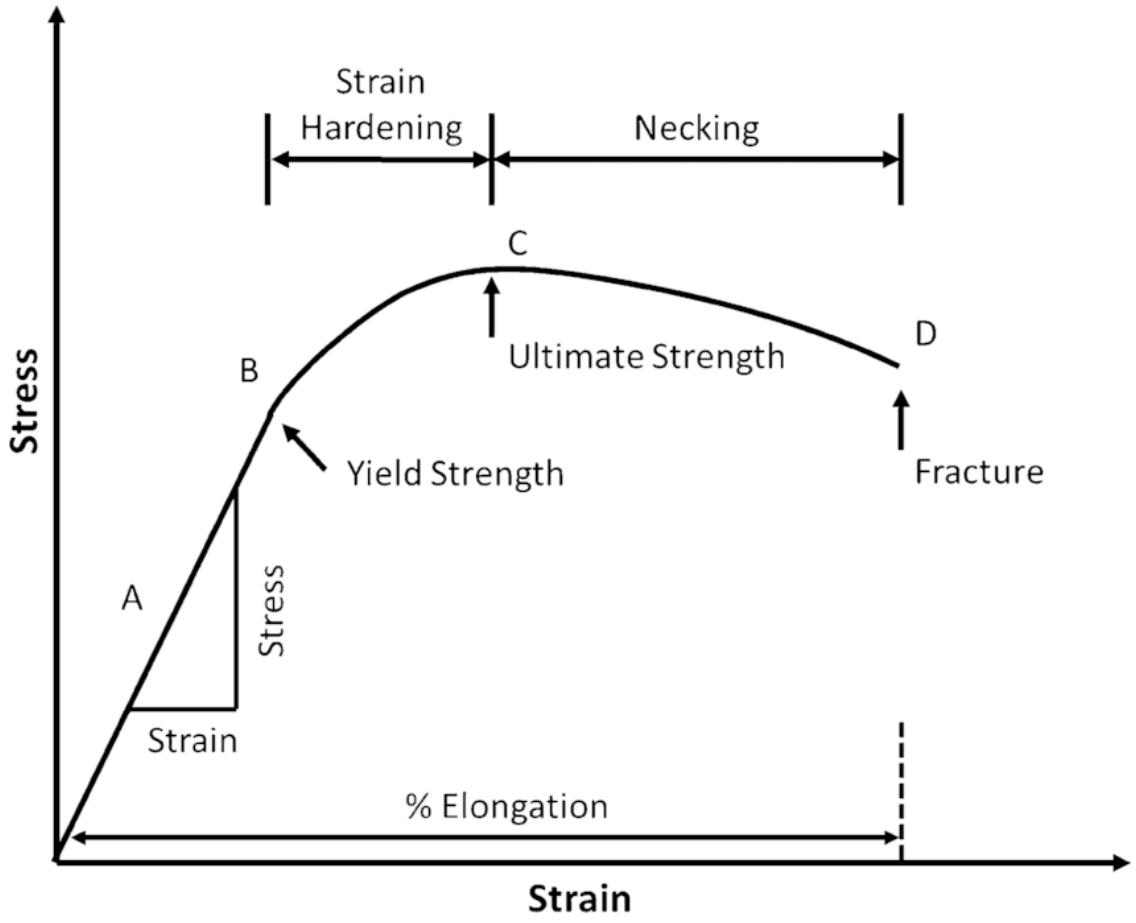

Figure 1.15 Stress-strain curve [96].

The strength of materials is defined as the ability to resist external forces applied to the materia without bending or breaking. Polymers, metals, and ceramics shown different strengths. Figure 1.15 shows the relationship between stress and strain. Important

parameters can be calculated for some materials using the curve obtained during uniaxial tensile test. The maximum stress that a materials can withstand under the force is defined as the ultimate tensile strength (UTS) (point C). The elastic region indicates that the material returns to its original shape without deformation when freed from the force effect. The plastic region, on the other hand, has undergone irreversible deterioration due to the force acting the materials. After the material exceeds the UTS, the neck begins to form in the materials. Young's modulus is calculated by the stress and slope at the linear point of the stress (point A). It constitutes a very essential for tissue engineering applications. The elastic limit indicated the ability of the material to withstand loads without breaking down. As the force continues to be applied, the material exhibits rupture or fracture behavior as at the D point.

1.5.2 Mechanical Properties of Semicrystalline Polymers

Semi-crystalline polymers consist of both tightly packed crystalline regions and randomly aligned amorphous regions. The crystal regions are formed by regularly aligned molecules that fold into spherical lamellae called spherulites [97]. The density of these crystal regions determines the overall crystallinity of the polymer, which can range from 10% to 80%. The amorphous regions of the polymer are structures that are randomly aligned between the crystal regions. These regions contain four different types of molecules: free-ended chains, loops, tie molecules (bridging), and floating molecules as presented in Figure 1.16 [98]. These complex structures are not fully understood, but ongoing studies have studied to shed more light on their distribution and how it affects the mechanical properties of the polymer. The mechanical properties of the polymer are influenced by a variety of factors, including the distribution of the crystal and amorphous regions, molecular weight, molecular orientations, molecular mass distribution, cross-linking, and temperature. Additionally, the recrystallization of dissolved polymers with the help of a solvent is also related to the distribution of these regions as the solvent is removed. Overall, understanding the complex structure of semicrystalline polymers and how it affects their mechanical properties is important for various applications, such as in the development of advanced materials and medical devices. Although the literature has not been able to fully explain their complex structures, studies are continuing to shed light on this area [98]. The distribution of these structures changes the mechanical properties of the polymer. In addition, the recrystallization of the dissolved polymer with the help of a solvent is related to the distribution of these regions as the solvent is removed [99].

At the same time, factors such as molecular weight, molecular orientations, molecular mass distribution, cross-linking, and temperature affect the mechanical properties of the polymer [100].

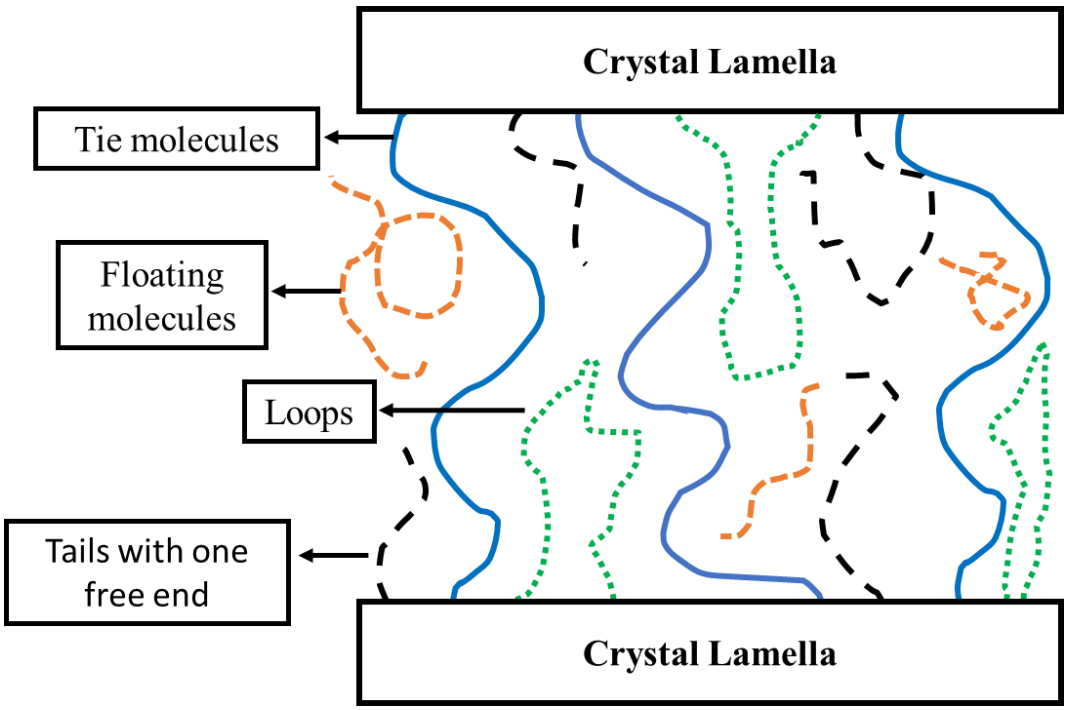

Figure 1.16 Structure of semicrystalline polymers [101], [102].

In the tensile test, the molecules in the amorphous regions form cavities perpendicular to the force direction, and this point where these cavities begin to form gives the yield stress value as seen in Figure 1.17. As the force continues to be applied, the stress between the nanocavities increases and forms microcavities. Since the formation of cavitations takes place in amorphous regions, it gives information about tie molecules and the distribution of molecules in other amorphous regions. The cavities coalesce, reducing the void volume and inactivating the tie molecules [101-102].

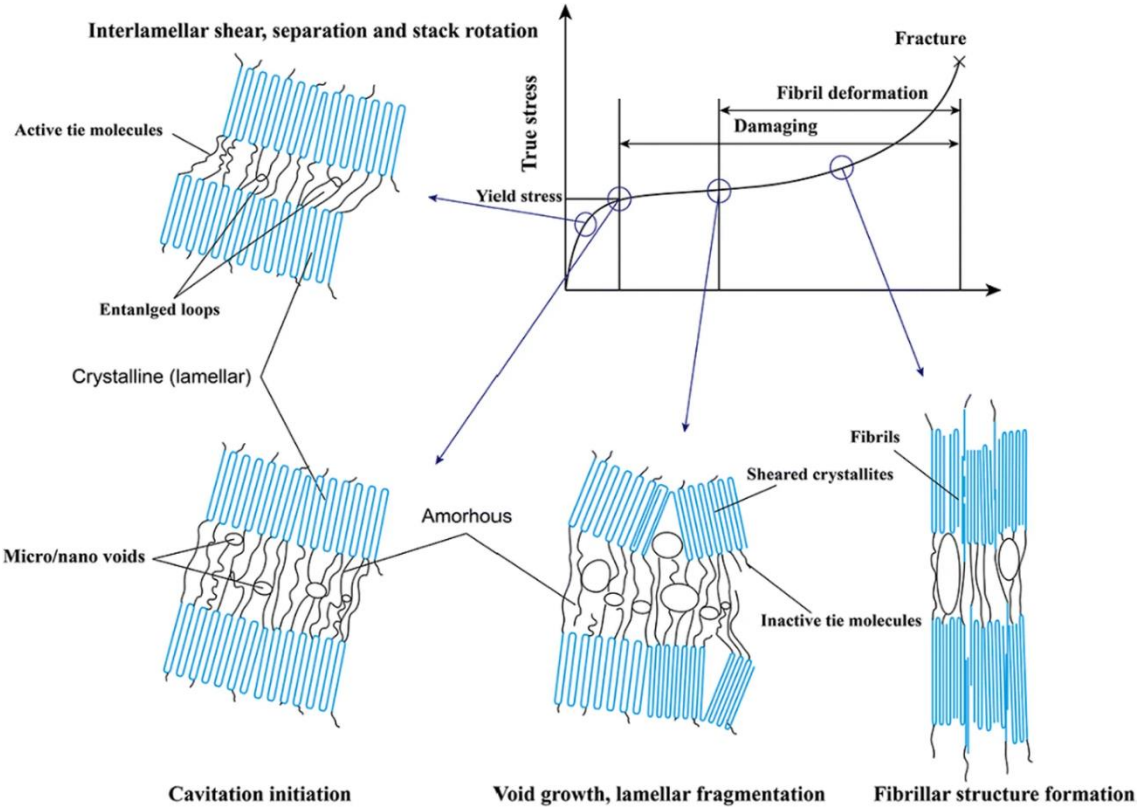

Figure 1.17 Deformation of semicrytalline polymers during uniaxixal tensile test [103].

Chapter 2

Materials And Methods

2.1 Materials

PCL (average Mn=80,000; CAS No. 24980-41-4), which is formed of 3 mm pellets, was purchased from Sigma–Aldrich (St. Louis, MO, USA) purchased from Sigma-Aldrich (St. Louis, MO, USA). Chloroform (CF) (CAS No. 102445.2500) and acedic acid (AA) (CAS No. 200-580-7) were purchased from Merk and dichloromethane (DCM) (CAS No. 75-09-2) were purchased from Sigma–Aldrich. A cartridge syringe of 3 ml volume (CONS-C-001) and a nozzle diameter of 0.41 mm (CONS-CBT-22G) were purchased from Axolotl Biosystems (Istanbul, Turkey).

2.2 Methods

2.2.1 Fabrication of PCL Scaffolds

In this study, to obtain homogeneous polymer solutions from PCL pellets were dissolved in CF, DCM and AA stirred at 50°C for 5 h, at 30°C for 5 h, at 60 °C for 6 h respectively (Figure 2.1). After the solutions were loaded into syringes, they were centrifuged at 2000 rpm for 2 minutes to eliminate air bubbles which are a limiting factor in the printing process.

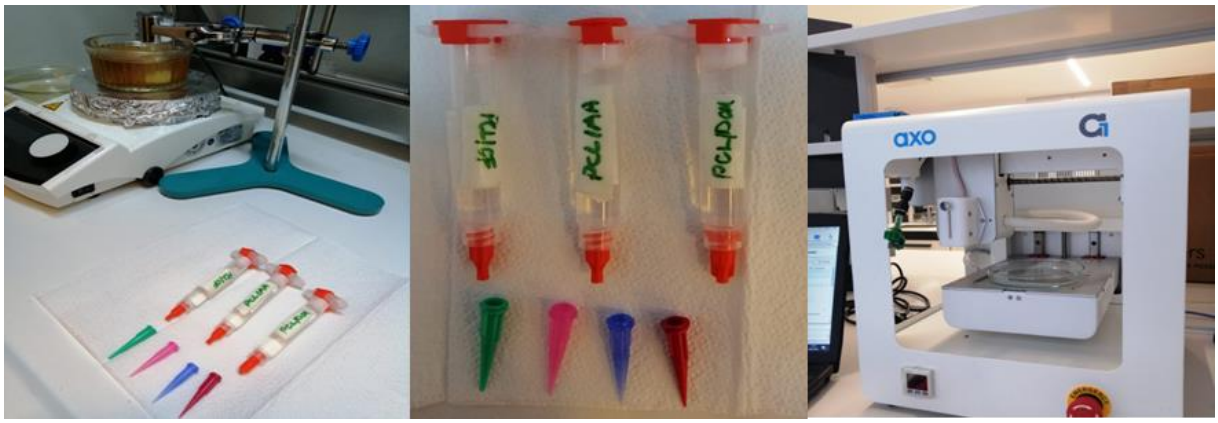

Figure 2.1 Experimental processes.

PCL scaffolds in a grid structure (height: 20 mm, length: 20 mm) were printed using an extrusion-based bioprinter (EBB) (Axolotl Biosystems, Istanbul, Turkey) as presented in Figure 2.2. The grid structure was designed with computer-aided design software (SOLIDWORKS, Waltham, MA, USA). The designed structure was converted into a ". stl" file using the Repetier Host program, which is provided by slicing 3D structures into 2D layers [104].

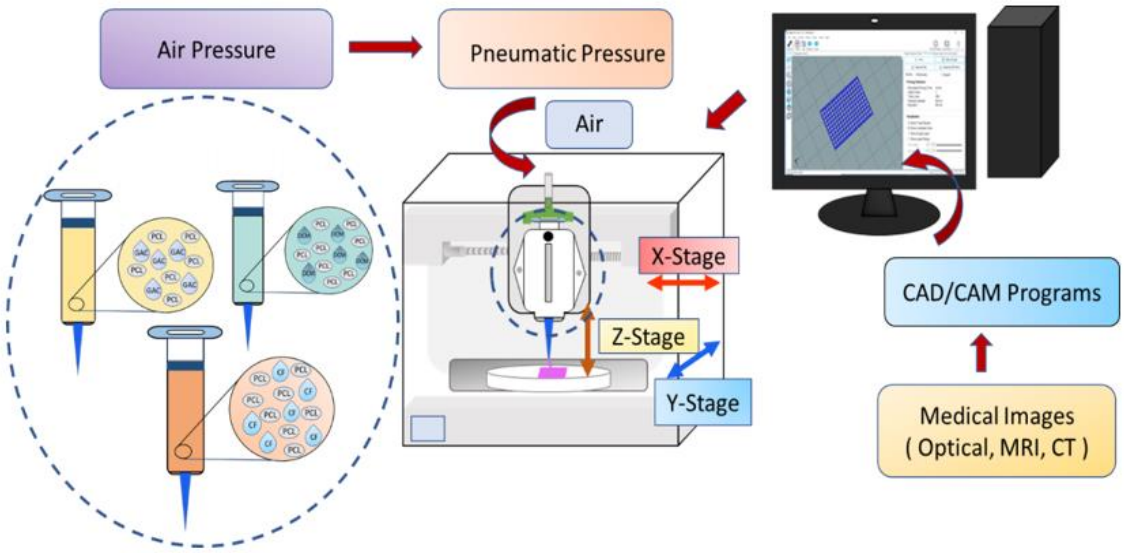

Figure 2.2 Representative image of a solution extrusion-based three-dimensional (3D) Bioprinter.

Solutions were prepared at 10%, 25%, 50%, and 75% concentrations to investigate the effect of viscosity on printability and mechanical behavior. To determine the printability of the solutions prepared at 10%, 25%, 50% and 75% polymer concentrations, z-offset values, nozzle size, pressure, speed and fill rates were evaluated. As seen in

Figure 2.3, 18 Gauge (G), 20 G, 22 G and 25 G nozzles were used. Z offset values of 0.2, 0.4, 0.6 and 0.8 mm were selected. All scaffolds are manufactured with 90° orientation.

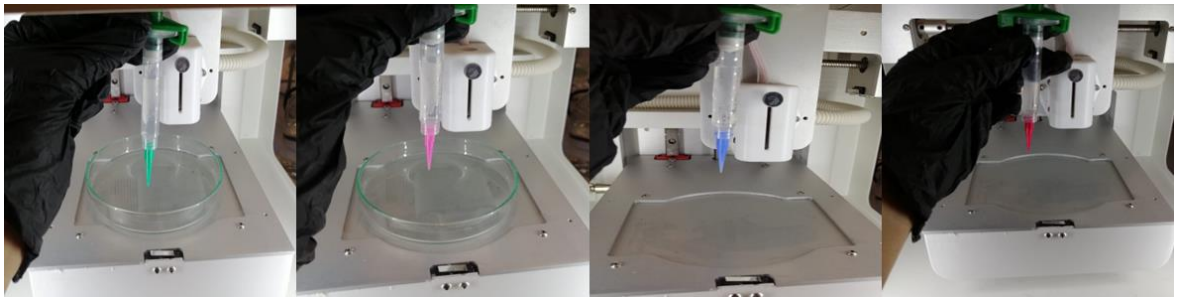

Figure 2.3 Investigation nozzles with different polymer concentration. (18G (green), 20G (pink), 22G (blue) and 25G (red)).

2.2.1.1 Evaluation of Solvent

To investigate the effect of solvent, DCM, AA, and CF solvents were used in the procedure. Scaffolds printed in 10%, 25%, 50% and 75% concentration with PCL dissolved with AA, DCM and CF were named PCL_AA, PCL_DCM and PCL_CF respectively. The effect of the solvent on printed structure was evaluated with a variety of pressure, speed and infill density parameter given below data (Figure 2.4).

2.2.1.2 Evaluation of Printing Speed

In order to investigate the effect of printing pressure on printability and mechanical properties, solutions were pressed at different speeds. 10% and 25% polymer concentrations were increased by increasing the speed of 5 mm/s in the speed range of 1-80 mm/s. 75% polymer concentration was printed by increasing the speed of 1 mm/s in the 1-10 mm/s speed range.

5 mm/s, 10 mm/s and 15 mm/s values were selected to evaluate the mechanical properties of the scaffolds printed with 50% PCL_CF and 50% PCL_DCM solutions. Solutions printed keeping constant pressure (480 kPa), infill density (50%), nozzle type (22 G) and z-offset value (0.4 mm).

2.2.1.3 Evaluation of Printing Pressure

The printing pressure range of the our device is 1-480 kPa and scaffolds with 30 kPa intervals were produced in this range for 10%, 25%, 50% and 75% polymer concentration keeping constant infill density(50%), nozzle size(22 G) and z-offset value

(0.4 mm). Solutions prepared with 75% polymer concentration were produced only with a pressure of 480 kPa.

In order to perform mechanical analyses at 50% polymer concentration, 3 different pressure values were determined at 3 different writing speeds and for each speed value. These scaffolds were determined according to the minimum, medium and maximum printable pressure values. 172 kPa, 310 kPa and 480 kPa pressures were selected to examine the change of scaffolds produced at 5 mm/s speed with writing pressure. 206 kPa, 345 kPa and 480 kPa pressure values were determined to examine the pressure effects of the scaffolds printed at 10 mm/s speed. 310 kPa, 396 kPa and 480 kPa pressures were used to examine the pressure effect on the scaffolds printed at 15 mm/s speed.

2.2.1.4 Evaluation of Infill Density

Scaffolds in 10% and 25% polymer concentration were printed in 10%, 25% and 50% infill density.The scaffolds were produced by increasing the 50% and 75% polymer concentration by 10% and increasing the infill density from 20% to 100%.

In order to examine the effect of infill density on mechanical behavior, structures with 50%, 70% and 90% infill density were produced. Solutions of polymers formed at 50% and 75% concentrations were used. 310 kPa printing pressure and 5 mm/s printing speed were used at 50% concentration. In speed and pressure investigations, it was seen at 5mm/s this speed that, 310 kPa pressure can be utilized. To investigate the 75% concentration infill density effect, scaffolds were produced at printing pressure of 480 kPa and speed of 5 mm/s.

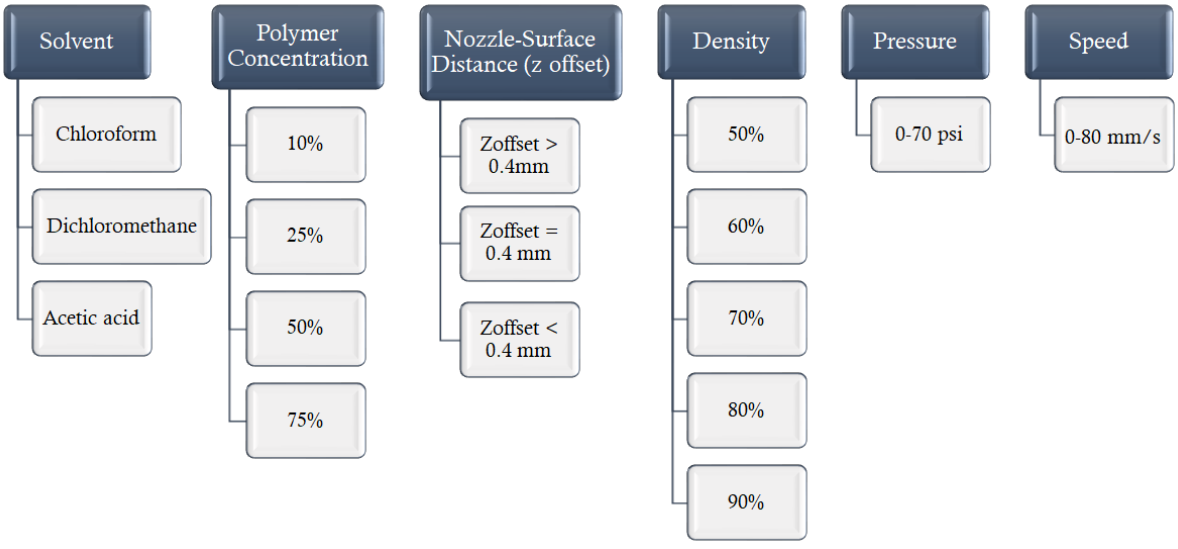

Figure 2.4 Diagram of investigated parameters throughout the experimental sets.

2.3. Morphological analysis

In this study, all scaffold's images were captured using a 20-megapixel camera positioned at a distance of approximately 20 centimeters from the subject which is proved to be a suitable distance for capturing images. Additionally, optical microscopy was employed to observe and analyze the morphology of printed samples in 25% concentration. A scanning electron microscope (SEM, ZEISS EVO LS10) was utilized for some scaffolds to evaluate their strut diameter, pore structures, microstructures, and detailed morphological analysis to identify effect of infill density and printing pressure. Before the SEM analysis, scaffolds were coated with a thin layer of gold (QUORUM, Q150R ES). The obtained SEM images were analyzed using ImageJ software.

2.4. Chemical analysis

A Fourier transform infrared spectroscopy (FT-IR) spectrum of the PCL scaffolds was assessed with a Nicolet 6700 spectrometer (Nicolet 6700, Thermo Scientific), wavelength 4000-400 cm^{-1}. FT-IR analysis was used to determine the interactions of molecules and functional groups in printed structures.

2.5. Mechanical testing

Uniaxixal tensile tests were performed to evaluate the mechanical properties of scaffolds formed by various combinations of process and device parameters. For each of the parameters, two specimens were manufactured with the dimension of 20mmx20mmx3mm. Each of the specimens were tested using a servo-hydraulic universal uniaxixal tensile testing machine Shimadzu AGS-X having a load capacity of 10 kN with a strain rate of 10^{-2} s^{-1} at room temperature.

The parameters to be examined for the mechanical test are selected, and these parameters are indicated in Figure 2.5. After testing the parameters on a variety of 3D Bioprinters, mechanical testing of saccolds was performed. As seen in the Figure 2.6, the mechanical properties of the scaffolds produced using different process parameters were

evaluated by the uniaxixal tensile test. The results obtained were compared with each other, and the process parmeters' effect on the structure was examined in detail.

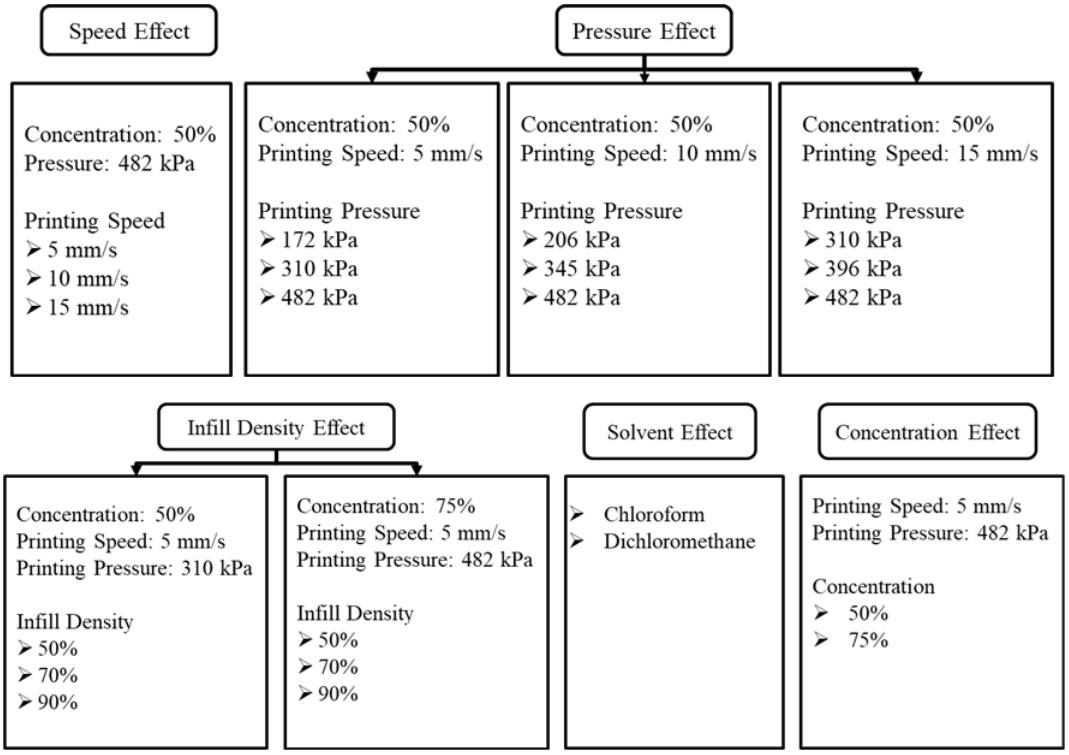

Figure 2.5 Diagram of investigated parameters throughout the experimental tensile test.

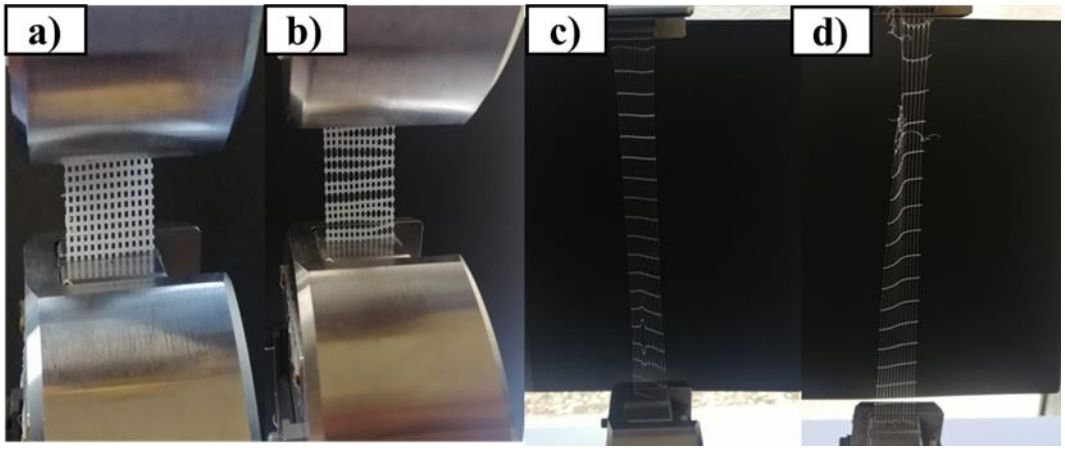

Figure 2.6 Tensile test of selected samples; (a) placing the sample between the jaws, (b) applying force in the z-axis direction, (c) deformation of the sample with elongation, (d) fracture of the samples.

Chapter 3

Results And Discussion

3.1. Morphological Evaluation of PCL Scaffolds

Solvents used in 3D bioprinting can have a direct impact on the morphological characteristics of printed structures, as observed through various imaging techniques such as optical microscopy, SEM, and camera imaging. Solvents can cause changes in the rheological properties of the bioink, leading to alterations in the shape, size, and surface features of the printed structures [105]. Therefore, it is important to carefully control the solvent composition and evaporation rate during bioprinting to ensure the desired morphological characteristics of the printed structures. During the printing process, the solvent will begin to evaporate from the bioink as it is deposited the layer. If the evaporation rate is too high, it can cause the bioink to dry out and become too viscous, making it difficult to print or resulting in poor print quality. On the other hand, if the evaporation rate is too low, the solvent may not evaporate quickly enough, leading to pooling or spreading of the bioink and distortion of the printed structure. Therefore, it is important to carefully control the rate of solvent evaporation during the bioprinting process to achieve the desired print quality and structure [106]. To ensure the mechanical stability and structural integrity of the printed scaffolds, the viscosity parameter was identified as the most crucial factor to consider prior to determining the process parameters. In the following sections, we will provide a detailed discussion of our findings and their implications for 3D bioprinting.

3.1.1 10% Polymer Concentration

High-resolution images were captured using a 20-megapixel camera in Figure 3.1. Analysis of the high-resolution images revealed that working with low concentrations of the bioink presented challenges in achieving the desired scaffold geometries. Despite

using high printing speeds, the fluidity of the bioink resulted in a lack of homogeneity in the printed structures, causing the struts to merge and disappear. As a result, the pore sizes were not clearly discernible, and the intended geometries could not be accurately reproduced. Therefore, this polymer concentration was not studied as it was not found suitable for the following parts of the study to characterize with the uniaxixal tensile test or SEM analysis.

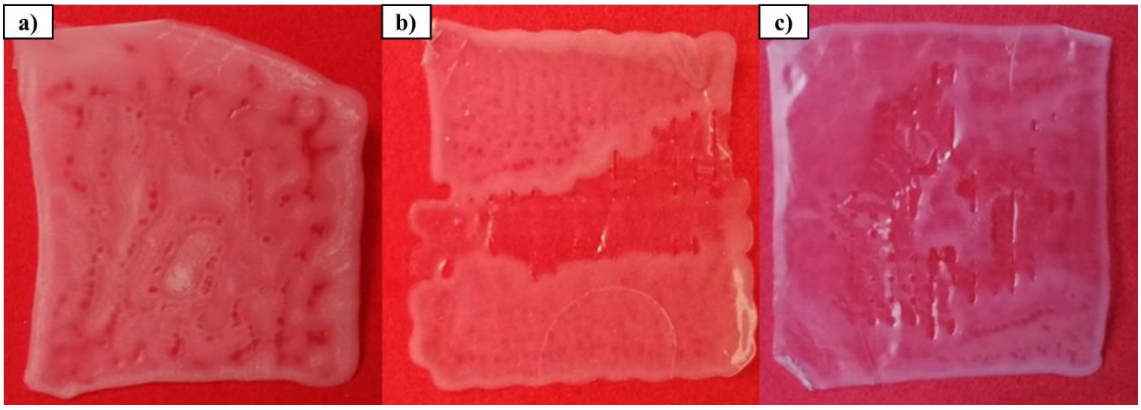

Figure 3.1 Scaffolds obtained from solutions prepared using AA, DCM, and CF using high printing speed (80 mm/s), respectively from a to c.

3.1.2 25% Polymer Concentration

Camera and optic microscope images were captured to describe the morphology of the scaffolds at 25% polymer concentration. According the images, 25% PCL solutions were found to be unsuitable for printability, even when high printing speeds were used, as evident from the results presented in Figure 3.2 and Figure 3.3. Among the scaffolds obtained across various experimental conditions, only a few exhibited open pore stuructures, as observed under an optical microscope in Figure 3.4. However, stabilizing the scaffold structure proved to be challenging, as the solvent evaporation time was excessively long [107]. As a result, this PCL concentration was deemed unsuitable for mechanical analysis based on the imaging results obtained.

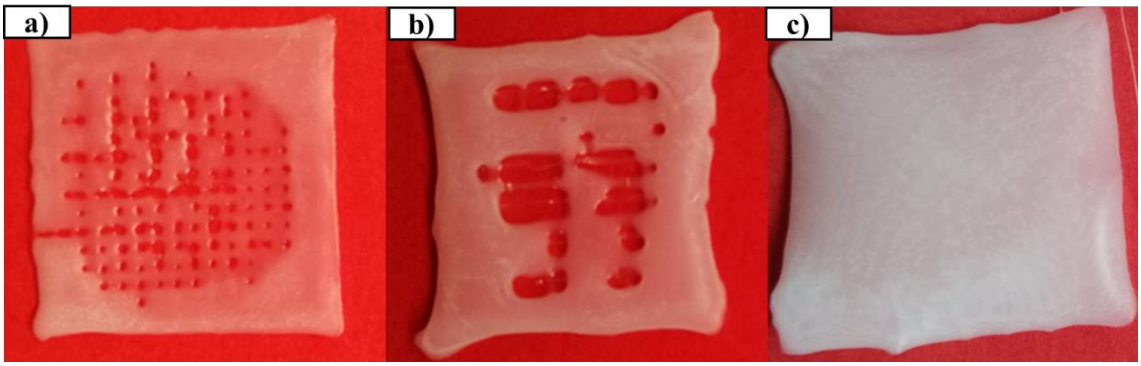

Figure 3.2 Scaffolds obtained at 65 kPa (a), 100 kPa (b) and 135 kPa (c) using the 80 mm/s printing speed of 25% PCL/DCM scaffolds.

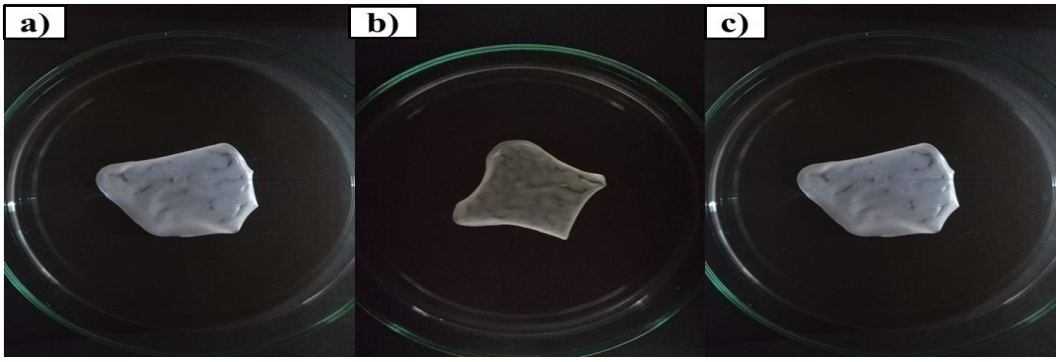

Figure 3.3 Scaffolds obtained at 65 kPa (a), 100 kPa (b) and 135 kPa (c) using the 80 mm/s printing speed of 25% PCL/AA scaffolds.

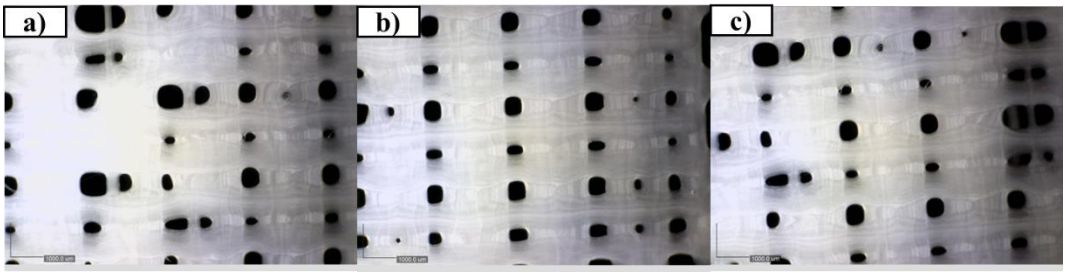

Figure 3.4 Optical microscope images of scaffolds printed at different speed with 65 kPa.

3.1.3 50% Polymer Concentration

In order to evaluate the printability of scaffold samples at 50% polymer concentration, we conducted an analysis using camera, optic microscopy images and SEM techniques. We also investigated whether there were any changes in the morphological properties of the scaffolds when adjusting printing parameters such as

pressure, speed, and infill density ratio. In our experiments involving AA solvent, we were unable to achieve the desired grid structure as shown in Figure 3.5 and Figure 3.6. One of its notable properties is its high boiling point, which is attributed to its strong intermolecular hydrogen bonding. The boiling point of acetic acid is 118.1 °C at standard atmospheric pressure, which is considerably higher than other organic compounds of similar molecular weight [108]. Furthermore, acetic acid has been observed to exhibit low volatility, meaning that it has a tendency to resist evaporation at room temperature. This behavior is due to intermolecular hydrogen bonding, which creates strong cohesive forces between acetic acid molecules, making it difficult for them to escape into the gas phase [109]. This caused a loss of structural integrity, leading to the merging of pores, as observed in Figure 3.6. The molecular structure and bonding of PCL material are influenced by the type of solvent used [110]. A detailed investigation of the effects of solvents on printed structures is presented in the Section 3.3.5.

PCL_CF and PCL_DCM scaffolds, as illustrated in Figures 3.8 and 3.10, scaffolds printed at a speed of 5 mm/s within the range of 172-480 kPa exhibited favorable morphological structure without any rupture. However, the images presented in Figure 3.9 demonstrated that PCL_DCM and PCL_CF scaffolds exhibited poor printability at a speed of 20 mm/s and required pressures above 172 kPa when printed at lower speeds. PCL_CF and PCL_DCM scaffolds exhibited high printability and structural stability when printed with desired geometries, whereas PCL_AA scaffolds demonstrated poor printability and stability. Therefore, we only conducted mechanical testing on PCL_DCM and PCL_CF scaffolds. After conducting experiments with various values as shown in Figure 2.4, we identified with respect to analysis of morphological data a range of optimal printability for scaffolds with 50% PCL polymer concentration presented in Figure 3.7. Through the use of optical and camera imaging, we were able to collect data on the open-pore process parameters without encountering issues such as rupturing or excessive

agglomeration. Uniaxial tensile testing was employed to evaluate the mechanical properties of the selected scaffolds.

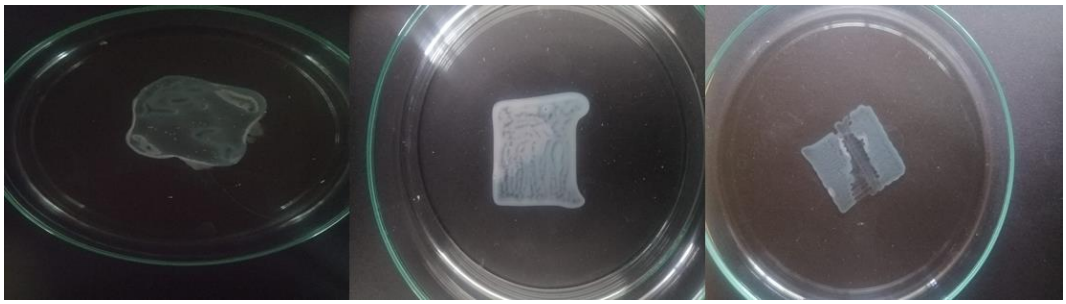

Figure 3.5 Images of PCL_AA scaffolds printed at 5 mm/s with different printing pressure.

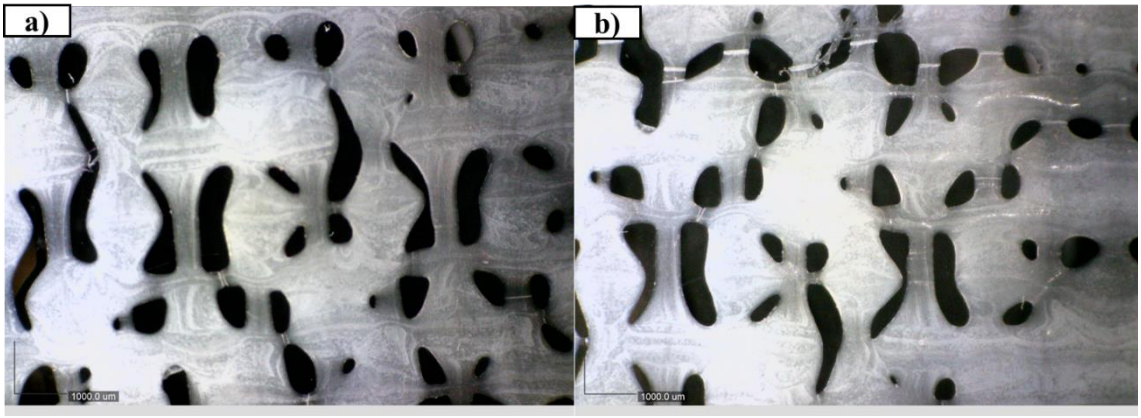

Figure 3. 6 Microscope images of PCL_AA scaffolds printed in 15 mm/s.

Following our morphological analysis of the printed scaffolds, a subset of the samples were chosen for further evaluation of their mechanical properties, as depicted in Figure 3.7. In Section 3.5, we conducted a comprehensive assessment of the mechanical properties of these selected scaffolds, with a focus on the specific details of their behavior under various mechanical tests. Our evaluation was conducted in accordance with

established scientific protocols and methodologies, ensuring the accuracy and reliability of our findings.

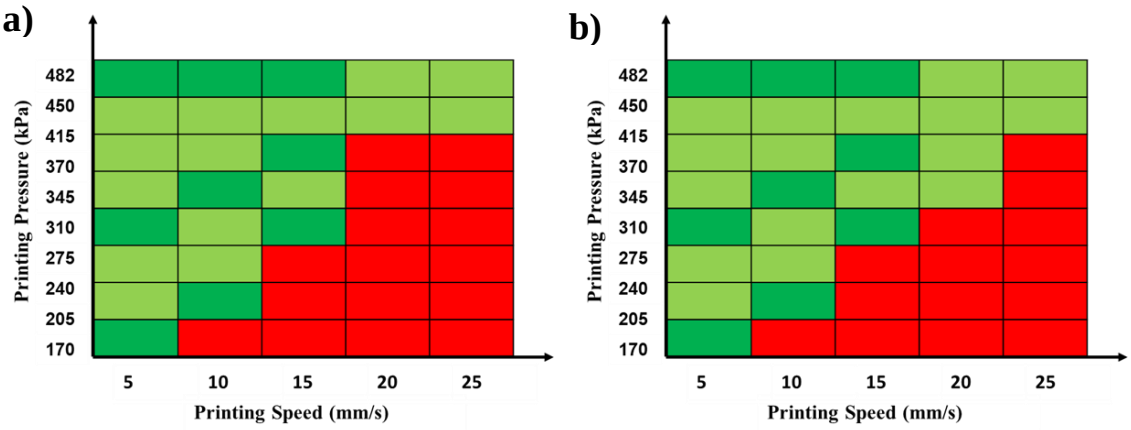

Figure 3. 7 Graph representing the structural integrity of the structures printed with 50% PCL/DCM and 50% PCL/CF scaffolds according to the speed and pressure variable, respectively (Low printability and high in red and light green, respectively, and scaffolds tested are represented by dark green; (a) PCL_DCM and (b) PCL_CF.

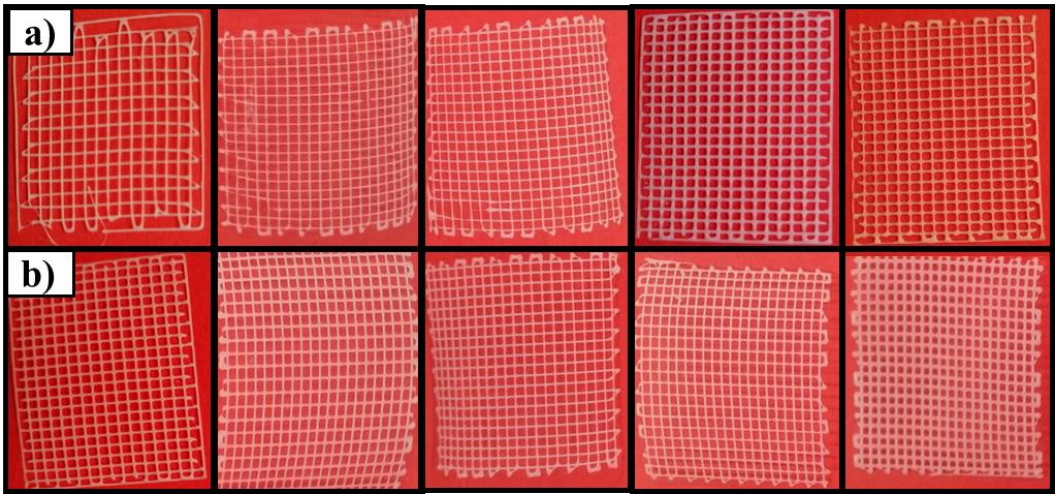

Figure 3.8 Scaffolds of PCL_DCM printed between 172-480 kPa at 5 mm/s printing speed.

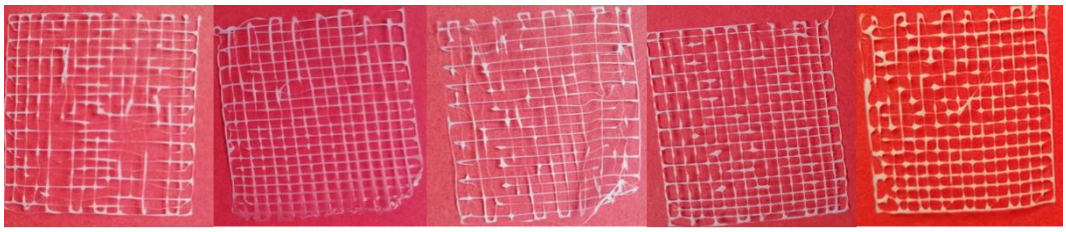

Figure 3.9 Printability of PCL_DCM scaffolds that are tested to be printed at pressures lower than 172 kPa and using printing speed more than 15 mm/s.

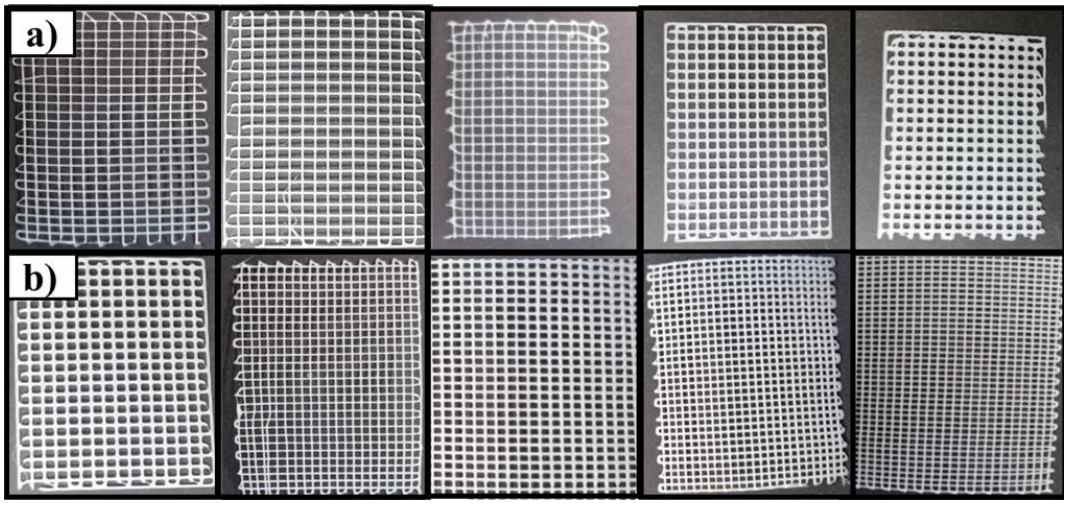

Figure 3.10 Scaffolds of PCL_CF printed between 172-428 kPa at 5 mm/s printing speed.

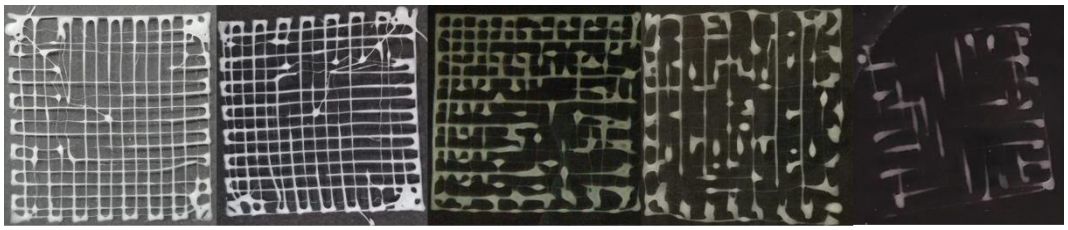

Figure 3.11 Printability of PCL_CF scaffolds that are tested to be written at pressures lower than 172 kPa and using printing speed more than 20 mm/s.

3.1.4 75% Polymer Concentration

A 20-megapixel camera of high resolution was utilized to capture the images. According the images and observations findings suggest to fabricate scaffolds with increasing concentrations at 75% concentration, it is necessary to employ low printing speed and high pressure. In Figure 3.12, scaffolds were fabricated at maximum printing pressure in our device (480 kPa) from 1 to 5 mm/s printing speed. There are agglomerations in scaffold with AA solvent, and pores disappear by closing completely

in the pores for printed scaffolds with a speed of 1 mm/s. It can be seen in Figure 3.12 ,increasing printing speed can lead to a decrease in the structural integrity of the printed scaffolds, which could result in the formation of ruptured structures. However, in scaffolds after 5 mm/s breaks started as seen in Figure 3.13, and also printability decreased. PCL_DCM and PCL_CF scaffolds produced at 5 mm/s were used to compare the mechanical responses of the scaffolds prepared with 50% concentration. In summary, high concentrations need to be printed at low printing speed with high pressure or using large diameter nozzles/needles.

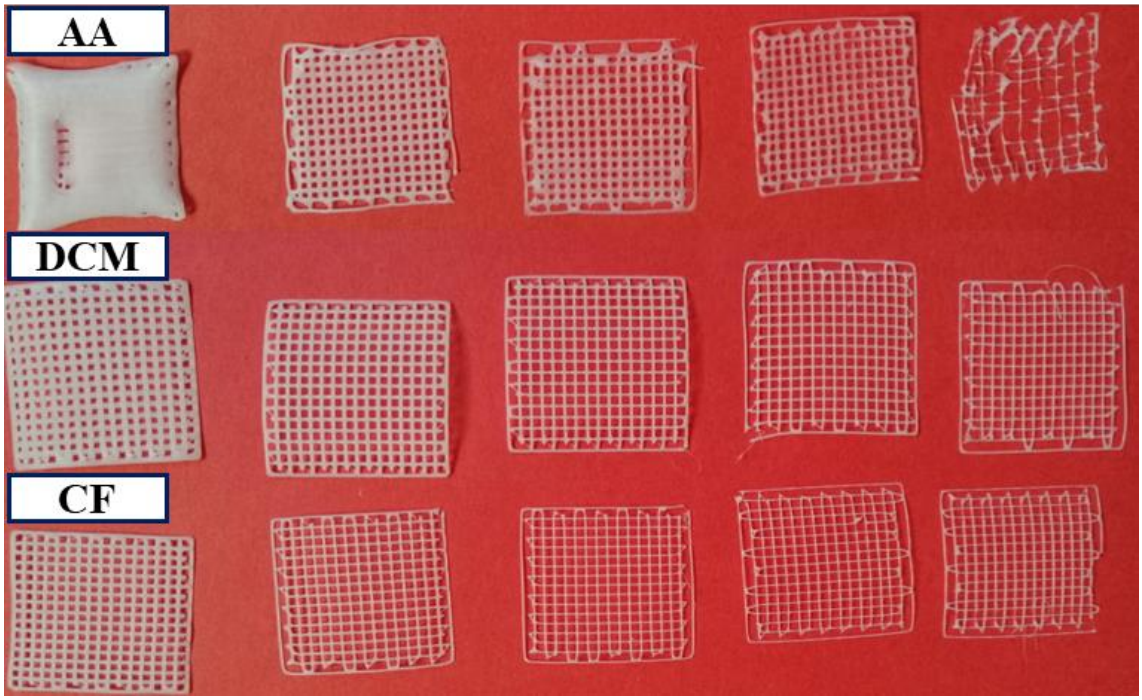

Figure 3.12 Scaffolds prepared at 75% polymer concentration.

Figure 3.13 Printability of PCL_DCM and PCL_CF scaffolds at speeds above 5 mm/s with 480 kPa.

3.2 Infill Density

Images were captured using a 20 megapixel camera with high resolution (Figure 3.14). SEM was utilized to analyze the morphology of at 50%, 70% and 90% infill densities as shown in Figure 3.15. The surface-to-volume ratio and pore characteristics were found to be noticeably impacted by changes in the process parameters, based on the SEM images results presented Figure 3.15. Essentially, modifications made to the process parameters had a significant influence on how pores were formed and distributed within the material, as well as the ratio of its surface area to its volume. The SEM analysis in Table 3.1 showed that increasing the infill density ratio led to a reduction in pore size, which is clearly observable in the morphology of the sample images. These findings suggest that the infill density ratio has a significant impact on the morphology of printed scaffolds and also may be a critical factor in determining its strength and performance. In the following sections (section 3.3.3), we will discuss infill density effect on mechanical properties.

Table 3.1 Strut diameters and pore sizes at different infill density ratios.

Infill Density	50%	70%	90%
Strut Diameter (µm)	380	390	350
Pore Size (µm)	1230	850	600

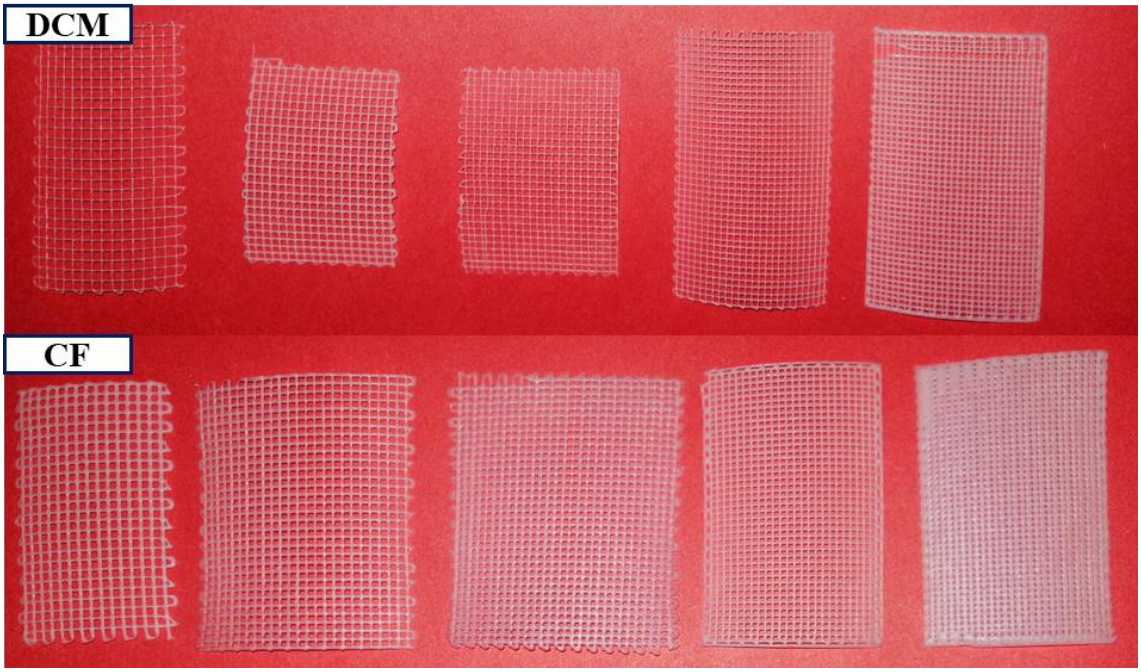

Figure 3.14 Images shown PCL_ DCM and PCL CF scaffolds with different infill density rates from 50% to 90% infill density respectively.

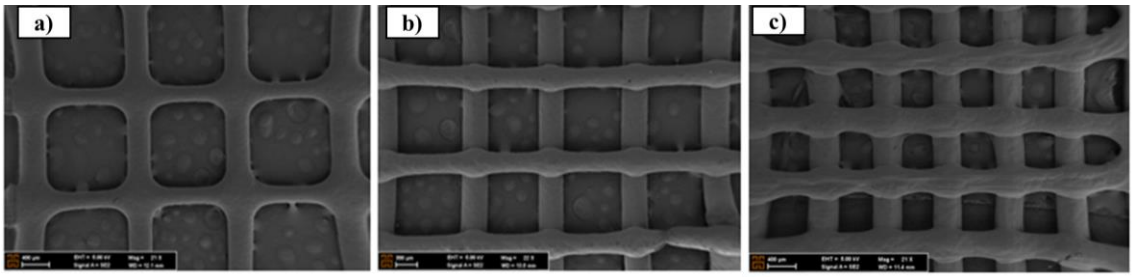

Figure 3.15 Evaluation of 50 PCL_CF scaffolds in SEM; a) printed with 60% infill density, b) 80% infill density and c) 99% infill density. All scaffolds were printed in 5 mm/s and 206 kPa.

3.3. FTIR Analysis

Fourier transform infrared spectroscopy (FTIR) analysis determines the interactions of molecules and functional groups in printed structures and evaluates the chemical structure of PCL scaffolds. The PCL scaffolds' FTIR spectrum was assessed with a Nicolet 6700 spectrometer (Nicolet 6700, Thermo Scientific). During the analysis, the wavelength was 4000-400 cm^{-1}. FTIR analysis result is presented in. The peak of the hydrogen-bonded hydroxyl group is around 3500 cm^{-1}, symmetric and asymmetric CH_2 stretching mode around 2943 and 2864 cm^{-1}[111] The absorption peak at 1720 cm^{-1} and

1470 cm^{-1} in the spectrum is C=O group, -CH2 bending vibrations respectively, C-O and C-C stretching in the crystalline phase around 1293 cm^{-1}, 1240 cm^{-1} correspond to C–C stretching vibrations (Figure 3.16) [112-113].

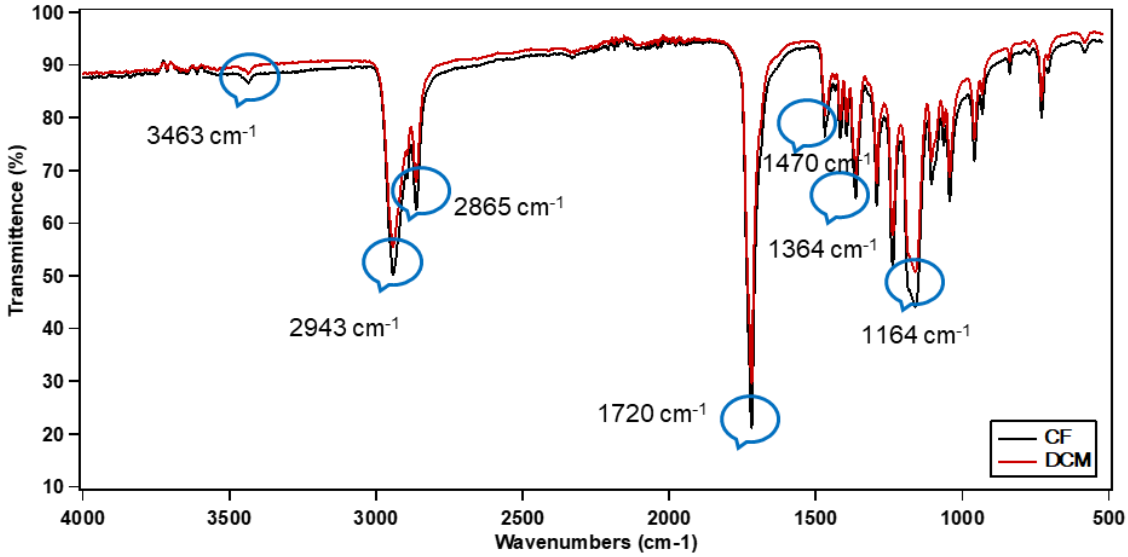

Figure 3. 16 FT-IR spectra of PCL scaffold with DCM and CF solvent.

3.5. Effect of 3D Printing Parameters on Mechanical Character of Scaffolds

3.5.1. Speed Effect

The effect of printing speed on the printing of PCL_DCM and PCL_CF structures was investigated. Specifically, the ex periment involved using three different printing speeds (5 mm/s, 10 mm/s and 15 mm/s) to examine the influence of speed on the quality and mechanical properties of the printed PCL structures. According to results presented in Figure 3.17 and Figure 3.18, it can be concluded that printing speed has a significant effect on the mechanical properties of PCL structures. PCL_DCM scaffolds printed at 5 mm/s had the highest Young's modulus value of 39.0 MPa, while PCL_DCM scaffolds printed at 10 mm/s and 15 mm/s showed their strength values with a decrease of approximately 60% (16.15 MPa) and 65% (13.83 MPa), respectively. It shows that scaffolds printed at 5mm/s were stiffer and more resistant to deformation than scaffolds printed at higher speeds of 10mm/s and 15mm/s. At 5 mm/s printing speed for PCL_DCM scaffolds may have led to a more densely packed and organized structure, resulting in

increased stiffness. PCL_CF scaffolds printed at speed of 5 mm/s showed a lower Young's modulus than PCL_DCM scaffolds (26.8 MPa). However, it showed elongation value of 1152% with an increase of approximately 25%. In addition, PCL_DCM and PCL_CF scaffolds have a UTS value of 6.4 MPa and 6.3 MPa and yield strength of 1.9 MPa and 1.7 MPa for printed at 5 mm/s, respectively. PCL_DCM scaffolds printed at 5 mm/s have a slightly higher UTS value and yield strength value compared to the PCL_CF scaffolds printed at the same speed.

For PCL_DCM scaffolds, increasing the printing speed from 5 mm/s to 15 mm/s significantly decreased Young's modulus. PCL_DCM and PCL_CF scaffolds printed with 15 mm/s exhibit the lowest Young's modulus. Results showed that higher printing speeds might result in a less rigid final product and more deformable. According the literature, increased printing speed causes a slight decrease of the polymer amount deposited on the surface per unit area, which can result in weak or ruptured structures [114]. On the other hand, for PCL_CF scaffolds, the highest Young's modulus (32.0 MPa) values were obtained for scaffold printed at 10 mm/s. It concluded that a moderate printing speed for PCL_CF scaffolds were more rigid and less deformable printed scaffolds at 5 mm/s (26.88 MPa) and 15 mm/s (18.0 MPa). In addition, it is clearly demonstrated in Figure 3.18 (b) that UTS and yield strength decreased significantly with increasing printing speeds. The results obtained show that it significantly changes the mechanical properties of the scaffolds printed with the solution formed with different solvents. Different solvents may have different abilities to dissolve the PCL material, which can affect the viscosity and rheological properties of the printing solution. Because solvents affect the molecular structure and bonding of the PCL material [110].

Fakhruddin et al. highlight the importance of optimizing extrusion pressure and printing speed parameters to achieve high-quality and precise 3D-printed structures. Their results showed that increasing the printing speed required a corresponding increase in extrusion pressure to prevent the formation of beading or other defects in the printed structure. Moreover, they found that printing at high pressure and low speed could lead to excessive material outflow and a loss of structural integrity [115]. As shown in this study, the polymer's appropriate printing pressure and printing speed values should be determined at the most optimum values for reasonable mechanical properties and printability.

Gentile et al. reported pure PCL membranes with electrospinning values of Young Modulus at 27.2 ± 4.4 MPa for tissue engineering applications [116]. In this study, it has been shown that more controlled, porous, and homogeneous structures can be obtained by using the 3D Bioprinting technique. In another study, Vurat et al investigated effect of molecular weight and printing speed on mechanical properties in PCL scaffolds. They showed that increasing the molecular weight of the polymer increased the mechanical strength conversely, but there was no significant difference in ductility. Additionally, it showed that the printing speed decreased the mechanical strength when the scaffolds with the same molecular weight were printed at different printing speeds [117]. Similarly, our experiment results presented that scaffolds obtained in slow printing speed (5 mm/s) were found to have higher mechanical strength than scaffolds obtained at fast printing speed conditions (10 mm/s and 15 mm/s) in PCL_DCM and PCL_CF scaffolds. On the other side, ductility changed in each different scaffold, but no direct positive or negative correlation was found between ductility and scaffolds produced with varying printing speeds.

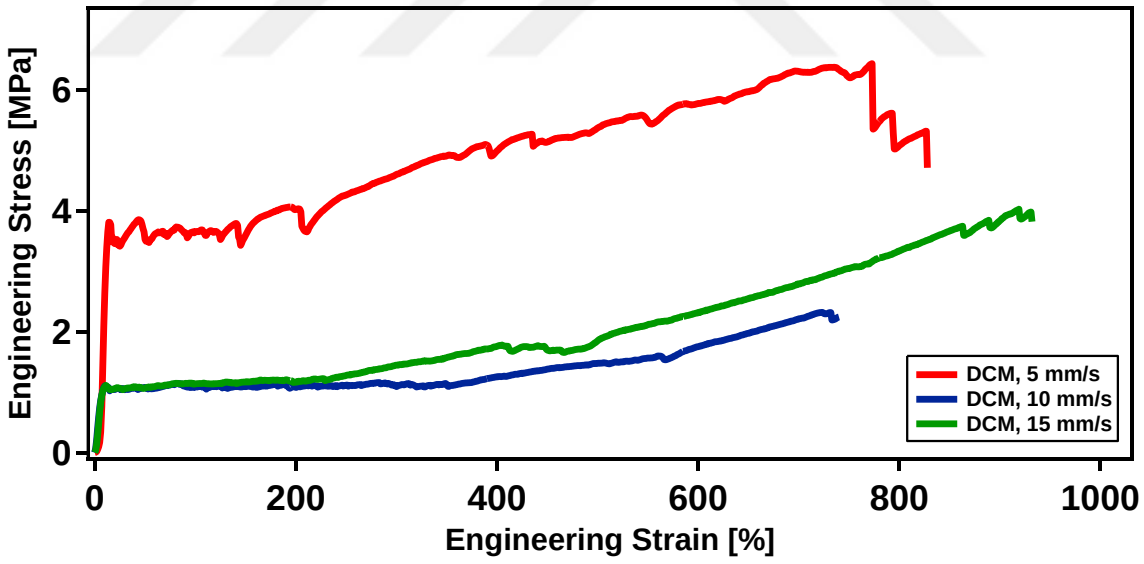

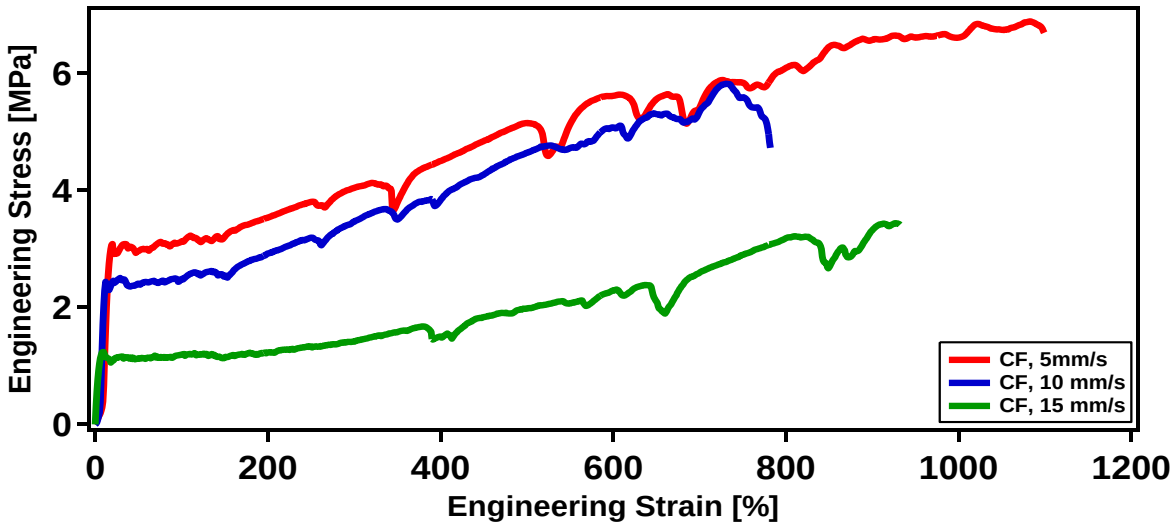

Figure 3.17 The engineering tensile stress-strain curves of printed PCL_DCM and PCL_CF at printing speeds of 5 mm/s, 10 mm/s and 15 mm/s.

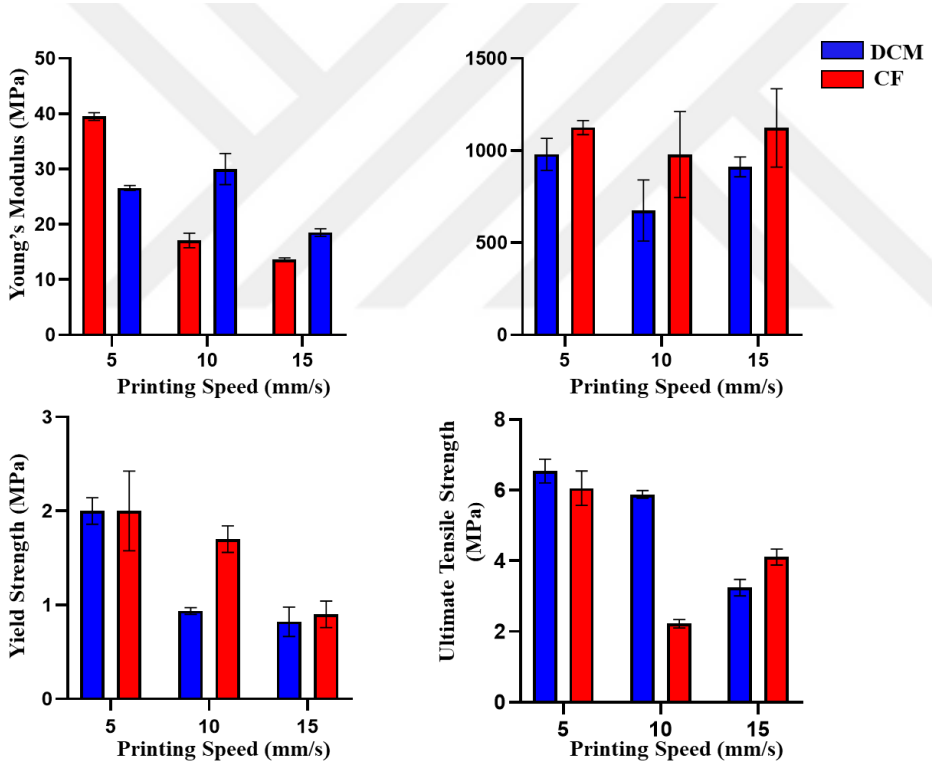

Figure 3.18 The effect of printing speed on PCL structures (a) Young's Modulus, (b) Elongation rate of scaffolds until failure of printed PCL_DCM and PCL_CF (c) Yield strength, and (d) UTS values of tested scaffolds (Blue column and red column are representative PCL_DCM and PCL_CF scaffolds, respectively).

Table 3.2 Process parameters and mechanical test results used to investigate the printing speed effect.

Concetration of Polymers	Process Parameters in 3D Bioprinting	Young's Modulus (MPa)	Yield Strength (MPa)	Ultimate Tensile Strength(MPa)	Elongation at Break(%)
50% PCL/DCM	V=5 mm/s P=480 kPa	39.00	1.9	6.4	919
	V=10 mm/s P=480 kPa	16.15	0.91	2.14	792
	V=15 mm/s P=480 kPa	13.85	0.93	3.14	950
50% PCL/CF	V=5 mm/s P=480 kPa	26.88	1.7	6.3	1152
	V=10 mm/s P=480 kPa	32.00	1.6	5.80	814
	V=15 mm/s P=480 kPa	18.00	0.8	3.41	950

3.5.2 Pressure Effect

Pressure is another significant process parameter that impacts the structure's printability, structural integrity, and mechanical properties. Firstly, the mechanical properties of the scaffolds produced at different speeds were investigated. Then, mechanical tests of the structure built to varying pressures at the same speeds were performed. Three different pressure values were selected for each printing speed (5 mm/s, 10 mm/s, and 15 mm/s). For each scaffolds, concentration and infill density were constant at %50. After that, the effect of the pressure was evaluated for PCL_DCM and PCL_CF scaffolds, as presented in Figure 3.19 and Figure 3.25 and their 3D surface response graph drawn in Figure 3.26 and Figure 3.29.

Based on the results demonstrated in Figure 3.19 and Figure 3.20, printed scaffold at 5 mm/s and 480 kPa printing pressure had the highest Young's modulus value of 39.00 for PCL_DCM and 26.88 MPa for PCL_CF . 310 kPa printing pressure shows that the lowest Young' modulus (13.0 MPa), yield strength (0.58 MPa), and UTS (3.1 MPa) in PCL_CF scaffolds compared to other scaffolds printed at 480 kPa and 172 kPa printing

pressure but they showed similar elongation (1152%) with 480 kPa printed scaffolds (1161%). For PCL_DCM scaffolds, 172 kPa printing pressure demonstrated the lowest Young' modulus (22.27 MPa), but it showed the highest elongation (1205%) over other scaffold printed at 480 kPa and 310 kPa printing pressure.

Table 3.3 Process parameters and mechanical test results used to investigate the printing pressure effect in printing speed of 5 mm/s.

Concetration of Polymers	Process Parameters in 3D Bioprinting	Young's Modulus (MPa)	Yield Strength (MPa)	Ultimate Tensile Strength(MPa)	Elongation at Break(%)
50% PCL/DCM	V=5 mm/s P=172 kPa	22.27	2.02	6.41	1205
	V=5 mm/s P=310 kPa	35.00	2.3	4.6	902
	V=5mm/s P=480 kPa	39.69	1.9	6.4	919
50% PCL/CF	V=5 mm/s P=172 kPa	24.48	1.05	4.65	640
	V=5 mm/s P=310 kPa	13.00	0.58	3.1	1161
	V=5 mm/s P=480 kPa	26.80	1.7	6.3	1152

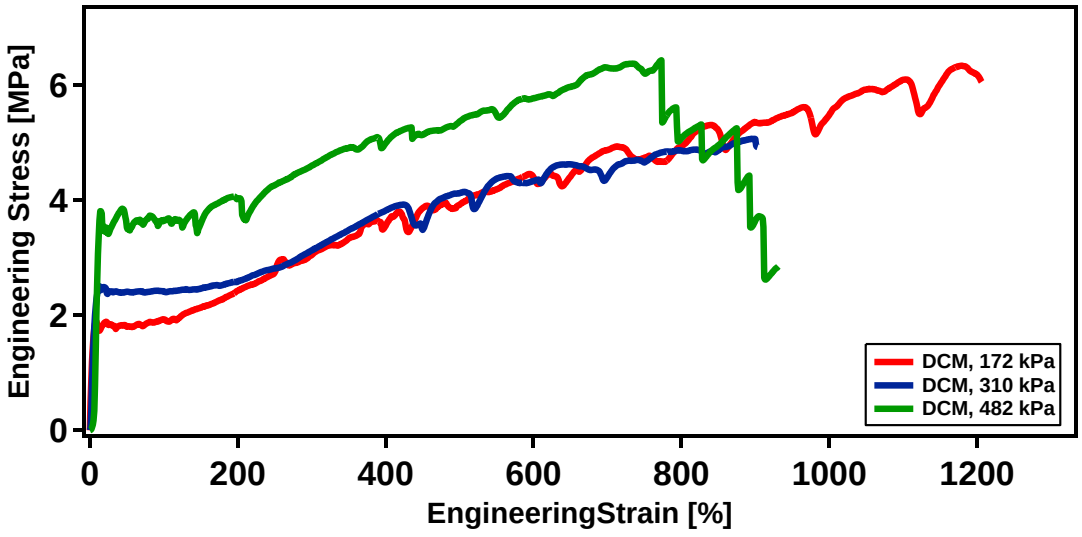

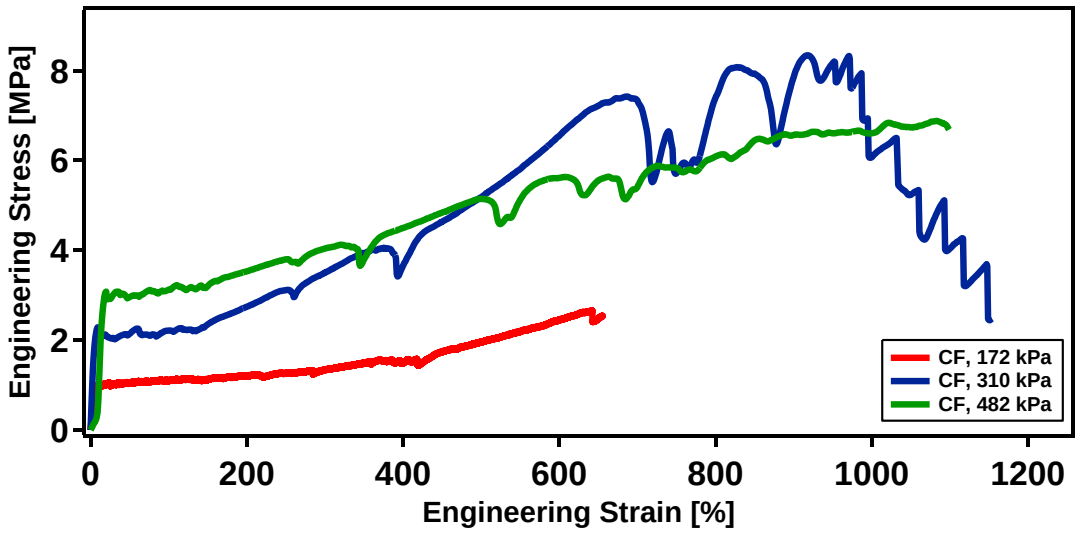

Figure 3.19 The engineering tensile stress-strain curves of printed PCL_DCM and PCL_CF at printing speeds of 5 mm/s.

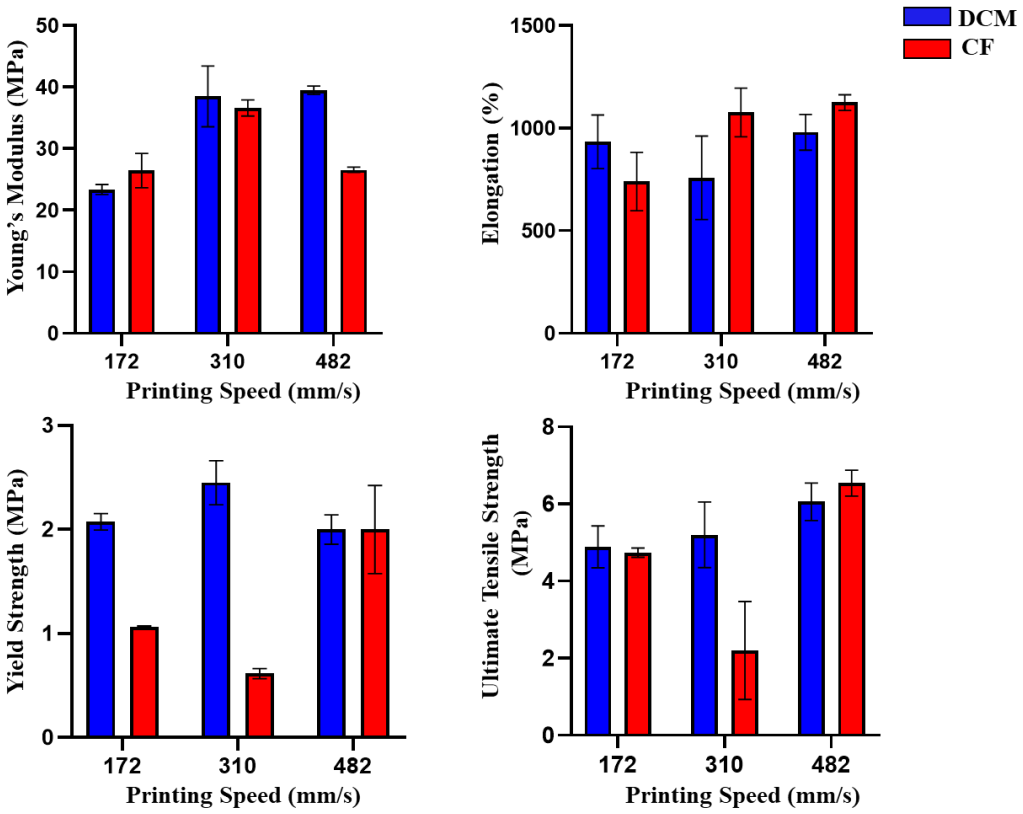

Figure 3.20 The effect of printing pressure on PCL scaffolds (a) Young's Modulus, (b) Elongation rate of scaffolds until failure of printed PCL_DCM and PCL_ CF (c) Yield strength, an, (d)UTS values of tested scaffold (Blue column and red column are representative PCL_DCM and PCL_CF scaffolds, respectively).

Printed scaffolds at 10 mm/s with 206 kPa, 345 kPa, and 480 kPa printing pressure were revealed in Figure 3.21 and Figure 3.22. Both PCL_DCM and PCL_CF printed at 345 kPa printing pressure indicated the highest Young's modulus, yield strength, and UTS and elongation. PCL_DCM scaffolds at printed 345 kPa printing pressure had incredibility values with increased of approximately 97% (22.42 MPa) for 206 kPa printing pressure and 167% (16.15 MPa) for 480 kPa printing pressure. On the other hand, PCL_CF scaffolds at 206 kPa, 345 kPa, and 480 kPa showed Young's modulus value of 21.44 MPa, 36.44 MPa, and 32.1 MPa, respectively. Additionally, PCL_CF exhibited the highest elongation with 1263% than scaffolds printed at 206 kPa (840% elongation) and 480 kPa (814% elongation). Similiarly, PCL_DCM scaffolds indicated the highest elongation with 1512% compared to printed at 206 kPa (1008%) and 480 kPa (792%).

Table 3.4 Process parameters and mechanical test results used to investigate the printing pressure effect in printing speed of 10 mm/s.

Concetration of Polymers	**Process Parameters in 3D Bioprinting**	**Young's Modulus (MPa)**	**Yield Strength (MPa)**	**Ultimate Tensile Strength(MPa)**	**Elongation at Break(%)**
50% PCL/DCM	V=10 mm/s P=206 kPa	22.44	1.65	5.59	1008
	V=10 mm/s P=345 kPa	43.20	2.6	7.65	1512
	V=10 mm/s P=480 kPa	16.15	0.93	2.14	792
50% PCL/CF	V=10 mm/s P=206 kPa	21.44	1.12	3.58	840
	V=10 mm/s P=345 kPa	36.44	1.45	6.67	1263
	V=10 mm/s P=480 kPa	32.10	0.9	5.80	814

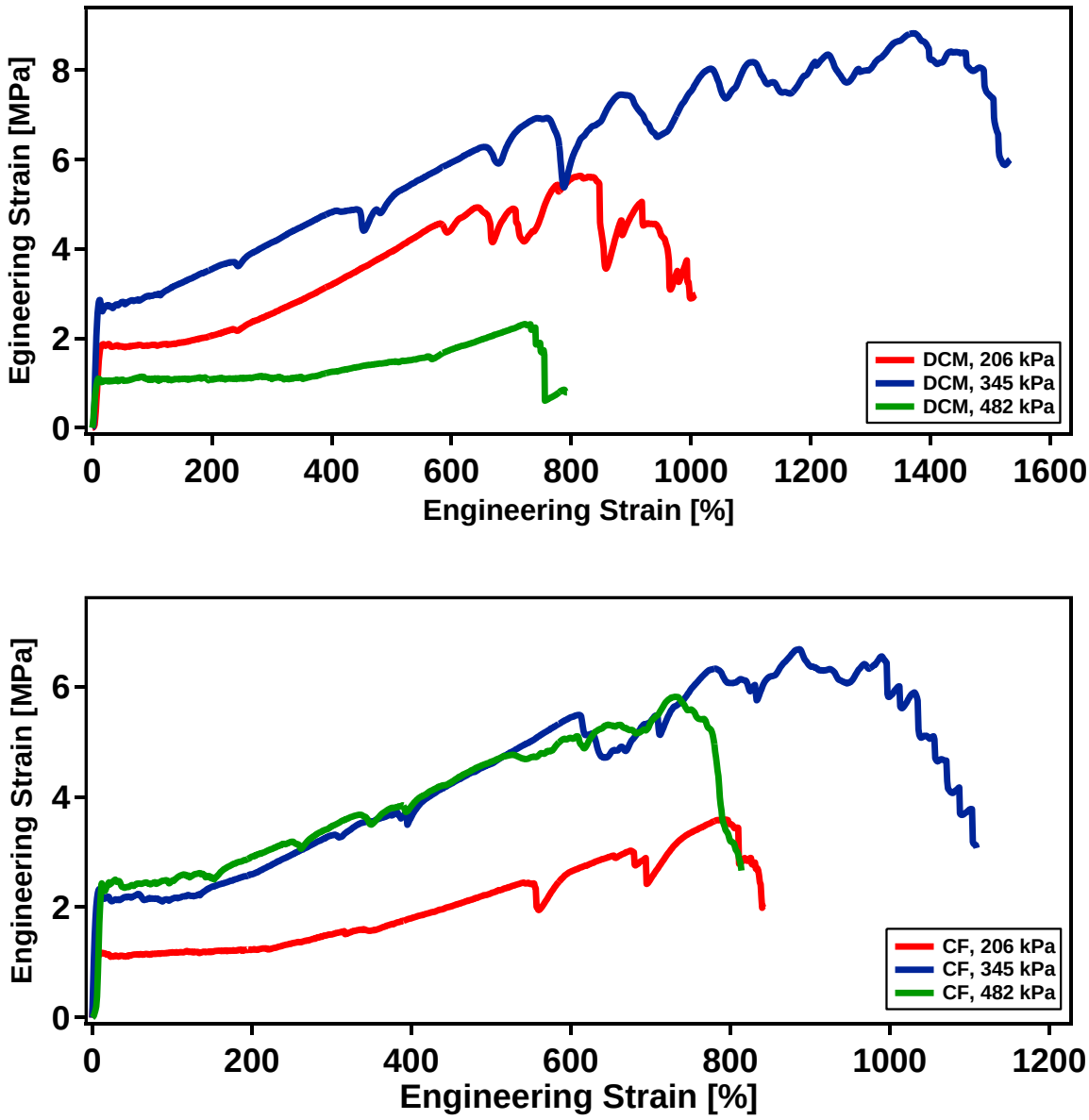

Figure 3.21 The engineering tensile stress-strain curves of printed PCL_DCM and PCL_CF scaffolds at printing speeds of 10 mm/s.

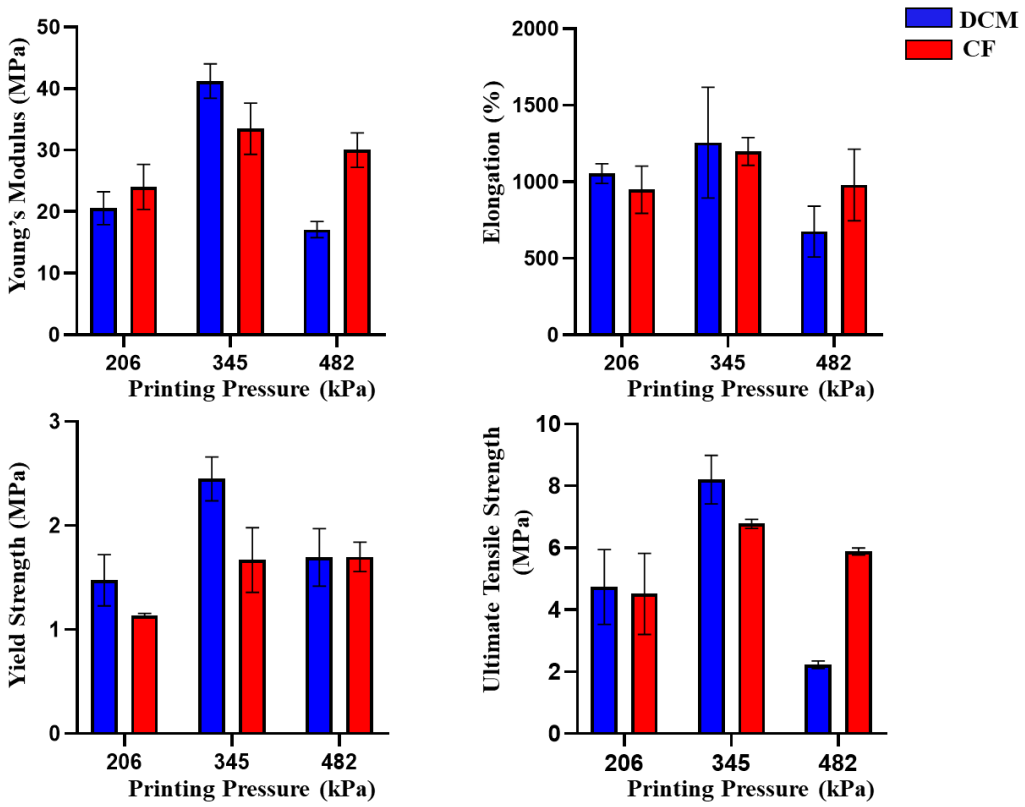

Figure 3.22 The effect of printing pressure on PCL scaffolds (a) Young's Modulus, (b) Elongation rate of scaffolds until failure of printed PCL_DCM and PCL_CF (c) Yield strength, and (d)UTS values of tested scaffolds (Blue column and red column are presentative PCL_DCM and PCL_CF scaffolds, respectively).

As stated in Figure 3.23 and Figure 3.24, printed scaffolds at 15 mm/s with moderate printing pressure (396 kPa) showed the highest Young's modulus and elongation which was 24.9 MPa and 1280% for PCL_DCM and 19.56 MPa and 1535% for PCL_CF scaffolds, repectively. At printed 310 kPa and 480 kPa printing pressure for PCL_DCM have Young modulus at 21.3 MPa and 13.85 MPa by decreasing about 14% and 45%, respectively. Moreover, PCL_DCM and PCL_CF scaffolds exhibited the highest strength values 6,28 MPa and 4.58 MPa at this printing pressure. Both PCL_DCM and PCL_CF scaffolds printed at 480 kPa printing pressure showed the lowest ductility values but they had similar results with 950% elongation and 973% elongation. Consequently, all results at printed 480 kPa demonstrated that lower printing speeds exhibited generally the highest Young's modulus and lowest elongation. At the same printing speed with different pressure values showed highest Young's modulus, elongation, and UTS except for scaffolds with printed 5 mm/s printing speed.

Table 3.5 Process parameters and mechanical test results used to investigate the printing pressure effect in printing speed of 15 mm/s.

Concetration Polymers	Process Parameters in 3D Bioprinting	Young's Modulus (MPa)	Yield Strength (MPa)	Ultimate Tensile Strength(MPa)	Elongation at Break(%)
50% PCL/DCM	V=15 mm/s P=310 kPa	21.3	1.12	4.84	953
	V=15 mm/s P=396 kPa	24.9	1.21	6.28	1280
	V=15 mm/s P=480 kPa	13.85	0.93	3.95	950
50% PCL/CF	V=15 mm/s P=310 kPa	16.95	0.81	3.11	1298
	V=15 mm/s P=396 kPa	19.56	1.31	4.58	1535
	V=15 mm/s P=480 kPa	18.0	0.83	3.41	973

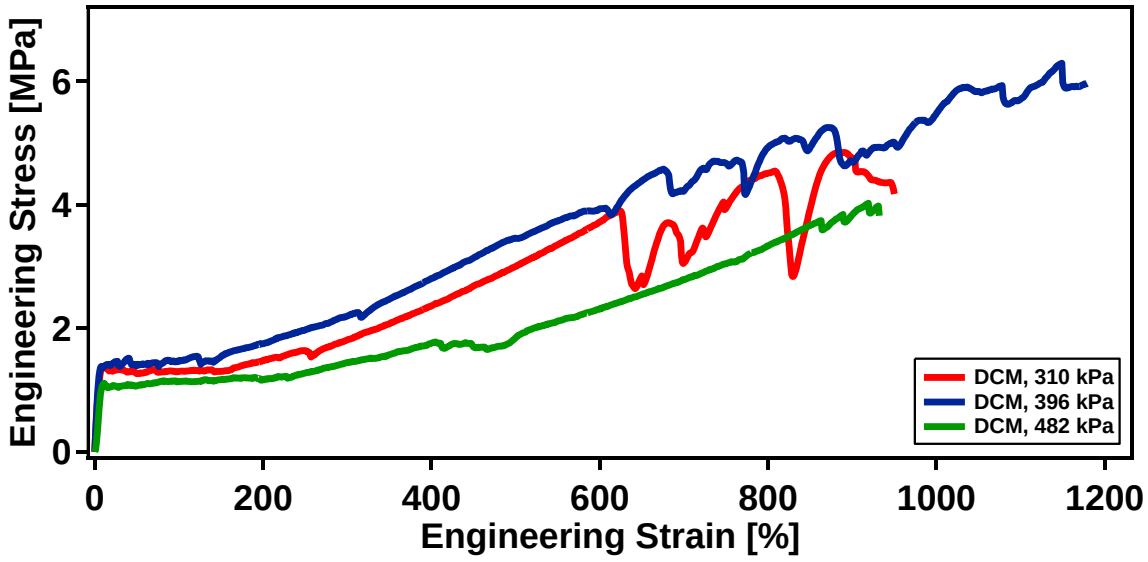

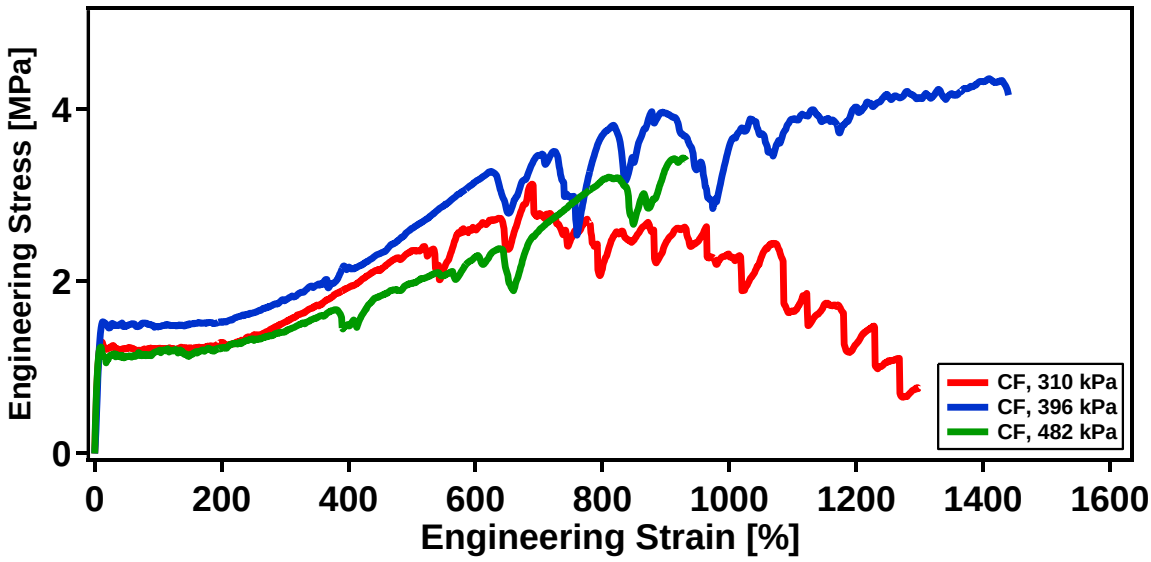

Figure 3.23 The engineering tensile stress-strain curves of printed PCL_DCM and PCL_CF scaffolds at printing speeds of 15 mm/s.

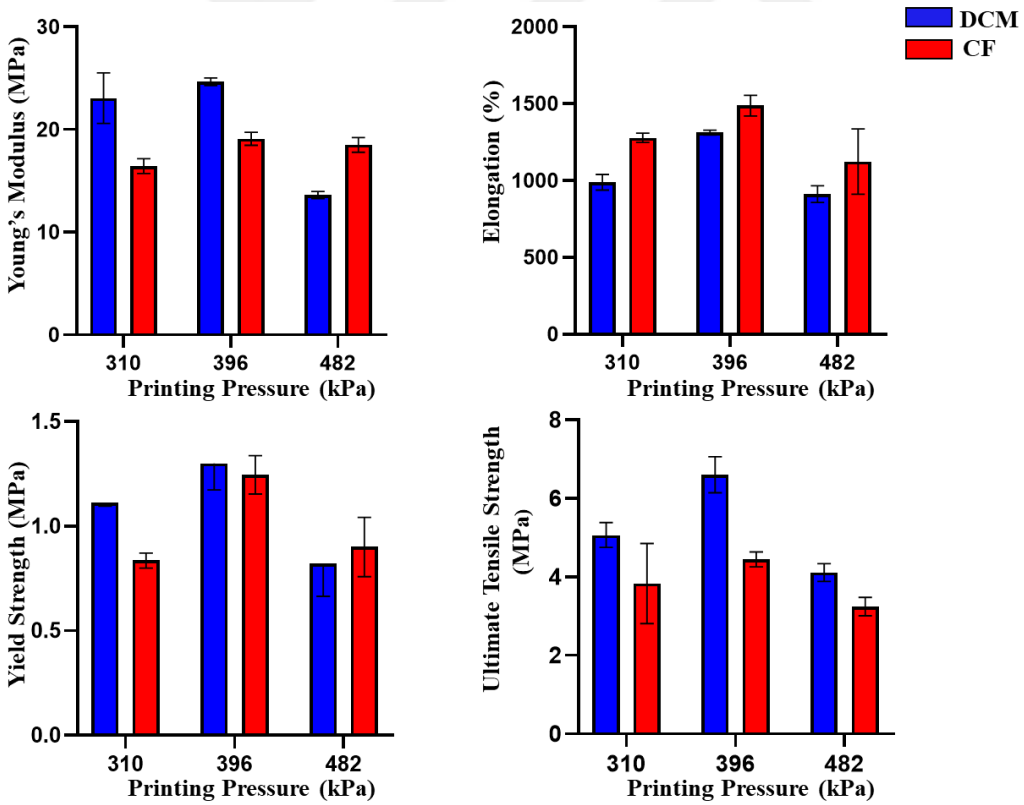

Figure 3.24 The effect of printing pressure on PCL scaffolds (a) Young's Modulus, (b) Elongation rate of scaffolds until failure of printed PCL_DCM and PCL_CF (c) Yield strength, and (d) UTS values of tested scaffolds (Blue column and red column are representative PCL_DCM and PCL_CF scaffolds, respectively).

According to the engineering stress-strain data for 10 mm/s and 15 mm/s printing speeds, moderate printing pressures show higher ultimate tensile strength (UTS) and ductility values. As pressure is decreased, UTS and ductility decrease. The reason is that the amount of material per unit printing area decreases below an optimum pressure value. UTS and ductility tend to decrease at more significant pressures compared to moderate printing pressures. Still, the change is more dramatic between medium and low printing pressures. It can be concluded that the pressure needs to be modified according to changing printing velocities which vary the amount of material per printing area, the concentration, which affects the viscosity, and solvent. The pressure needs to be increased for optimum mechanical properties for higher printing speeds. These comments can be strengthened using SEM images presented in Figure 3.25. The belongs to 396 kPa printing pressure, and it is moderate pressure in our study. As the pressure is decreased from 396 kPa to 310 kPa, the structure's thickness is decreasing, which can be concluded from the cone-like structure of moderate printing pressure and the flat structure of the low-pressure structure. This results in decrease in strength and ductility values, as discussed before. At higher pressures, the smoothness of the surface is changed. Also, in Figure 3.25 the printing quality is lower than that of moderate printing pressure. So, at higher and lower magnification images, both high pressure and low pressure make the structure far from the optimum. Lower pressure decreases the amount of material, and higher pressure makes the structure quality low [118].

Our study highlights the importance of balancing pressure and speed to achieve continuous, uniform filaments with minimal defects. Printing at very low pressures (172 Kpa, 206 Kpa and 310 kPa) can resulted in a significant reduction in deposition and the formation, while printing at very high pressures (480 kPa) can led to cause nonlinear responses. Increasing printing pressure can lead to a denser and stronger printed structure, while reducing pressure can result in a more porous structure with lower mechanical strength. This is because higher pressure can help in pushing the material more tightly together, reducing the amount of voids, and enhancing the bonding between them. However, the optimal printing pressure should be determined based on the specific printing material and printing process parameters to achieve the desired mechanical properties while avoiding any negative impacts on the printing process [119]. Therefore, it is essential to carefully optimize printing conditions to ensure successful 3D bioprinting outcomes [120].

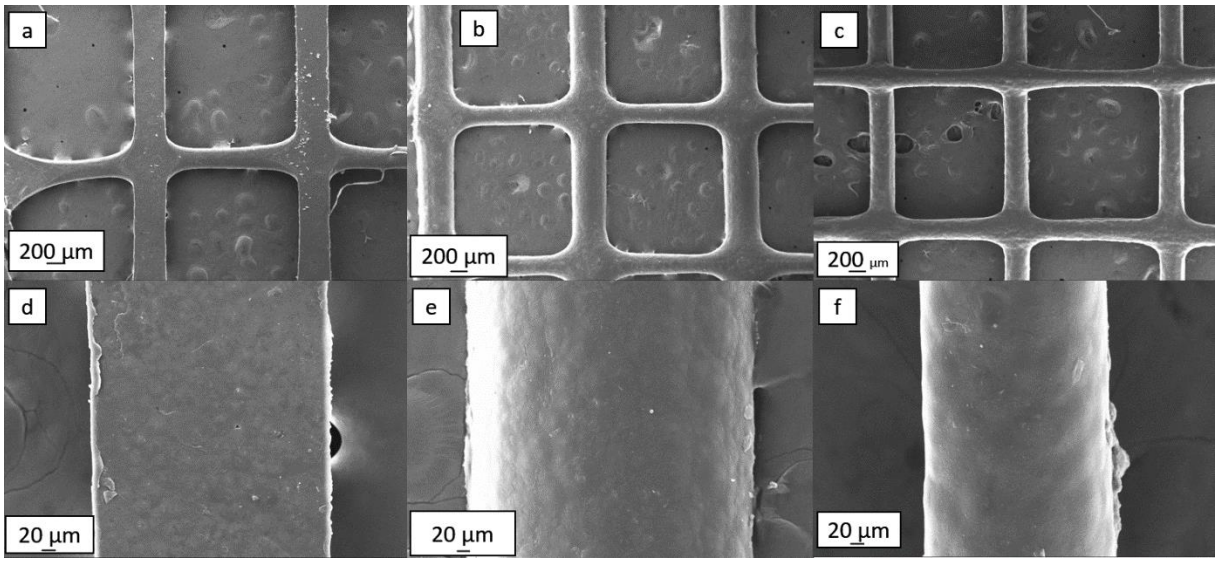

Figure 3.25 SEM images of 15 mm/s printing pressure PCL_CF and the printing pressures are 310, 396 and 480 kPa, respectively from a to c. The bottom images belong to the higher magnification of the top images.

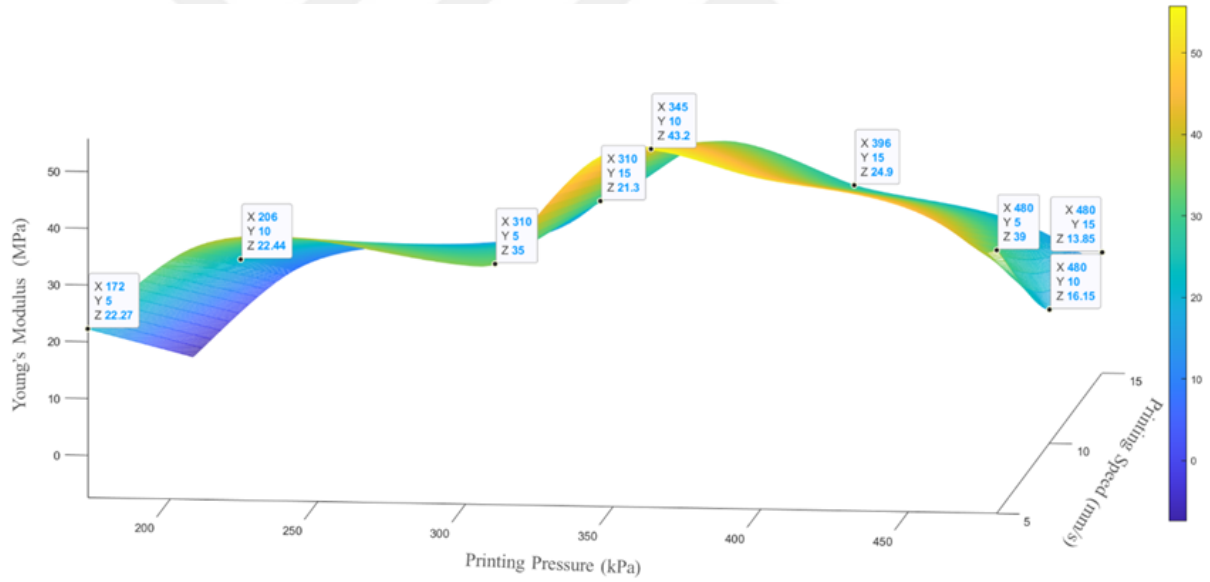

Figure 3.26 Response surface plots (3D) for PCL_DCM scaffolds showing the effects of different printing pressure and printing speed on Young's Modulus.

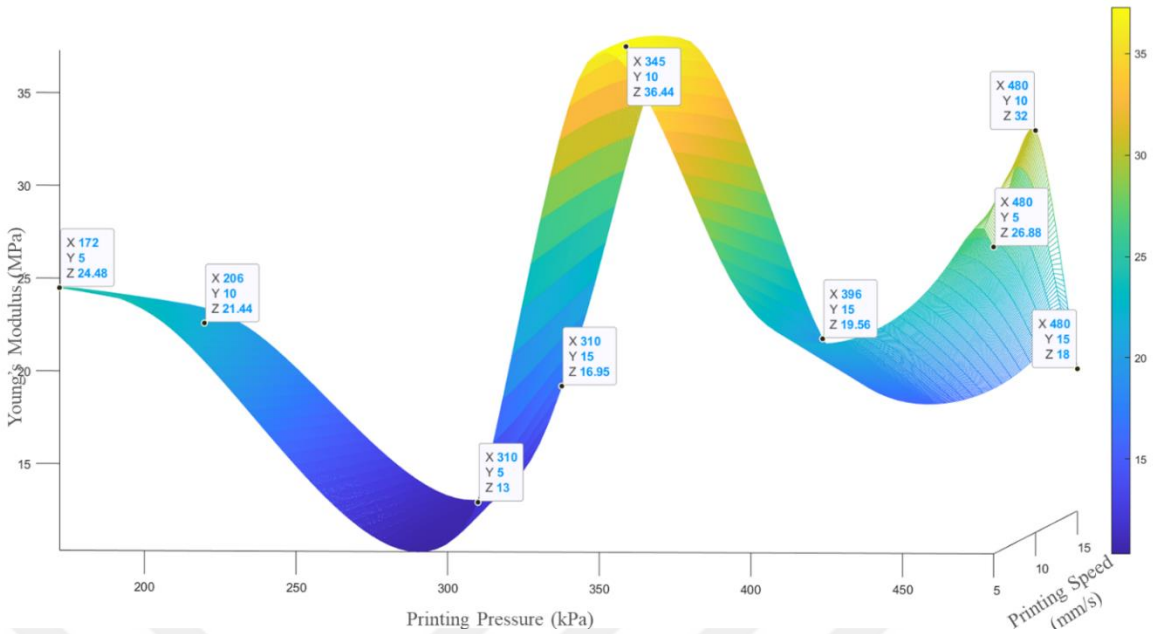

Figure 3.27 Response surface plots (3D) for PCL_CF scaffolds showing the effects of different printing pressure and printing speed on Young's Modulus.

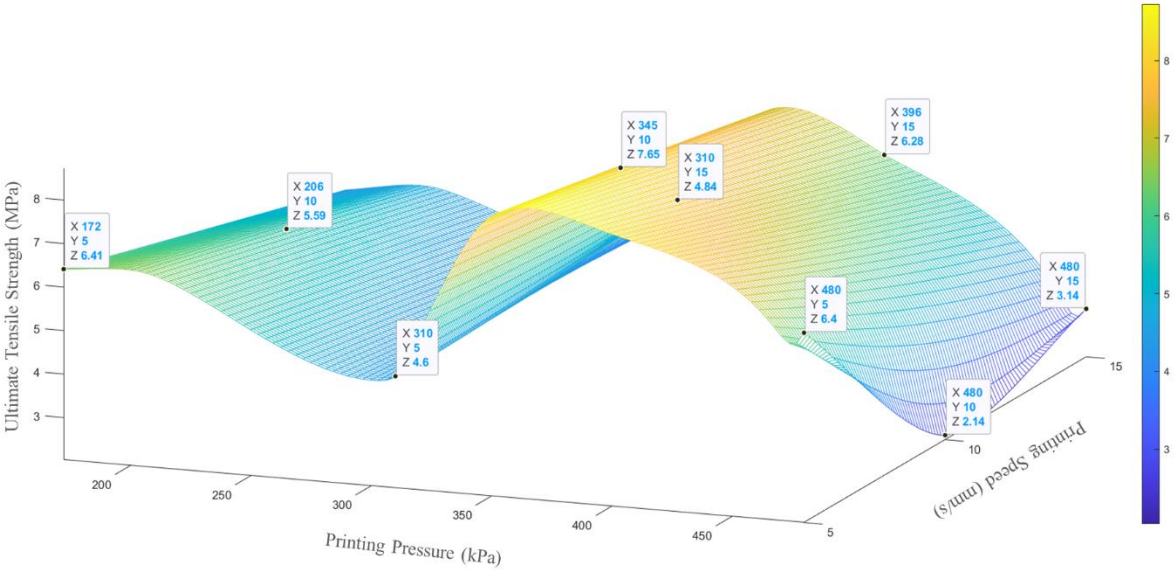

Figure 3.28 Response surface plots (3D) for PCL_DCM scaffolds showing the effects of different printing pressure and printing speed on UTS.

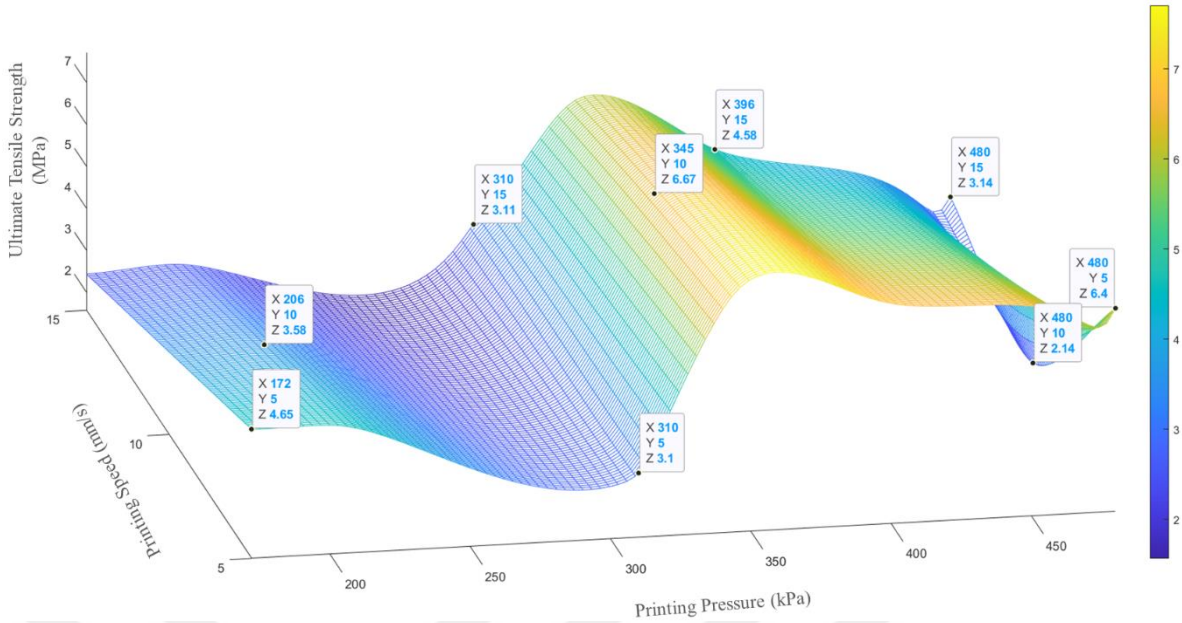

Figure 3.29 Response surface plots (3D) for PCL_CF scaffolds showing the effects of different printing pressure and printing speed on UTS.

3.3.3. Infill Density Effect

The infill density rate is another important parameter in 3D bioprinting that can affect the mechanical properties of the scaffold. Infill density alter porosity and number of struts in printed structure. As the infill density rate increases, more PCL solution is deposited on the surface. Therefore, it can lead to a decrease in porosity and an increase in the number of struts which can lead to an increase in mechanical strength [121-122]. Moreover, infill density changes a percentage of the total scaffold volume [123]. They show higher mechanical strength as the stress distribution can be spread across more struts as increase infill density.

In this study, the mechanical properties of the scaffolds created with three different infill density; 50%, 70% and 90% at both 50% and 75% concentration were evaluated. Increased levels of infill density in both concentration groups indicated that the ductility and strength values increased as describe in Figure 3.26 and Figure 3.27. Investigation at 50% PCL concentration, the printed scaffolds at 90% infill density showed the highest Young's modulus, which was 44.8 MPa for PCL_CF and 50.06 MPa for PCL_DCM scaffolds. Printed scaffolds with a 50% infill density indicate that PCL_DCM and PCL_CF scaffolds have the lowest Young's modulus at 35.0 MPa and 22.42 MPa with a decrease of approximately 31% and 50%, respectively. Considering the 70% infill

density, Young's modulus with values of 41.1 MPa and 37.55 MPa for PCL_DCM and PCL_CF increased compared to 50% infill density, but it has lower value than scaffolds printed with 90% infill density. In addition, increasing infill density ratios from 50% to 90% remarkably increased UTS values by approximately 89% and 52% for PCL_DCM and PCL_CF scaffolds, respectively. In contrast, there is no direct relation between elongation and infill density at concentration of 50 %.

On the other hand, when scaffolds were tested at 75% PCL concentration, Young's modulus value and UTS increased as the infill density value increased. These results indicate that higher infill density leads to higher values of Young's modulus and UTS for both concentration groups. Although increasing the value of infill density improves strength in the scaffolds, but it reduces their ductility values. The fracture strain of PCL_DCM scaffolds reduced slightly by around 17% from 891% to 758%. On the other hand, for the PCL_CF scaffolds, the fracture strain decreased gradually by approximately 47% from 663% to 433% as the infill density increased.

Chou et al. analyzed that increasing infill density (65% and 80%) increases strength and ductility [106]. In another study, Tanveer et al. investigated the effect of infill density (25%, 50%, 75%, and 100%) on the mechanical properties of 3D printed ABS parts. They found that increasing infill density led to higher tensile strength, but also increased the stiffness and reduced the ductility on printed structure [124]. While decreasing infill density increases the pore diameters, and so increased porosity causes stress concentration during the uniaxixal tensile test and therefore shows lower mechanical properties [106-107]. In other words, when scaffolds begin to deform during the uniaxixal tensile test, the struts cannot carry loads evenly. As the deformation progresses, it reduces the number of stretched struts that are subjected to stress due to the struts of scaffolds ruptured. However, with increasing infill density ratios, they are dispersed between the neighboring strip chains after the ruptured struts [125]. Overall, our results show that printed scaffolds with high infill density ratios showed higher strength than printed scaffolds with low infill density ratios [126].

Table 3.6 Process parameters and mechanical test results used to investigate the infill density effect in polymer concentration of 75%.

Concetration Polymers	Process Parameters in 3D Bioprinting	Young's Modulus (MPa)	Yield Strength (MPa)	Ultimate Tensile Strength(MPa)	Elongation at Break(%)
75% PCL/DCM	I.D= 50% V=5 mm/s P=480 kPa	35.00	2.3	4.6	902
	I.D= 70% V=5 mm/s P=480 kPa	41.1	1.8	6.43	703
	I.D= 90% V=5 mm/s P=480 kPa	50.06	2.3	8.7	887
75% PCL/CF	I.D= 50% V=5 mm/s P=480 kPa	22.42	1.8	6.87	1126
	I.D= 70% V=5 mm/s P=480 kPa	37.55	1.3	8.18	1161
	I.D= 90% V=5 mm/s P=480 kPa	44.8	3.6	10.48	884

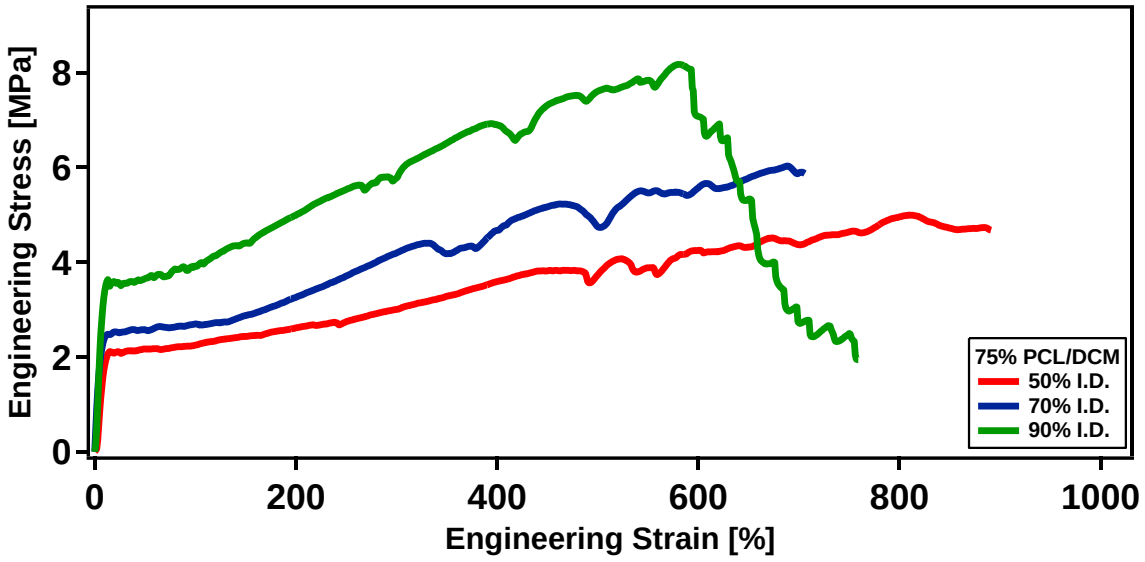

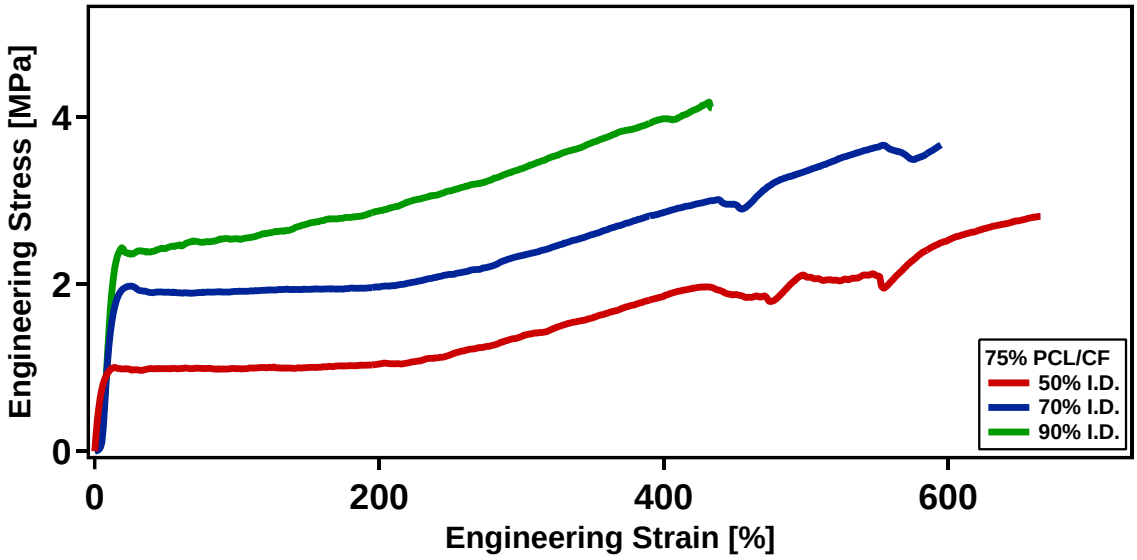

Figure 3.30 The engineering tensile stress-strain curves of printed 75% PCL_DCM and PCL_CF at infill densities of 50%, 70%, and 90%, respectively.

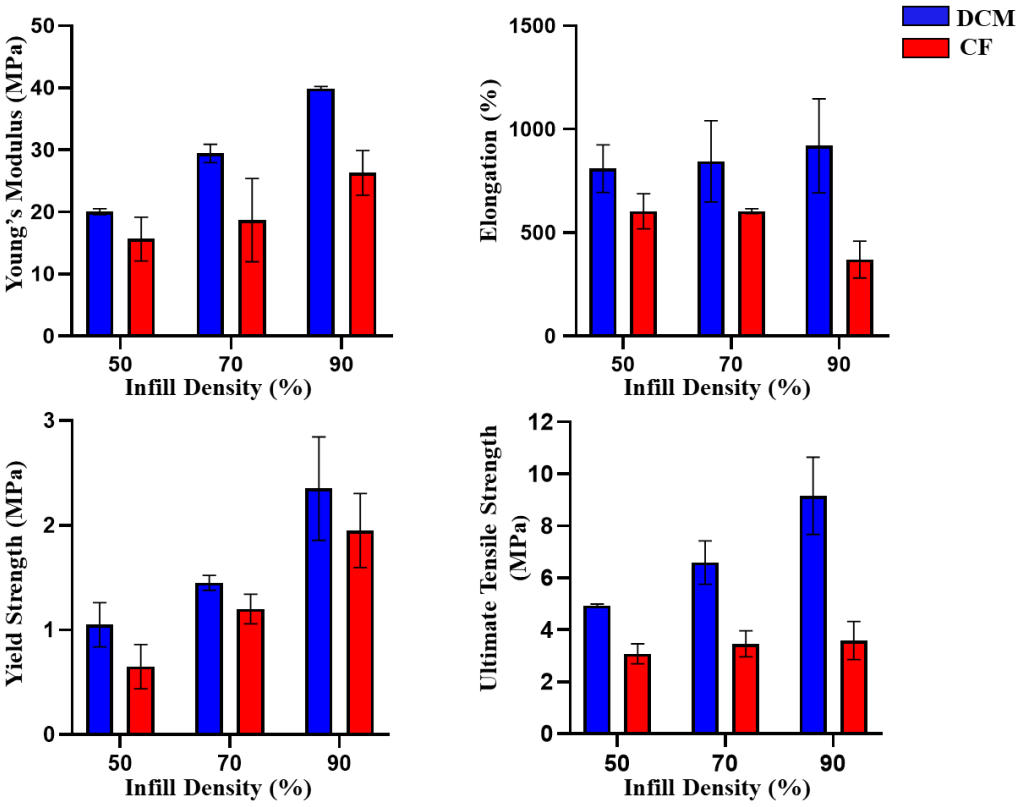

Figure 3.31 The effect of infill densities on the mechanical behavior of 75% PCL/DCM and 75% PCL/CF; (a) Young's Modulus, (b) Elongation rate of scaffolds until failure of printed PCL_DCM and PCL_CF, (c) Yield strength, and (d) UTS

values of tested scaffolds (Blue column and red column representative PCL_DCM and PCL_CF scaffolds, respectively).

Table 3.7 Process parameters and mechanical test results used to investigate the infill density effect in polymer concentration of 50%.

Concetration Polymers	Process Parameters in 3D Bioprinting	Young's Modulus (MPa)	Yield Strength (MPa)	Ultimate Tensile Strength(MPa)	Elongation at Break(%)
50% PCL/DCM	I.D= 50% V=5 mm/s P=310 kPa	19.7	1.2	4.89	891
	I.D= 70% V=5 mm/s P=310 kPa	23.38	1.4	6.0	706
	I.D= 90% V=5 mm/s P=310 kPa	40.13	2.0	8.11	758
50% PCL/CF	I.D= 50% V=5 mm/s P=310 kPa	13.14	0.5	2.81	663
	I.D= 70% V=5 mm/s P=310 kPa	13.93	1.3	3.12	595
	I.D= 90% V=5 mm/s P=310 kPa	23.75	2.2	4.10	433

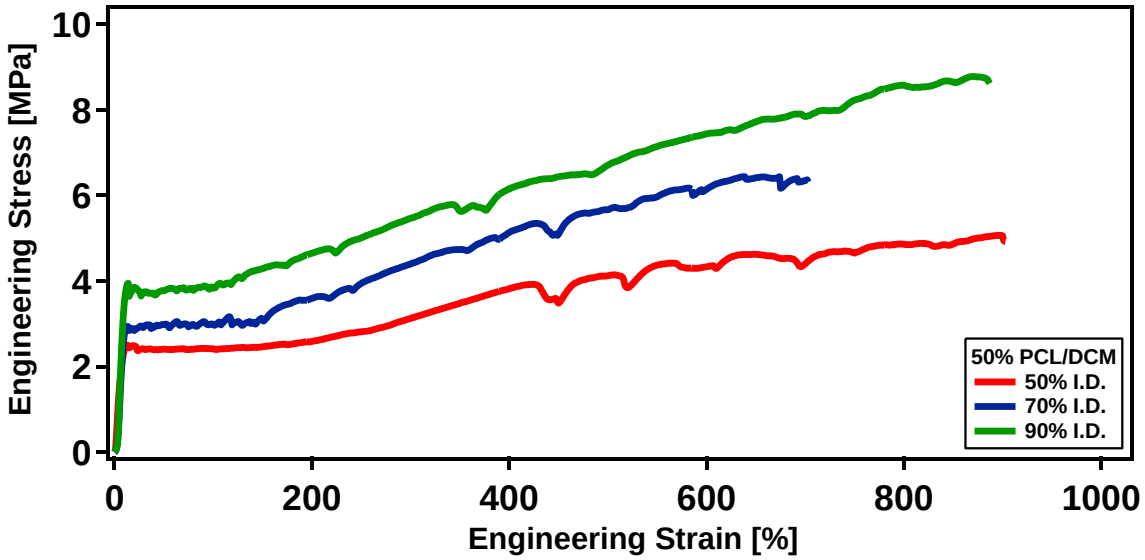

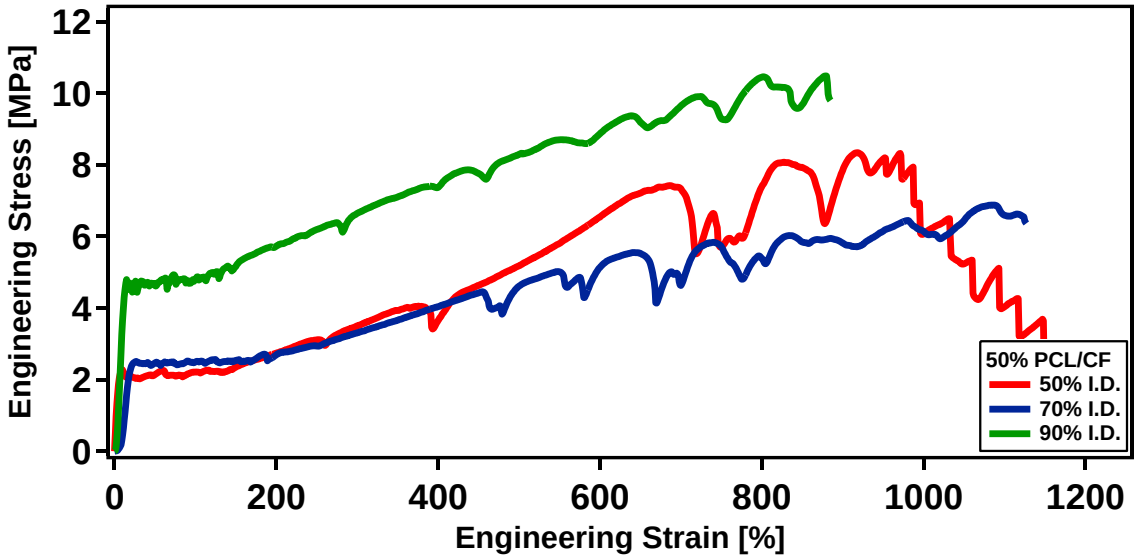

Figure 3.32 The engineering tensile stress-strain curves of printed 50 % PCL scaffolds with PCL_DCM and PCL_CF at infill densities of 50%, 70%, and 90%, respectively.

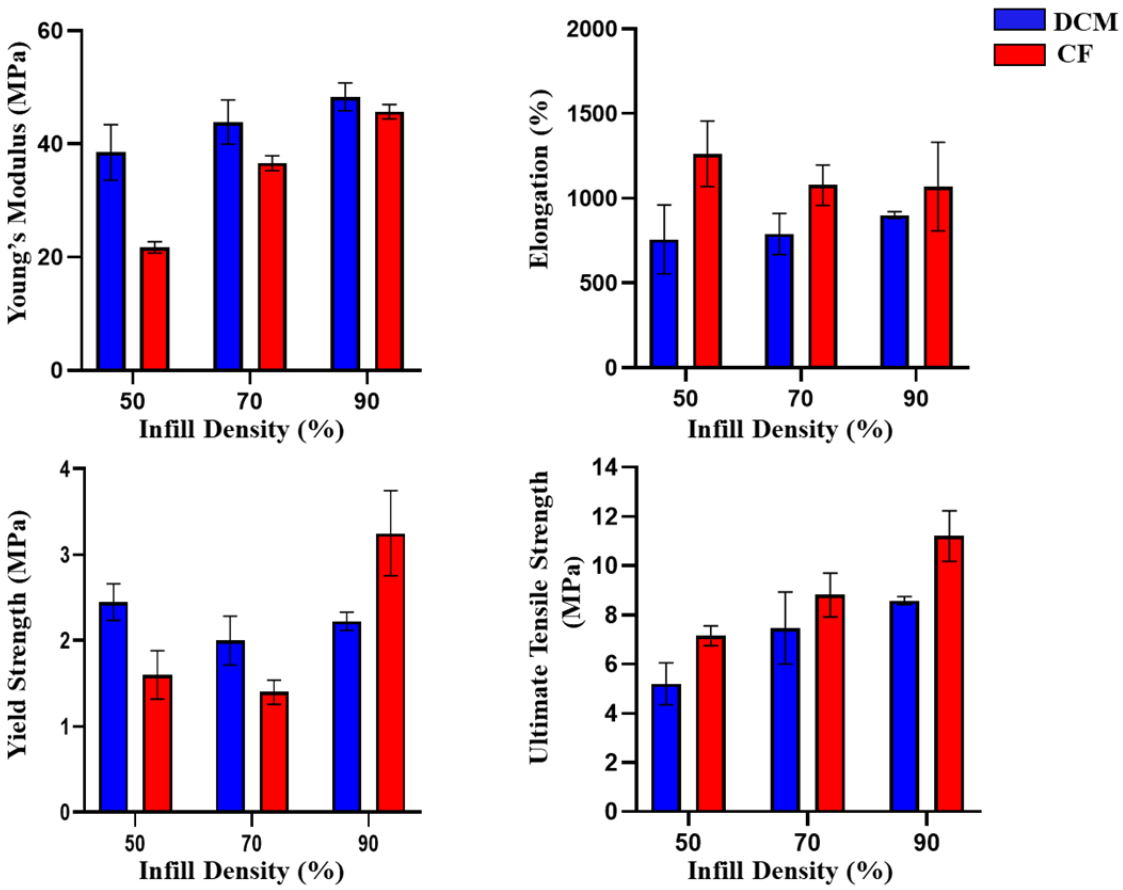

Figure 3.33 The effect of infill densities on the mechanical behavior of 50 % PCL/DCM and 50% PCL/CF. (a) Young's Modulus, (b) Elongation rate of scaffolds

until failure of printed PCL_DCM and PCL_CF, (c) Yield strength, and (d) UTS values of tested (Blue column and red column representative PCL_DCM and PCL_CF scaffolds, respectively).

3.3.4. Concentration Effect

To ensure the structural integrity of the printed structure, there are several important factors to consider when using polymers for 3D bioprinting. First, the polymer concentration should be optimized to achieve the desired viscosity and mechanical properties. Viscosity directly affects the flow of the material through the printing nozzle and the ability of the printed material to maintain its shape during and after printing [59].

The scaffolds prepared with four different concentrations (10% , 25%, 50% and 75%) were examined in this study. The structures of the scaffolds at concentration of 10% and 25%. PCL could not form a solid structure due to their longer evaporation time. In this respect, the choice of solvents with appropriate volatility is crucial to maintain the structural integrity of the printed scaffold in our study. Rapid evaporation of the solvent leads to quick solidification of the structure which makes it easier to print. Moreover, rapid evaporation enhances printability and ensures printing across a wider range of parameters [107]. The scaffolds prepared with 50% and 75% polymer concentrations demonstrated a considerable enhancement in printability and mechanical characteristics of the structure. 50% concentration provides a broad range of possibilities for printing speed and pressure. On the other hand, the scaffolds made with 75% polymer concentration exhibited structural integrity when printed at speeds ranging from 1 mm/s to 5 mm/s with high printing pressure (480 kPa). In summary, higher concentrations of polymer require more pressure and lower printing speeds to maintain their structural integrity during printing [107]. In Figure 3.31, it can be observed that the mechanical properties of the scaffolds produced at a printing speed of 5 mm/s and different concentrations show a decrease in Young's modulus as the concentration ratio increases. In Figure 3.30, Young's modulus decreases from 26.88 MPa to 13.14 MPa for PCL_CF scaffolds decreasing by approximately 51% and from 39.0 MPa to 19.7 MPa for PCL_DCM scaffolds reducing by about %49 at 75% concentration. Especially for PCL_CF scaffolds, their ductility changed significantly from 1152% fracture strain reducing to 663% reducing by approximately 43%, as increased concentration from 50%

to 75%. Additionally, scaffolds with a 75% polymer concentration exhibited lower tensile strength and UTS compared to the 50% polymer concentration in both solvents.

Considering the ease of adjusting process parameters and the mechanical analysis results, a polymer concentration of 50% has the potential to be more widely applicable in many studies. Therefore, we conducted our analyses on scaffolds prepared with 50% polymer concentration when evaluating most process parameters such as printing speed and printing pressure. Chen et al. also used DCM solvent to prepare PCL at different concentration ratios and found that increasing concentration ratios did not lead to molecular realignment due to the rapid volatility [127].

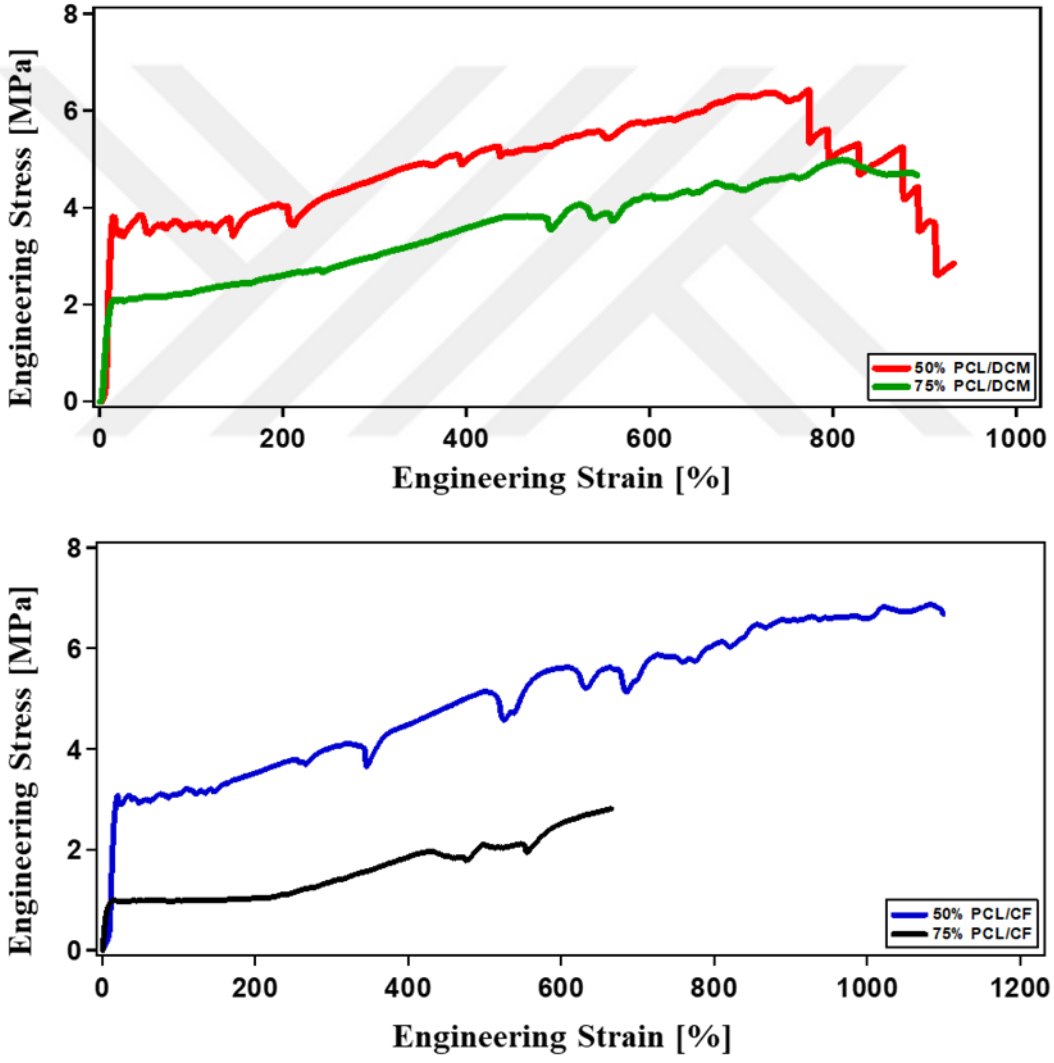

Figure 3.26 The engineering tensile stress-strain curves of printed 50 % PCL_DCM and 50% PCL_CF, and 75% PCL_DCM and 50% PCL_CF.

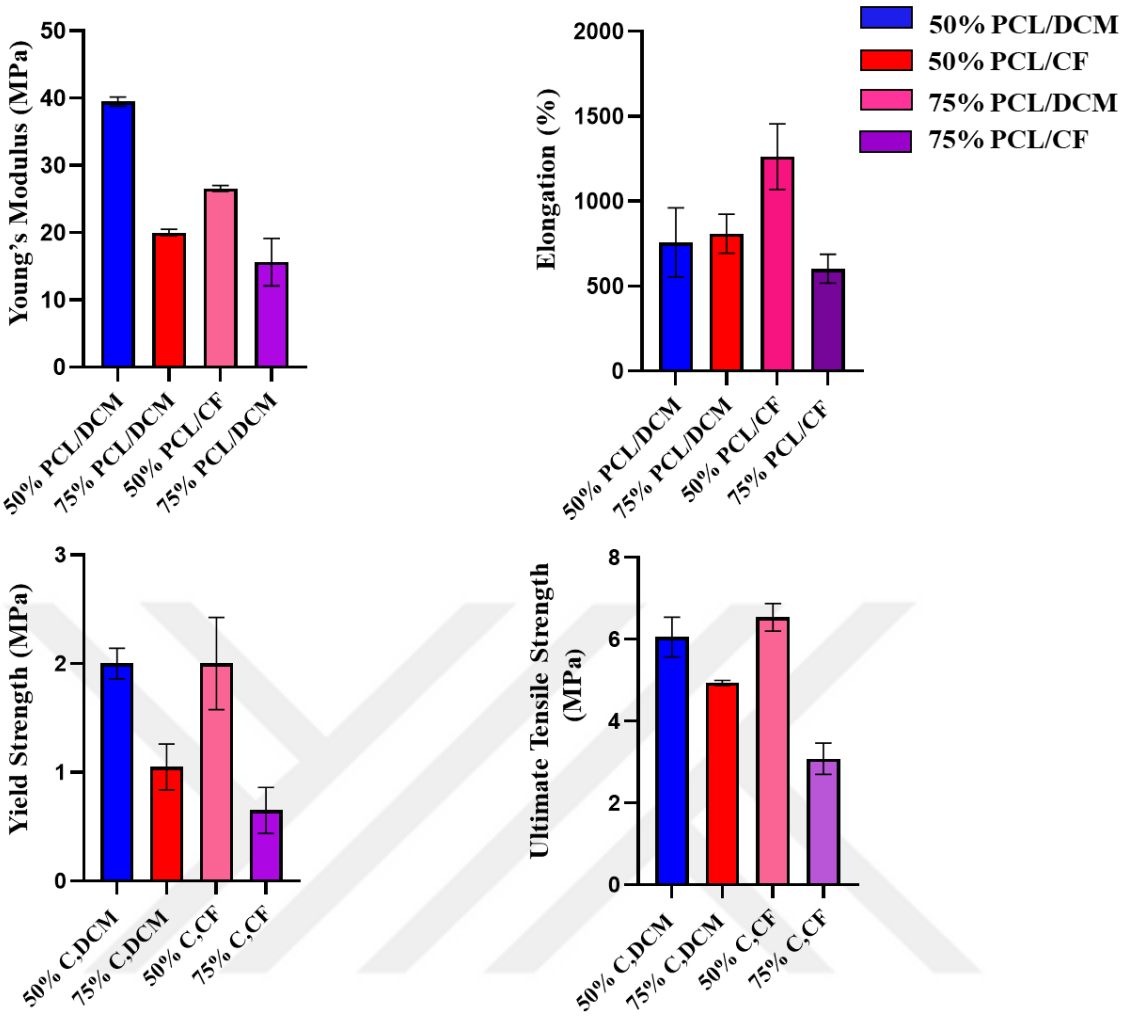

Figure 3.34 50% and 75% concentration PCL scaffolds printed at 50% infill density, 5 mm/s and 480 kPa. (a) Young's modulus, (b) fracture strain of scaffolds until failure of printed PCL_DCM and PCL_CF, (c) Yield strength, and (d)UTS values of tested scaffolds.

3.3.5. Solvent Effect

PCL is soluble in many solvents such as dimethylformamide (DMF), 1-methyl-2-pyrrolidone (NMP), tetrahydrofuran (THF), dichloromethane (DCM), acetic acid (AA), acetone (AC), chloroform (CF), and dimethyl sulfoxide (DMSO) [110]. In this study, in the beginning, three different solvents were used to evaluate the effects of the solvent on the printability and to investigate the effect on the mechanical behavior of the produced structures. In this study, DCM, AA, and CF solvents were used to dissolve PCL. To investigate the solvent effect, the printed structure was investigated concerning the uniaxixal tensile test results of the scaffolds produced with the values mentioned above,

including the printing pressures, printing speeds, infill densities, and concentrations. As the solvent's boiling point decreases, the solvent's volatility increases [110]. The sequence of boiling point is: AA (118 °C) > CF (61 °C) > DCM (40 °C) [128]. The study with acetic acid was not continued, as it caused the closure and disappearance of the pore structures in the structure due to long-term solidification. As evaluated in the above sections, it is seen that the scaffolds printed with DCM solvent have higher Young's modulus values. On the other hand, the ductility behavior is generally higher in CF scaffolds. Still, as the infill ratio and polymer concentration increased, the fracture strain of the CF scaffolds decreased significantly, as seen from Figure 3.27 to Figure 3.30. The results obtained indicate that the mechanical properties of the printed scaffolds can be significantly affected by the solvents used to dissolve the polymer. Different solvents can affect the viscosity, surface tension, and evaporation rate of the polymer solution, which in turn can affect the printing quality and the resulting mechanical properties of the printed scaffolds. For example, the use of solvents with high volatility can result in faster solvent evaporation and therefore faster solidification of the printed structure[106], leading to a more dense and rigid structure with higher mechanical strength. On the other hand, the use of solvents with lower volatility may result in slower evaporation and slower solidification, leading to a less dense and more flexible structure with lower mechanical strength .

PCL is a semicrystalline polymer, and semicrystalline polymers contain crystalline and amorphous regions. Crystallization nucleation sites can change with different solvent and their evaporation time therefore, the crystalline parts of PCL and the amorphous regions of PCL continue to be reorganized after printing and throughout the solidification period [129]. Along the drying time of the structure, the crystal regions affect the diffusion of the solvent, so the crystallinity ratios change [130]. In the literature, it has been stated that increasing the volume fraction decreases the flexibility between the chains, and this causes the delay of crystallization. As a result of the decrease in the interaction between the crystalline and amorphous regions, the crystallization rates also decrease [131]. These results can explain that the structures' mechanical properties at 75% concentration show that they are mechanically weaker, and their ductile behaviors are lower than 50% concentration. Considering all the data, PCL_DCM scaffolds ' stiffness were higher than PCL_CF scaffolds, especially at low speeds and high-pressure ranges. Although the ductility behaviors of the scaffolds produced at the same printing speed and

printing pressure using 50% concentration and 50% infill density parameters were close to each other, it was observed that the PCL_CF scaffolds showed more ductility. However, as the infill density increases for 75% concentration, the fracture strain of PCL_DCM scaffolds remain within specific ranges, while a significant decrease was revealed for CF scaffolds.

Length of polymers affects the mechanical properties of materials. As the length of the polymers is increased in unit volume, molecular weight of materials is increased correspondingly and, this is a strengthening mechanism. So, molecular weight of materials are indications of mechanical properties [132]. Semicrystalline polymer structures include both amorphous and crystalline regions and the fraction is effective on mechanical behavior [97-132]. Bondings between the chains effects the mechanical properties [125-132]. Crystalline structure density is also effective on mechanical behavior [132-133]. Moreover, dense orientation of crystalline region increases the density and molecular weight [132-134]. Knowing this knowledge, mechanical behavior results that are described above are effective on microstructures of 3D printed polymeric structures. Fractions of crystalline regions, length of chains and bonds between the chains can be changed as a result of the change in printing parameters. The aforementioned effects can be investigated using detailed SEM and uniaxixal tensile analysis. From the results it can be concluded that optimum pressure and speed can change according to the solvent and its concentration. Also, at the optimum values, the chain length, molecular weight and crystallizations can be maximized.

Table 3.8 Results of all scaffolds with mechanical tests.

Polymers Concentration	Infill Density (%)	Speed (mm/s)	Pressure (kPa)	Young Modulus (MPa)	Yield Strength (MPa)	Ultimate Tensile Strength (MPa)	Elongation(%)
50% PCL/CF	50	5	172	24.48 28.42	1.05 1.07	4.65 4.82	920 840
50% PCL/CF	50	5	310	35.68 37.55	1.5 1.3	9.44 8.18	993 1161
50% PCL/CF	50	5	480	26.26 26.88	2.3 1.7	6.78 6.3	1098 1152

50% PCL/CF	50	10	206	26.63 21.44	1.15 1.12	5.44 3.58	1058 840
50% PCL/CF	50	10	345	36.44 30.53	1.45 1.89	6.67 6.88	1134 1263
50% PCL/CF	50	10	480	28 32	1.8 1.6	5.96 5.80	1144 814
50% PCL/CF	50	15	310	15.92 16.95	0.86 0.81	4.55 3.11	1256 1298
50% PCL/CF	50	15	396	19.56 18.66	1.31 1.18	4.58 4.31	1535 1439
50% PCL/CF	50	15	480	19 18	1 0.8	3.08 3.41	1273 973
50% PCL/DCM	50	5	172	23.93 22.78	2.13 2.02	5.27 4.5	841 713
50% PCL/DCM	50	5	310	35 42	2.3 2.6	4.6 5.8	902 614
50% PCL/DCM	50	5	480	39 40	1.9 2.1	6.4 5.71	919 1041
50% PCL/DCM	50	10	206	22.44 18,66	1,65 1,3	5,59 2,88	1008 1099
50% PCL/DCM	50	10	345	39,25 43.2	2.3 2,6	8,76 7,65	1512 1000
50% PCL/DCM	50	10	480	18 16.15	0.96 0.91	2.31 2.14	558 792
50% PCL/DCM	50	15	310	24,80 21,3	1,1 1,12	5,29 4,84	1024 953
50% PCL/DCM	50	15	396	24,39 24,91	1,39 1,21	6,93 6,28	1323 1300

50% PCL/DCM	50	15	480	13.36 13.85	0.71 0.93	4.27 3.95	874 950
50% PCL/CF	50	5	310	22.42 21.03	1.8 1.4	6.87 7.44	1126 1399
50% PCL/CF	70	5	310	35.68 37.55	1.5 1.3	9.44 8.18	993 1161
50% PCL/CF	90	5	310	46.6 44.8	2.9 3.6	11.93 10.48	1254 884
50% PCL/DCM	50	5	310	35 42	2.3 2.6	4.6 5.8	902 614
50% PCL/DCM	70	5	310	46.65 41.1	2.2 1.8	8.5 6.43	875 703
50% PCL/DCM	90	5	310	50.06 46.59 42.28	2.3 2.1 2.2	8.7 8.47 8.11	887 976 915
75% PCL/CF	50	5	480	13.14 18.11	0.5 0.8	2.81 3.35	663 543
75% PCL/CF	70	5	480	13.93 23.44	1.3 1.1	3.11 3.82	595 612
75% PCL/CF	90	5	480	23.75 28.85	2.2 1.1	4.11 3.07	433 307
75% PCL/DCM	50	5	480	20.38 19.7	0,9 1.2	4.89 4.98	728 891
75% PCL/DCM	70	5	480	30.48 28.38	1.5 1.4	7.18 6.00	983 706
75% PCL/DCM	90	5	480	40.13 39.69	2 2.7	8.11 10.21	758 1080

Chapter 4

Conclusion and Future Prospects

4.1 Conclusions

3D bioprinting technology is a tissue scaffold production technique. This technology has become increasingly important in recent years, aims to print artificial tissues and organs that have biological activity and can fulfill physiological functions, thus solving the problem of tissues and organs that are insufficient to fulfill their functions. Bioprinted structures are currently being studied as potential transplantable grafts for tissue restoration, advanced in vitro models to aid in cancer research, testing of drugs, and potential alternatives to animal experiments.

In our study investigated the effects of various process parameters on the mechanical properties printed PCL scaffolds. PCL was selected as the as the material of choice for our experimental investigations. Because, PCL exhibited superior mechanical properties, making it an attractive material for use in tissue engineering and biomedical engineering applications. Obtained results in terms of printability and mechanical demonstrate that bioink concentration, printing speed, printing pressure, nozzle size, z-offset value, solvent, and infill density are all critical factors that influence the printability and mechanical properties of printed PCL scaffolds.

The solvent were found to be important factors in determining the mechanical properties of the printed scaffolds. Specifically, the use of DCM solvent showed higher stiffness results. Additionally, increasing the polymer concentration was found to be a simple and effective way to improve the mechanical strength and stiffness of the printed scaffolds. However, it is important to note that the optimal polymer concentration may vary depending on the specific scaffold design and intended application. While higher polymer concentrations generally led to improved mechanical properties, above a certain

concentration for our study at 50% polymer concentration, the mechanical properties started to plateau or even decrease as seen at 75% concentration. Increasing the PCL_CF concentration from 50% to 75% led to a significant decrease in ductility by approximately 43%. Furthermore, scaffolds with a 75% polymer concentration exhibited lower tensile strength and ultimate tensile strength compared to the 50% polymer concentration in both solvents.

Furthermore, optimizing the nozzle size and z-offset value was found to be important for improving the morphological and mechanical properties of the printed scaffolds. A nozzle gauge of 22 G and a z-offset value of 0.4 mm were found to be optimal for printing PCL scaffolds with high-quality morphological and mechanical properties among the z-offsett value of 0.2 and 0.6 mm in optic microscopy and observations examinations.

In terms of printing speed and pressure, the results suggest that slower printing speeds and moderate printing pressures are preferred for achieving high-quality PCL scaffolds with good mechanical properties. PCL_DCM scaffolds printed at a slower speed of 5 mm/s exhibited the highest Young's modulus of 39.0 MPa, whereas scaffolds printed at faster speeds of 10 mm/s and 15 mm/s demonstrated a reduction in strength values of approximately 60% (16.15 MPa) and 65% (13.83 MPa), respectively.On the other hand, low printing speeds and high printing pressures can led to weaker mechanical properties for some case, while moderate printing pressures were found to be optimal for achieving good mechanical properties. PCL_CF scaffolds printed at a moderate speed of 10 mm/s exhibited the highest Young's modulus of 32.0 MPa, indicating that they were more rigid and less deformable compared to scaffolds printed at slower (5 mm/s) and faster (15 mm/s) speeds with Young's moduli of 26.88 MPa and 18.0 MPa, respectively.

The effect of infill density on mechanical properties examined 50%, 70 % and 90%. 50% PCL and 75% PCL concentration, the highest Young's modulus values for PCL_CF and PCL_DCM scaffolds were obtained at a 90% infill density. Scaffolds printed with a 50% infill density in 50% PCL concentration showed the lowest Young's modulus values, with reductions of approximately 31% and 50% for PCL_DCM and PCL_CF, respectively. For both concentration, increasing the infill density from 50% to 90% significantly increased the UTS. However, there was no clear relationship between elongation and infill density at both concentration.

Overall, the findings of this study provide valuable insights into the optimization of process parameters for PCL scaffolds and could inform the design and fabrication of PCL-based tissue engineering scaffolds for various biomedical applications. However, further research is needed to explore the effect of other process parameters, such as nozzle diameter and layer thickness, on the mechanical properties of 3D-printed PCL scaffolds, as well as to evaluate the in vivo biocompatibility and functionality of these scaffolds.

4.2 Societal Impact and Contribution to Global Sustainability

3D bioprinting technology, an increasingly important technique in tissue engineering, aims to print artificial tissues and organs capable of biological activity and performing physiological functions to address the issue of insufficiently functioning tissues and organs. Structures created with bioprinting are currently being investigated as potential transplantable grafts for tissue restoration, advanced in vitro models to assist in cancer research, and potential alternatives to animal experiments for drug testing. Additionally, it is crucial for Turkey to conduct more research using 3D bioprinting technology, which has rapidly advanced in the field of tissue engineering in recent years, to elevate the country's position in international competition, as outlined in the 11th Development Plan.

The PCL polymer, which will be used in the thesis study, is frequently used in various biomedical research due to its characteristics such as low melting temperature, good solubility, slow biodegradation rate, and compatibility with biological tissues. PCL enables the production of scaffolds with the desired morphology and mechanical strength. Moreover, PCL solutions are commonly preferred in 3D bioprinting techniques and other tissue fabrication methods due to their suitable viscosity. The thesis study aims to examine the effects of density, solvent type, and device parameters on the printability and mechanical behavior of the PCL structures. This comprehensive investigation aims to determine scaffolds that support cell adhesion for various tissue types, facilitate gas and nutrient exchange, and exhibit the desired mechanical strength. The successful completion of the study is expected to significantly contribute to the field by accelerating research efforts and making substantial contributions to the global literature through the extensive range of data obtained.

4.3 Future Prospects

The outcomes of this thesis study have significant implications for the mechanical application of tissue engineering and regenerative medicine. The creation of scaffolds with the desired pore structures, mechanical properties, and biocompatibility is crucial for the production of functional tissues and organs in the laboratory. The knowledge obtained from this study can aid in the creation of such scaffolds by providing insights into the optimal polymer concentrations, solvents, and device parameters for printing PCL structures with desired mechanical properties and pore structures.

Moreover, the data obtained from this study could be used to perform mechanical analyses using software such as Ansys, which can provide insights into the structural stability and mechanical behavior of PCL scaffolds under different loading conditions. These simulations could inform the design of scaffolds with enhanced mechanical properties, leading to the development of more effective treatments for tissue injuries and diseases.

In conclusion, the results of this study can contribute significantly to the advancement of the field of tissue engineering and regenerative medicine by providing new knowledge on the optimal parameters for printing PCL structures with desired mechanical properties. The application of mechanical analysis tools such as Ansys can further inform the design of scaffolds with enhanced mechanical properties, which could ultimately lead to the development of functional tissues and organs for use in regenerative medicine.

BIBLIOGRAPHY

[1] M. E. Furth and A. Atala, 'Tissue Engineering: Future Perspectives', *Principles of Tissue Engineering: Fourth Edition*, pp. 83–123, Jan. 2014, doi: 10.1016/B978-0-12-398358-9.00006-9.

[2] Y. Kim, H. Ko, I. K. Kwon, and K. Shin, 'Extracellular Matrix Revisited: Roles in Tissue Engineering', *Int Neurourol J*, vol. 20, no. Suppl 1, p. S23, May 2016, doi: 10.5213/INJ.1632600.318.

[3] H. R. C. Screen, D. E. Berk, K. E. Kadler, F. Ramirez, and M. F. Young, 'Tendon Functional Extracellular Matrix', *J Orthop Res*, vol. 33, no. 6, p. 793, Jun. 2015, doi: 10.1002/JOR.22818.

[4] X. Lin, S. Patil, Y. G. Gao, and A. Qian, 'The Bone Extracellular Matrix in Bone Formation and Regeneration', *Front Pharmacol*, vol. 11, p. 757, May 2020, doi: 10.3389/FPHAR.2020.00757/BIBTEX.

[5] T. Hoshiba and T. Yamaoka, 'CHAPTER 1 Extracellular Matrix Scaffolds for Tissue Engineering and Biological Research', pp. 1–14, Dec. 2019, doi: 10.1039/9781788015998-00001.

[6] J. K. Mouw, G. Ou, and V. M. Weaver, 'Extracellular matrix assembly: a multiscale deconstruction', *Nature Reviews Molecular Cell Biology 2014 15:12*, vol. 15, no. 12, pp. 771–785, Nov. 2014, doi: 10.1038/nrm3902.

[7] M. Xue and C. J. Jackson, 'Extracellular Matrix Reorganization During Wound Healing and Its Impact on Abnormal Scarring', *Adv Wound Care (New Rochelle)*, vol. 4, no. 3, p. 119, Mar. 2015, doi: 10.1089/WOUND.2013.0485.

[8] R. E. McClelland, R. Dennis, L. M. Reid, J. P. Stegemann, B. Palsson, and J. M. Macdonald, 'Tissue Engineering', in *Introduction to Biomedical Engineering*, Elsevier Inc., 2011, pp. 273–357. doi: 10.1016/B978-0-12-374979-6.00006-X.

[9] B. P. Chan and K. W. Leong, 'Scaffolding in tissue engineering: General approaches and tissue-specific considerations', in *European Spine Journal*, Dec. 2008. doi: 10.1007/s00586-008-0745-3.

[10] G. Huang *et al.*, 'Engineering three-dimensional cell mechanical microenvironment with hydrogels', *Biofabrication*, vol. 4, no. 4, Dec. 2012, doi: 10.1088/1758-5082/4/4/042001.

[11] F. J. O'Brien, 'Biomaterials & scaffolds for tissue engineering', *Materials Today*, vol. 14, no. 3, pp. 88–95, 2011, doi: 10.1016/S1369-7021(11)70058-X.

[12] B. Thavornyutikarn, N. Chantarapanich, K. Sitthiseripratip, G. A. Thouas, and Q. Chen, 'Bone tissue engineering scaffolding: computer-aided scaffolding techniques', *Prog Biomater*, vol. 3, no. 2–4, pp. 61–102, Jul. 2014, doi: 10.1007/s40204-014-0026-7.

[13] J. Beniak, P. Križan, and M. Matúš, 'Accuracy of Rapid Prototyped Models with Using of FDM Technology', *Applied Mechanics and Materials*, vol. 613, pp. 390–395, 2014, doi: 10.4028/WWW.SCIENTIFIC.NET/AMM.613.390.

[14] C. Mota, D. Puppi, F. Chiellini, and E. Chiellini, 'Additive manufacturing techniques for the production of tissue engineering constructs', *J Tissue Eng Regen Med*, vol. 9, no. 3, pp. 174–190, Mar. 2015, doi: 10.1002/TERM.1635.

[15] C. Lueders, B. Jastram, R. Hetzer, and H. Schwandt, 'Rapid manufacturing techniques for the tissue engineering of human heart valves', *Eur J Cardiothorac Surg*, vol. 46, no. 4, pp. 593–601, Oct. 2014, doi: 10.1093/EJCTS/EZT510.

[16] M. B. Murphy and A. G. Mikos, 'Polymer Scaffold Fabrication', *Principles of Tissue Engineering*, pp. 309–321, Jan. 2007, doi: 10.1016/B978-012370615-7/50026-3.

[17] J. Reignier and M. A. Huneault, 'Preparation of interconnected poly(ε-caprolactone) porous scaffolds by a combination of polymer and salt particulate leaching', *Polymer (Guildf)*, vol. 47, no. 13, pp. 4703–4717, Jun. 2006, doi: 10.1016/J.POLYMER.2006.04.029.

[18] S. Khorshidi *et al.*, 'A review of key challenges of electrospun scaffolds for tissue-engineering applications', *J Tissue Eng Regen Med*, vol. 10, no. 9, pp. 715–738, Sep. 2016, doi: 10.1002/TERM.1978.

[19] A. Al-Abduljabbar and I. Farooq, 'Electrospun Polymer Nanofibers: Processing, Properties, and Applications', *Polymers*, vol. 15, no. 1. MDPI, Jan. 01, 2023. doi: 10.3390/polym15010065.

[20] A. Haider, S. Haider, and I. K. Kang, 'A comprehensive review summarizing the effect of electrospinning parameters and potential applications of nanofibers in biomedical and biotechnology', *Arabian Journal of Chemistry*, vol. 11, no. 8, pp. 1165–1188, Dec. 2018, doi: 10.1016/J.ARABJC.2015.11.015.

[21] S. Khorshidi *et al.*, 'A review of key challenges of electrospun scaffolds for tissue-engineering applications', *J Tissue Eng Regen Med*, vol. 10, no. 9, pp. 715–738, Sep. 2016, doi: 10.1002/TERM.1978.

[22] H. Y. Mi, X. Jing, J. McNulty, M. R. Salick, X. F. Peng, and L. S. Turng, 'Approaches to Fabricating Multiple-Layered Vascular Scaffolds Using Hybrid Electrospinning and Thermally Induced Phase Separation Methods', *Ind Eng Chem Res*, vol. 55, no. 4, pp. 882–892, Feb. 2016, doi: 10.1021/ACS.IECR.5B03462.

[23] R. Vasita and D. S. Katti, 'Nanofibers and their applications in tissue engineering', *International Journal of Nanomedicine*, vol. 1, no. 1. pp. 15–30, 2006. doi: 10.2147/nano.2006.1.1.15.

[24] J. Avossa, G. Herwig, C. Toncelli, F. Itel, and R. M. Rossi, 'Electrospinning based on benign solvents: current definitions, implications and strategies', *Green Chemistry*, vol. 24, no. 6. Royal Society of Chemistry, pp. 2347–2375, Mar. 07, 2022. doi: 10.1039/d1gc04252a.

[25] Z. Li, M. bin Xie, Y. Li, Y. Ma, J. S. Li, and F. Y. Dai, 'Recent progress in tissue engineering and regenerative medicine', *J Biomater Tissue Eng*, vol. 6, no. 10, pp. 755–766, Oct. 2016, doi: 10.1166/JBT.2016.1510.

[26] W. Ma *et al.*, 'Membrane formation by thermally induced phase separation: Materials, involved parameters, modeling, current efforts and future directions', *J Memb Sci*, vol. 669, Mar. 2023, doi: 10.1016/J.MEMSCI.2022.121303.

[27] J. J. Blaker, J. C. Knowles, and R. M. Day, 'Novel fabrication techniques to produce microspheres by thermally induced phase separation for tissue engineering and drug delivery', *Acta Biomater*, vol. 4, no. 2, pp. 264–272, Mar. 2008, doi: 10.1016/J.ACTBIO.2007.09.011.

[28] B. E. Uygun, T. Bou-Akl, M. Albanna, and H. W. T. Matthew, 'Membrane thickness is an important variable in membrane scaffolds: Influence of chitosan membrane structure on the behavior of cells', *Acta Biomater*, vol. 6, no. 6, pp. 2126–2131, 2010, doi: 10.1016/j.actbio.2009.11.018.

[29] J. F. Kim, J. H. Kim, Y. M. Lee, and E. Drioli, 'Thermally induced phase separation and electrospinning methods for emerging membrane applications: A review', *AIChE Journal*, vol. 62, no. 2, pp. 461–490, Feb. 2016, doi: 10.1002/AIC.15076/ABSTRACT.

[30] D. Gorth and T. J. Webster, 'Matrices for tissue engineering and regenerative medicine', *Biomaterials for Artificial Organs*, pp. 270–286, Jan. 2011, doi: 10.1533/9780857090843.2.270.

[31] O. A. M. Abdelaal and S. M. H. Darwish, 'Review of rapid prototyping techniques for tissue engineering scaffolds fabrication', *Advanced Structured Materials*, vol. 29, pp. 33–54, 2013, doi: 10.1007/978-3-642-31470-4_3/COVER.

[32] M. K. Joshi, H. R. Pant, A. P. Tiwari, H. J. kim, C. H. Park, and C. S. Kim, 'Multi-layered macroporous three-dimensional nanofibrous scaffold via a novel gas foaming technique', *Chemical Engineering Journal*, vol. 275, pp. 79–88, Sep. 2015, doi: 10.1016/J.CEJ.2015.03.121.

[33] 'Analytical freeze-drying', *Techniques and Instrumentation in Analytical Chemistry*, vol. 24, no. C, pp. 11–41, Jan. 2002, doi: 10.1016/S0167-9244(02)80004-X.

[34] F. Wahid, T. Khan, Z. Hussain, and H. Ullah, 'Nanocomposite scaffolds for tissue engineering; properties, preparation and applications', *Applications of Nanocomposite Materials in Drug Delivery*, pp. 701–735, Jan. 2018, doi: 10.1016/B978-0-12-813741-3.00031-5.

[35] B. Thavornyutikarn, N. Chantarapanich, K. Sitthiseripratip, G. A. Thouas, and Q. Chen, 'Bone tissue engineering scaffolding: computer-aided scaffolding techniques', *Prog Biomater*, vol. 3, no. 2–4, pp. 61–102, Jul. 2014, doi: 10.1007/S40204-014-0026-7.

[36] M. A. Ghalia and Y. Dahman, 'Advanced nanobiomaterials in tissue engineering: Synthesis, properties, and applications', *Nanobiomaterials in Soft Tissue Engineering: Applications of Nanobiomaterials*, pp. 141–172, Jan. 2016, doi: 10.1016/B978-0-323-42865-1.00006-4.

[37] R. B. Kristiawan, F. Imaduddin, D. Ariawan, Ubaidillah, and Z. Arifin, 'A review on the fused deposition modeling (FDM) 3D printing: Filament processing, materials, and printing parameters', *Open Engineering*, vol. 11, no. 1. De Gruyter Open Ltd, pp. 639–649, Jan. 01, 2021. doi: 10.1515/eng-2021-0063.

[38] R. Landers and R. Mülhaupt, ‘Desktop manufacturing of complex objects, prototypes and biomedical scaffolds by means of computer-assisted design combined with computer-guided 3D plotting of polymers and reactive oligomers’, *Macromol. Mater. Eng*, vol. 282, pp. 17–21, 2000, doi: 10.1002/1439-2054.

[39] S. H. Riza, S. H. Masood, and C. Wen, ‘Laser-Assisted Additive Manufacturing for Metallic Biomedical Scaffolds’, *Comprehensive Materials Processing*, vol. 10, pp. 285–301, Jan. 2014, doi: 10.1016/B978-0-08-096532-1.01017-7.

[40] K. S. Munir, Y. Li, and C. Wen, ‘Metallic scaffolds manufactured by selective laser melting for biomedical applications’, *Metallic Foam Bone: Processing, Modification and Characterization and Properties*, pp. 1–23, Jan. 2017, doi: 10.1016/B978-0-08-101289-5.00001-9.

[41] D. White, ‘Rapid Prototyping Processes’, *Encyclopedia of Materials: Science and Technology*, pp. 8003–8009, Jan. 2001, doi: 10.1016/B0-08-043152-6/01439-X.

[42] J. N. Dementyeva, R. N. Kashapov, N. F. Kashapov, and L. N. Kashapov, ‘Disadvantages of the selective laser sintering technology in the manufacture models for investment casting’, *IOP Conf Ser Mater Sci Eng*, vol. 570, no. 1, Aug. 2019, doi: 10.1088/1757-899X/570/1/012015.

[43] S. Agarwal, S. Saha, V. K. Balla, A. Pal, A. Barui, and S. Bodhak, ‘Current Developments in 3D Bioprinting for Tissue and Organ Regeneration–A Review’, *Front Mech Eng*, vol. 0, p. 90, Oct. 2020, doi: 10.3389/FMECH.2020.589171.

[44] Muskan, D. Gupta, and N. P. Negi, ‘3D bioprinting: Printing the future and recent advances’, *Bioprinting*, vol. 27, p. e00211, Aug. 2022, doi: 10.1016/J.BPRINT.2022.E00211.

[45] Y. W. Ding, X. W. Zhang, C. H. Mi, X. Y. Qi, J. Zhou, and D. X. Wei, ‘Recent advances in hyaluronic acid-based hydrogels for 3D bioprinting in tissue engineering applications’, *Smart Mater Med*, vol. 4, pp. 59–68, Jan. 2023, doi: 10.1016/J.SMAIM.2022.07.003.

[46] J. Xiongfa, Z. Hao, Z. Liming, and X. Jun, ‘Recent advances in 3D bioprinting for the regeneration of functional cartilage’, *Regenerative Med*, vol. 13, no. 1, pp. 73–87, Jan. 2018, doi: 10.2217/RME-2017-0106.

[47] I. T. Ozbolat, W. Peng, and V. Ozbolat, ‘Application areas of 3D bioprinting’, *Drug Discov Today*, vol. 21, no. 8, pp. 1257–1271, Aug. 2016, doi: 10.1016/J.DRUDIS.2016.04.006.

[48] P. S. Zieliński, P. K. R. Gudeti, T. Rikmanspoel, and M. K. Włodarczyk-Biegun, ‘3D printing of bio-instructive materials: Toward directing the cell’, *Bioact Mater*, vol. 19, pp. 292–327, Jan. 2023, doi: 10.1016/j.bioactmat.2022.04.008.

[49] J. Groll *et al.*, ‘A definition of bioinks and their distinction from biomaterial inks’, *Biofabrication*, vol. 11, no. 1, p. 013001, Nov. 2018, doi: 10.1088/1758-5090/AAEC52.

[50] A. Fatimi, O. V. Okoro, D. Podstawczyk, J. Siminska-Stanny, and A. Shavandi, ‘Natural Hydrogel-Based Bio-Inks for 3D Bioprinting in Tissue Engineering: A Review’, *Gels 2022, Vol. 8, Page 179*, vol. 8, no. 3, p. 179, Mar. 2022, doi: 10.3390/GELS8030179.

[51] Muskan, D. Gupta, and N. P. Negi, ‘3D bioprinting: Printing the future and recent advances’, *Bioprinting*, vol. 27, p. e00211, Aug. 2022, doi: 10.1016/J.BPRINT.2022.E00211.

[52] J. Groll *et al.*, ‘A definition of bioinks and their distinction from biomaterial inks’, *Biofabrication*, vol. 11, no. 1, p. 013001, Nov. 2018, doi: 10.1088/1758-5090/AAEC52.

[53] S. v. Murphy and A. Atala, ‘3D bioprinting of tissues and organs’, *Nature Biotechnology 2014 32:8*, vol. 32, no. 8, pp. 773–785, Aug. 2014, doi: 10.1038/nbt.2958.

[54] S. Boularaoui, G. al Hussein, K. A. Khan, N. Christoforou, and C. Stefanini, ‘An overview of extrusion-based bioprinting with a focus on induced shear stress and its effect on cell viability’, *Bioprinting*, vol. 20, p. e00093, Dec. 2020, doi: 10.1016/J.BPRINT.2020.E00093.

[55] J. Yu *et al.*, ‘Current advances in 3D bioprinting technology and its applications for tissue engineering’, *Polymers*, vol. 12, no. 12. MDPI AG, pp. 1–30, Dec. 01, 2020. doi: 10.3390/polym12122958.

[56] D. Song, Y. Xu, S. Liu, L. Wen, and X. Wang, ‘Progress of 3d bioprinting in organ manufacturing’, *Polymers*, vol. 13, no. 18. MDPI, Sep. 01, 2021. doi: 10.3390/polym13183178.

[57] S. Vijayavenkataraman, J. Y. H. Fuh, and W. F. Lu, ‘3D printing and 3D bioprinting in pediatrics’, *Bioengineering*, vol. 4, no. 3. MDPI AG, Sep. 01, 2017. doi: 10.3390/bioengineering4030063.

[58] V. Keriquel *et al.*, ‘In situ printing of mesenchymal stromal cells, by laser-assisted bioprinting, for in vivo bone regeneration applications’, *Sci Rep*, vol. 7, no. 1, Dec. 2017, doi: 10.1038/s41598-017-01914-x.

[59] J. Yu *et al.*, ‘Current Advances in 3D Bioprinting Technology and Its Applications for Tissue Engineering’, *Polymers (Basel)*, vol. 12, no. 12, pp. 1–30, Dec. 2020, doi: 10.3390/POLYM12122958.

[60] K. Hölzl, S. Lin, L. Tytgat, S. Van Vlierberghe, L. Gu, and A. Ovsianikov, ‘Biofabrication TOPICAL REVIEW • OPEN ACCESS Bioink properties before, during and after 3D bioprinting’, *Biofabrication*, vol. 8, p. 32002, 2016, doi: 10.1088/1758-5090/8/3/032002.

[61] Y. Wang, X. Yuan, B. Yao, S. Zhu, P. Zhu, and S. Huang, ‘Tailoring bioinks of extrusion-based bioprinting for cutaneous wound healing’, *Bioact Mater*, vol. 17, pp. 178–194, Nov. 2022, doi: 10.1016/J.BIOACTMAT.2022.01.024.

[62] R. Levato, T. Jungst, R. G. Scheuring, T. Blunk, J. Groll, and J. Malda, ‘From Shape to Function: The Next Step in Bioprinting’, *Advanced Materials*, vol. 32, no. 12, p. 1906423, Mar. 2020, doi: 10.1002/ADMA.201906423.

[63] S. Derakhshanfar, R. Mbeleck, K. Xu, X. Zhang, W. Zhong, and M. Xing, ‘3D bioprinting for biomedical devices and tissue engineering: A review of recent trends and advances’, *Bioact Mater*, vol. 3, no. 2, pp. 144–156, Jun. 2018, doi: 10.1016/J.BIOACTMAT.2017.11.008.

[64] K. Dzobo, K. S. C. M. Motaung, and A. Adesida, ‘Recent Trends in Decellularized Extracellular Matrix Bioinks for 3D Printing: An Updated Review’, *Int J Mol Sci*, vol. 20, no. 18, Sep. 2019, doi: 10.3390/IJMS20184628.

[65] ‘3D Printer Z Offset: Simply Explained | All3DP’. https://all3dp.com/2/z-offset-3d-printing-how-to-adjust-it/ (accessed Apr. 05, 2023).

[66] ‘How to Calibrate the Z-Offset on the E2 3D Printer’. https://www.raise3d.com/academy/how-to-calibrate-the-z-offset-on-the-e2-3d-printer/ (accessed Apr. 05, 2023).

[67] Z. Fu, V. Angeline, and W. Sun, ‘Evaluation of Printing Parameters on 3D Extrusion Printing of Pluronic Hydrogels and Machine Learning Guided Parameter Recommendation’, *Int J Bioprint*, vol. 7, no. 4, pp. 179–189, 2021, doi: 10.18063/IJB.V7I4.434.

[68] G. Huang *et al.*, ‘Engineering three-dimensional cell mechanical microenvironment with hydrogels’, *Biofabrication*, vol. 4, no. 4. Dec. 2012. doi: 10.1088/1758-5082/4/4/042001.

[69] H. Liu, G. Zheng, X. Cheng, X. Yang, and G. Zhao, ‘Simulation Analysis of the Influence of Nozzle Structure Parameters on Material Controllability’, *Micromachines (Basel)*, vol. 11, no. 9, Sep. 2020, doi: 10.3390/MI11090826.

[70] İ. Böğrekci, P. Demircioğlu, H. Saygın Sucuoğlu, and O. Turhanlar, ‘THE EFFECT OF THE INFILL TYPE AND DENSITY ON HARDNESS OF 3D PRINTED PARTS’.

[71] ‘3D Printing Infill: The Basics for Perfect Results | All3DP’. https://all3dp.com/2/infill-3d-printing-what-it-means-and-how-to-use-it/ (accessed Apr. 05, 2023).

[72] F. N. Alaribe, S. L. Manoto, and S. C. K. M. Motaung, ‘Scaffolds from biomaterials: advantages and limitations in bone and tissue engineering’, *Biologia 2016 71:4*, vol. 71, no. 4, pp. 353–366, Dec. 2016, doi: 10.1515/BIOLOG-2016-0056.

[73] J. K. Cho, Y. G. Jin, S. J. Rha, S. J. Kim, and J. H. Hwang, ‘Biochemical characteristics of four marine fish skins in Korea’, *Food Chem*, vol. 159, pp. 200–207, Sep. 2014, doi: 10.1016/j.foodchem.2014.03.012.

[74] M. N. Collins, G. Ren, K. Young, S. Pina, R. L. Reis, and J. M. Oliveira, ‘Scaffold Fabrication Technologies and Structure/Function Properties in Bone Tissue Engineering’, *Advanced Functional Materials*, vol. 31, no. 21. John Wiley and Sons Inc, May 01, 2021. doi: 10.1002/adfm.202010609.

[75] M. C. Echave, P. Sánchez, J. L. Pedraz, and G. Orive, ‘Progress of gelatin-based 3D approaches for bone regeneration’, *J Drug Deliv Sci Technol*, vol. 42, pp. 63–74, Dec. 2017, doi: 10.1016/J.JDDST.2017.04.012.

[76] S. Bhatia, ‘Natural Polymers vs Synthetic Polymer’, in *Natural Polymer Drug Delivery Systems*, Springer International Publishing, 2016, pp. 95–118. doi: 10.1007/978-3-319-41129-3_3.

[77] M. S. B. Reddy, D. Ponnamma, R. Choudhary, and K. K. Sadasivuni, ‘A Comparative Review of Natural and Synthetic Biopolymer Composite Scaffolds’, *Polymers (Basel)*, vol. 13, no. 7, Apr. 2021, doi: 10.3390/POLYM13071105.

[78] R. Dwivedi *et al.*, ‘Polycaprolactone as biomaterial for bone scaffolds: Review of literature’, *J Oral Biol Craniofac Res*, vol. 10, no. 1, pp. 381–388, Jan. 2020, doi: 10.1016/J.JOBCR.2019.10.003.

[79] R. Augustine, E. A. Dominic, I. Reju, B. Kaimal, N. Kalarikkal, and S. Thomas, ‘Electrospun polycaprolactone membranes incorporated with ZnO nanoparticles as skin substitutes with enhanced fibroblast proliferation and wound healing’, *RSC Adv*, vol. 4, no. 47, pp. 24777–24785, Jun. 2014, doi: 10.1039/C4RA02450H.

[80] E. Ercolani, C. Del Gaudio, and A. Bianco, ‘Vascular tissue engineering of small-diameter blood vessels: reviewing the electrospinning approach’, *J Tissue Eng Regen Med*, vol. 9, no. 8, pp. 861–888, Aug. 2015, doi: 10.1002/TERM.1697.

[81] J. P. Abriata *et al.*, ‘Development, characterization and biological in vitro assays of paclitaxel-loaded PCL polymeric nanoparticles’, *Materials Science and Engineering: C*, vol. 96, pp. 347–355, Mar. 2019, doi: 10.1016/J.MSEC.2018.11.035.

[82] T. K. Merceron *et al.*, ‘A 3D bioprinted complex structure for engineering the muscle-tendon unit’, *Biofabrication*, vol. 7, no. 3, Jun. 2015, doi: 10.1088/1758-5090/7/3/035003.

[83] C. X. F. Lam, M. M. Savalani, S. H. Teoh, and D. W. Hutmacher, ‘Dynamics of in vitro polymer degradation of polycaprolactone-based scaffolds: accelerated versus simulated physiological conditions’, *Biomedical Materials*, vol. 3, no. 3, p. 034108, Aug. 2008, doi: 10.1088/1748-6041/3/3/034108.

[84] A. C. Daly, G. M. Cunniffe, B. N. Sathy, O. Jeon, E. Alsberg, and D. J. Kelly, ‘3D Bioprinting of Developmentally Inspired Templates for Whole Bone Organ Engineering’, *Adv Healthc Mater*, vol. 5, no. 18, pp. 2353–2362, 2016, doi: 10.1002/adhm.201600182.

[85] F. Pati *et al.*, ‘Printing three-dimensional tissue analogues with decellularized extracellular matrix bioink’, *Nat Commun*, vol. 5, 2014, doi: 10.1038/ncomms4935.

[86] J. H. Shim, J. S. Lee, J. Y. Kim, and D. W. Cho, ‘Bioprinting of a mechanically enhanced three-dimensional dual cell-laden construct for osteochondral tissue engineering using a multi-head tissue/organ building system’, *Journal of Micromechanics and Microengineering*, vol. 22, no. 8, Aug. 2012, doi: 10.1088/0960-1317/22/8/085014.

[87] H. Lee, S. Ahn, L. J. Bonassar, and G. Kim, ‘Cell(MC3T3-E1)-printed poly(ϵ-caprolactone)/alginate hybrid scaffolds for tissue regeneration’, *Macromol Rapid Commun*, vol. 34, no. 2, pp. 142–149, Jan. 2013, doi: 10.1002/MARC.201200524.

[88] L. Ruiz-Cantu, A. Gleadall, C. Faris, J. Segal, K. Shakesheff, and J. Yang, ‘Multi-material 3D bioprinting of porous constructs for cartilage regeneration’, *Materials Science and Engineering: C*, vol. 109, p. 110578, Apr. 2020, doi: 10.1016/J.MSEC.2019.110578.

[89] A. Kosik-Kozioł, M. Heljak, and W. Święszkowski, ‘Mechanical properties of hybrid triphasic scaffolds for osteochondral tissue engineering’, *Mater Lett*, vol. 261, p. 126893, Feb. 2020, doi: 10.1016/J.MATLET.2019.126893.

[90] J. Yu *et al.*, ‘Fabrication of a polycaprolactone/alginate bipartite hybrid scaffold for osteochondral tissue using a three-dimensional bioprinting system’, *Polymers (Basel)*, vol. 12, no. 10, pp. 1–16, Oct. 2020, doi: 10.3390/POLYM12102203.

[91] J. H. Park *et al.*, ‘Experimental Tracheal Replacement Using 3-dimensional Bioprinted Artificial Trachea with Autologous Epithelial Cells and Chondrocytes’, *Scientific Reports 2019 9:1*, vol. 9, no. 1, pp. 1–11, Feb. 2019, doi: 10.1038/s41598-019-38565-z.

[92] T. T. Tran, Z. A. Hamid, and K. Y. Cheong, ‘A Review of Mechanical Properties of Scaffold in Tissue Engineering: Aloe Vera Composites’, *J Phys Conf Ser*, vol. 1082, no. 1, p. 012080, Aug. 2018, doi: 10.1088/1742-6596/1082/1/012080.

[93] C. F. Guimarães, L. Gasperini, A. P. Marques, and R. L. Reis, ‘The stiffness of living tissues and its implications for tissue engineering’, *Nature Reviews Materials*, vol. 5, no. 5. Nature Research, pp. 351–370, May 01, 2020. doi: 10.1038/s41578-019-0169-1.

[94] T. Billiet, M. Vandenhaute, J. Schelfhout, S. Van Vlierberghe, and P. Dubruel, ‘A review of trends and limitations in hydrogel-rapid prototyping for tissue engineering’, *Biomaterials*, vol. 33, no. 26, pp. 6020–6041, Sep. 2012, doi: 10.1016/J.BIOMATERIALS.2012.04.050.

[95] ‘Tensile Test Experiment | Michigan Technological University’. https://www.mtu.edu/materials/k12/experiments/tensile/ (accessed Oct. 25, 2022).

[96] U. K. Murmu *et al.*, ‘Mechanical Properties of Crystalline and Semicrystalline Polymer Systems’, in *Encyclopedia of Materials: Plastics and Polymers*, Elsevier, 2022, pp. 917–927. doi: 10.1016/b978-0-12-820352-1.00248-0.

[97] Z. S. ˇ pitalsk, T. Bleha, and P. Cifra, ‘Energy Elasticity of Tie Molecules in Semicrystalline Polymers’, *Macromol. Theory Simul*, vol. 11, pp. 513–524, 2002, doi: 10.1002/1521-3919(20020601)11:5.

[98] U. K. Murmu *et al.*, ‘Mechanical Properties of Crystalline and Semicrystalline Polymer Systems’, in *Encyclopedia of Materials: Plastics and Polymers*, Elsevier, 2022, pp. 917–927. doi: 10.1016/b978-0-12-820352-1.00248-0.

[99] S. S. Wong, S. A. Altinkaya, and S. K. Mallapragada, ‘Drying of semicrystalline polymers: Mathematical modeling and experimental characterization of poly(vinyl alcohol) films’, *Polymer (Guildf)*, vol. 45, no. 15, pp. 5151–5161, Jul. 2004, doi: 10.1016/J.POLYMER.2004.05.037.

[100] S. S. Wong, S. A. Altinkaya, and S. K. Mallapragada, ‘Drying of semicrystalline polymers: Mathematical modeling and experimental characterization of poly(vinyl alcohol) films’, *Polymer (Guildf)*, vol. 45, no. 15, pp. 5151–5161, Jul. 2004, doi: 10.1016/J.POLYMER.2004.05.037.

[101] S. Castagnet and Y. Deburck, ‘Relative influence of microstructure and macroscopic triaxiality on cavitation damage in a semi-crystalline polymer’,

Materials Science and Engineering A, vol. 448, no. 1–2, pp. 56–66, Mar. 2007, doi: 10.1016/j.msea.2006.11.100.

[102] Y. Zhang, P. Y. Ben Jar, S. Xue, and L. Li, 'Quantification of strain-induced damage in semi-crystalline polymers: a review', *Journal of Materials Science*, vol. 54, no. 1. Springer New York LLC, pp. 62–82, Jan. 01, 2019. doi: 10.1007/s10853-018-2859-2.

[103] Y. Zhang, P. Y. Ben Jar, S. Xue, and L. Li, 'Quantification of strain-induced damage in semi-crystalline polymers: a review', *Journal of Materials Science*, vol. 54, no. 1. Springer New York LLC, pp. 62–82, Jan. 01, 2019. doi: 10.1007/s10853-018-2859-2.

[104] J. Lai, C. Wang, and M. Wang, '3D printing in biomedical engineering: Processes, materials, and applications', *Applied Physics Reviews*, vol. 8, no. 2. American Institute of Physics Inc., Jun. 01, 2021. doi: 10.1063/5.0024177.

[105] B. Zhang, R. Cristescu, D. B. Chrisey, and R. J. Narayan, 'Solvent-based extrusion 3D printing for the fabrication of tissue engineering scaffolds', *Int J Bioprint*, vol. 6, no. 1, pp. 28–42, 2020, doi: 10.18063/ijb.v6i1.211.

[106] P. Y. Chou, Y. C. Chou, Y. H. Lai, Y. T. Lin, C. J. Lu, and S. J. Liu, 'Fabrication of Drug-Eluting Nano-Hydroxylapatite Filled Polycaprolactone Nanocomposites Using Solution-Extrusion 3D Printing Technique', *Polymers (Basel)*, vol. 13, no. 3, pp. 1–13, Feb. 2021, doi: 10.3390/POLYM13030318.

[107] I. T. Ozbolat, '3D Bioprinting: Fundamentals, Principles and Applications', *3D Bioprinting: Fundamentals, Principles and Applications*, pp. 1–342, Nov. 2016.

[108] I. M. Smallwood, 'Acetic acid', *Handbook of Organic Solvent Properties*, pp. 265–267, Jan. 1996, doi: 10.1016/B978-0-08-052378-1.50067-0.

[109] F. Kh. Tukhvatullin, U. N. Tashkenbaev, A. Zhumaboev, and Z. Mamatov, 'Intermolecular hydrogen bonds in acetic acid and its solutions', *Journal of Applied Spectroscopy 1999 66:4*, vol. 66, no. 4, pp. 501–505, Jul. 1999, doi: 10.1007/BF02675376.

[110] X. Qin and D. Wu, 'Effect of different solvents on poly(caprolactone)(PCL) electrospun nonwoven membranes', *J Therm Anal Calorim*, vol. 107, no. 3, pp. 1007–1013, Mar. 2012, doi: 10.1007/S10973-011-1640-4/FIGURES/9.

[111] F. C. Bayram, M. F. Kapçı, A. Yuruk, I. A. Isoglu, and B. Bal, 'Investigations of strain rate, size, and crack length effects on the mechanical response of polycaprolactone electrospun membranes', *Proceedings of the Institution of Mechanical Engineers, Part E: Journal of Process Mechanical Engineering*, vol. 235, no. 6, pp. 1957–1970, Dec. 2021, doi: 10.1177/09544089211024065.

[112] M. Kök, M. E. Pekdemir, E. Özen Öner, M. Coşkun, and S. Hekim, 'MWCNT nanocomposite films prepared using different ratios of PVC/PCL: Combined FT-IR/DFT, thermal and shape memory properties', *J Mol Struct*, vol. 1279, p. 134989, May 2023, doi: 10.1016/J.MOLSTRUC.2023.134989.

[113] B. Sowmya and P. K. Panda, 'Electrospinning of poly(ε-caprolactone) (PCL) and poly ethylene glycol (PEG) composite nanofiber membranes using methyl ethyl ketone (MEK) and N N'-dimethyl acetamide (DMAc) solvent mixture for anti-

adhesion applications', *Mater Today Commun*, vol. 33, p. 104718, Dec. 2022, doi: 10.1016/J.MTCOMM.2022.104718.

[114] M. Pivar, D. Gregor-Svetec, and D. Muck, 'Effect of printing process parameters on the shape transformation capability of 3D printed structures', *Polymers (Basel)*, vol. 14, no. 1, Jan. 2022, doi: 10.3390/polym14010117.

[115] K. Fakhruddin, M. S. A. Hamzah, and S. I. A. Razak, 'Effects of extrusion pressure and printing speed of 3D bioprinted construct on the fibroblast cells viability', *IOP Conf Ser Mater Sci Eng*, vol. 440, no. 1, p. 012042, Oct. 2018, doi: 10.1088/1757-899X/440/1/012042.

[116] P. Gentile, K. McColgan-Bannon, N. C. Gianone, F. Sefat, K. Dalgarno, and A. M. Ferreira, 'Biosynthetic PCL-graft-Collagen Bulk Material for Tissue Engineering Applications', *Materials (Basel)*, vol. 10, no. 7, Jun. 2017, doi: 10.3390/MA10070693.

[117] M. PARMAKSIZ and M. VURAT, 'MECHANICAL EVALUATION OF 3D PRINTED POLYCAPROLACTONE SCAFFOLDS: EFFECT OF MOLECULAR WEIGHT', *International Journal of 3D Printing Technologies and Digital Industry*, vol. 5, no. 2, pp. 251–258, Aug. 2021, doi: 10.46519/IJ3DPTDI.966777.

[118] K. Fakhruddin, S. I. Abd Razak, M. A. Murad, N. H. Mat Nayan, and S. Sa'adon, 'Effect of pressure and infill density parameter setting on morphological and mechanical properties of polycaprolactone printed scaffold using desktop 3D bioprinter', in *Journal of Physics: Conference Series*, Institute of Physics Publishing, Nov. 2019. doi: 10.1088/1742-6596/1372/1/012073.

[119] S. Naghieh, M. D. Sarker, N. K. Sharma, Z. Barhoumi, and X. Chen, 'Printability of 3D Printed Hydrogel Scaffolds: Influence of Hydrogel Composition and Printing Parameters', *Applied Sciences 2020, Vol. 10, Page 292*, vol. 10, no. 1, p. 292, Dec. 2019, doi: 10.3390/APP10010292.

[120] E. Sodupe-Ortega, A. Sanz-Garcia, A. Pernia-Espinoza, and C. Escobedo-Lucea, 'Accurate calibration in multi-material 3D bioprinting for tissue engineering', *Materials*, vol. 11, no. 8, Aug. 2018, doi: 10.3390/ma11081402.

[121] S. F. Khan, H. Zakaria, Y. L. Chong, M. A. M. Saad, and K. Basaruddin, 'Effect of infill on tensile and flexural strength of 3D printed PLA parts', in *IOP Conference Series: Materials Science and Engineering*, Institute of Physics Publishing, Nov. 2018. doi: 10.1088/1757-899X/429/1/012101.

[122] G. Turnbull *et al.*, '3D bioactive composite scaffolds for bone tissue engineering', *Bioact Mater*, vol. 3, no. 3, pp. 278–314, Sep. 2017, doi: 10.1016/J.BIOACTMAT.2017.10.001.

[123] M. J. Jahir-Hussain, N. A. Maaruf, N. E. F. Esa, and N. Jusoh, 'The effect of pore geometry on the mechanical properties of 3D-printed bone scaffold due to compressive loading', *IOP Conf Ser Mater Sci Eng*, vol. 1051, no. 1, p. 012016, Feb. 2021, doi: 10.1088/1757-899x/1051/1/012016.

[124] M. Qamar Tanveer, G. Mishra, S. Mishra, and R. Sharma, 'Effect of infill pattern and infill density on mechanical behaviour of FDM 3D printed Parts- a current

review', *Mater Today Proc*, vol. 62, pp. 100–108, Jan. 2022, doi: 10.1016/j.matpr.2022.02.310.

[125] G. R. Hamed, 'Molecular Aspects of the Fatigue and Fracture of Rubber', *Rubber Chemistry and Technology*, vol. 67, no. 3, pp. 529–536, Jul. 1994, doi: 10.5254/1.3538689.

[126] L. A. Chicos *et al.*, 'Infill Density Influence on Mechanical and Thermal Properties of Short Carbon Fiber-Reinforced Polyamide Composites Manufactured by FFF Process', *Materials*, vol. 15, no. 10, May 2022, doi: 10.3390/ma15103706.

[127] J. M. Chen, D. Lee, J. W. Yang, S. H. Lin, Y. T. Lin, and S. J. Liu, 'Solution Extrusion Additive Manufacturing of Biodegradable Polycaprolactone', *Applied Sciences 2020, Vol. 10, Page 3189*, vol. 10, no. 9, p. 3189, May 2020, doi: 10.3390/APP10093189.

[128] K. A. G. Katsogiannis, G. T. Vladisavljević, and S. Georgiadou, 'Porous electrospun polycaprolactone (PCL) fibres by phase separation', *Eur Polym J*, vol. 69, pp. 284–295, Aug. 2015, doi: 10.1016/J.EURPOLYMJ.2015.01.028.

[129] A. Gupper and S. G. Kazarian, 'Study of solvent diffusion and solvent-induced crystallization in syndiotactic polystyrene using FT-IR spectroscopy and imaging', *Macromolecules*, vol. 38, no. 6, pp. 2327–2332, Mar. 2005, doi: 10.1021/MA0476590.

[130] M. O. Ngui and S. K. Mallapragada, 'Mechanistic investigation of drying regimes during solvent removal from poly(vinyl alcohol) films', *J Appl Polym Sci*, vol. 72, no. 14, pp. 1913–1920, 1999, doi: 10.1002/(SICI)1097-4628(19990628)72:14<1913::AID-APP12>3.0.CO;2-L.

[131] I. Castilla-Cortázar, A. Vidaurre, B. Marí, and A. J. Campillo-Fernández, 'Morphology, Crystallinity, and Molecular Weight of Poly(ε-caprolactone)/Graphene Oxide Hybrids', *Polymers (Basel)*, vol. 11, no. 7, 2019, doi: 10.3390/POLYM11071099.

[132] W. D. Callister and D. G. Rethwisch, *Materials Science and Engineering*. Wiley. [Online]. Available: https://books.google.com.tr/books?id=99UeMAEACAAJ

[133] S. Patlazhan and Y. Remond, 'Structural mechanics of semicrystalline polymers prior to the yield point: A review', *J Mater Sci*, vol. 47, no. 19, pp. 6749–6767, Oct. 2012, doi: 10.1007/S10853-012-6620-Y.

[134] 'FreiDok plus - Understanding of the mechanical response of semicrystalline polymers based on the block-like substructure of crystalline lamellae'. https://freidok.uni-freiburg.de/data/273 (accessed Nov. 26, 2022).

CURRICULUM VITAE

2015 – 2019	B.Sc., Biomedical Engineering, Erciyes University, Kayseri, TURKEY
2011 – 2013	M.Sc., Bioengineering Engineering,Abdullah Gul University,Kayseri, TURKEY

Experience

Abdullah Gul University

- Researcher in Tubitak Project
- 10 Jul 2022-15 May 2023

Elmaslar Medical

- Biomedical Engineer
- 10 Jul 2021- 01 Sept 2021

Konya Beyhekim Hospital Konya (Turkey)-

- Biomedical Engineer intern
- 6 Jul 2018–7 Sept 2018

Yuksek Ihtisas Research Hospital

- Ankara (Turkey)-Biomedical Engineer intern
- 15 Jul 2017–13 Sept 2017